

Spring 5-2015

Deformation Post-Doming: New mapping of the Oliverian Jefferson Dome, Mt. Dartmouth 7.5' Quadrangle, New Hampshire

Michelle Devoe
mdevoe@bates.edu

Follow this and additional works at: <http://scarab.bates.edu/honorstheses>

Recommended Citation

Devoe, Michelle, "Deformation Post-Doming: New mapping of the Oliverian Jefferson Dome, Mt. Dartmouth 7.5' Quadrangle, New Hampshire" (2015). *Honors Theses*. 115.
<http://scarab.bates.edu/honorstheses/115>

This Open Access is brought to you for free and open access by the Capstone Projects at SCARAB. It has been accepted for inclusion in Honors Theses by an authorized administrator of SCARAB. For more information, please contact batesscarab@bates.edu.

Deformation Post-Doming:

New mapping of the Oliverian Jefferson Dome,

Mt. Dartmouth 7.5' Quadrangle,

New Hampshire

Bates College Department of Geology Honors Thesis

Presented to the Faculty of the Department of Geology, Bates College,
in partial fulfillment of the requirements for the Degree of Bachelor of Science

by

Michelle Cyr Devoe

Lewiston, Maine

March 30th, 2015

ABSTRACT

The Mt. Dartmouth 7.5' quadrangle, located west of the Presidential Range, contains the central southern portion of the Jefferson Dome. The Jefferson Dome is the largest and northernmost of the Oliverian Domes which outcrop along the Bronson Hill Anticlinorium, the resultant structure of convergent, orogenic forces on the Ordovician Bronson Hill volcanic arc. With a grant from the USGS NHGS EdMap StateMap program, the Mt. Dartmouth 7.5' quadrangle was remapped at the 1:24,000 scale for a detailed understanding of the rock types, structural geology, and petrology of the Jefferson Dome. These new findings produced a more complete understanding of the tectonic forces that have affected the Jefferson Dome.

This study identifies four new lithotectonic units within the Jefferson Dome, including the coarse-grained varieties Oo1bc and Oo1hc, and the porphyritic varieties Oo1bcx and Oo1hx. The compositions of the Oliverian Plutonic members range from biotite and/or hornblende-bearing quartz alkali feldspar syenites, quartz syenites, and granites. The strong marginal foliation and weaker core fabrics, seen throughout the Oliverian Domes in the Bronson Hill Anticlinorium, was not observed. Instead foliation intensity was found to vary across the dome revealing both doming patterns and post-doming structures.

Through analysis of doming related foliation using equal-area stereographic projections, it was determined that the quadrangle contained the two limbs of the Jefferson Dome which are oriented at $061^{\circ}, 41^{\circ}$ SE and $279^{\circ}, 10^{\circ}$ NW and form an interlimb angle of 130° . The hingeline of the Jefferson Dome was determined to be $62^{\circ}, 13^{\circ}$ using a Cylindrical Best Fit test. The axial surface was determined to be $245^{\circ}, 76^{\circ}$. The resulting fold is classified as a gently plunging, steeply dipping, gentle antiform (Fleuty, 1964).

Post-Doming dextral S-C fabrics were identified in three locations. A correlation between strongly developed foliation, shearing, and steeply-dipping foliation was identified at Appleby Mountain. A correlation between strongly developed foliation, shearing and the presence of porphyry was identified at Mill Brook. Based on these correlations, three dextral shear zones were mapped, two discrete narrow zones in Mill Brook and one broader zone on Appleby Mountain.

Crenulated S-C fabrics were observed on Appleby Mountain suggesting a third phase of deformation in the dome. These folds may be related to movement on the Pine Peak Fault, the major boundary between the Oliverian rocks to the NW and the Silurian Rangeley Formation and Bretton Woods Granite to the SE.

The dome-like structure of the foliation, the presence of S-C fabrics, and the crenulations in the S-C fabrics, can be used to infer the deformational events that have affected the dome and the order in which they occurred. Based on an observed limit of doming in the already refolded nappes of the Silurian and Devonian Rangeley and Littleton Formations (Eusden, 2010), the doming is believed to have occurred during the late Devonian late Acadian or Early Carboniferous Neocadian orogeny. The dextral shear zones followed in the Carboniferous-Permian Alleghanian orogeny producing structures similar in motion to the same aged Norumbega Fault (Hooke and Winski, 2014; Ludman et al., 1999). The crenulations of the earlier fabrics occurred due to motion along the either the Pine Peak Fault or Ammonoosuc Fault during the Mesozoic (Roden-Tice et al., 2009; Hardcastle et al., 1990).

ACKNOWLEDGEMENTS

I would like to start with the biggest and most sincere thank you to my advisor, Dyk Eusden. The enthusiasm and liveliness you approach life with is transmitted through to your students during lecture, field trips, or in this case, seven weeks in the hot, buggy New Hampshire woods. Your positivity has helped me see through every challenge to understanding.

A whole-hearted thank you to the rest of the Geology Department-- Bev, Mike, Genevieve, Gene, Marita, Phil—thank you for your continued support and inspiration over the years.

I would also like to thank the USGS EdMap StateMap Program and the New Hampshire Geological Survey for providing us with the grants which supported our summer research.

To all the geodes-- thank you for the endless support, laughs, and all those late nights in Coram. And of course, the biggest of love and thanks to my friends and family for their support in all my endeavors.

TABLE OF CONTENTS

Introduction.....	8
Overview.....	8
Study Area.....	11
Previous Mapping.....	11
Tectonic History of the Northern Appalachians.....	14
Tectonic Models: Bronson Hill Arc.....	18
Doming Theories.....	23
Foliation in the field.....	24
Significance of Study.....	24
Methods.....	25
Field Mapping Methods.....	25
Laboratory Mapping Methods.....	26
Thin Section Production.....	27
Mineralogical Analysis.....	28
Transmitted Light Microscopy.....	28
Scanning Electron Microscopy-Energy Dispersive Spectroscopy.....	29
Structural Analysis.....	31
Stereographic Projections.....	31
Results.....	32
Map Contacts and Units.....	32
Overview.....	32
Oo1b.....	35
Oo1bx.....	38
Oo1bc.....	38
Oo1bcx.....	38
Oo1h.....	39
Oo1hx.....	40

Oo1hc.....	42
Oal.....	42
Possibilities for Future Work.....	44
Structural Analysis.....	45
Using Foliation to Construct the Shape and Orientation of the Dome.....	45
The Dome	45
Shear Zones.....	47
Crenulations on Appleby Mountain.....	49
Discussion.....	50
Overview.....	50
Origin of the Oliverian Suite and Ammonoosuc Volcanics.....	50
Magmatic Differentiation and Timing of Intrusion.....	51
Asymmetry and Orientation of the Jefferson Dome.....	51
The Expected Ammonoosuc Volcanic Mantle.....	52
Appleby and Mill Brook Shear Zones.....	53
Dextral Shear Sense.....	55
The Dome: Three Stages of Deformation.....	58
The Silicified Zone and Quartz Veins.....	58
Deformation History of the Northeast.....	59
Conclusions.....	59
References.....	61
Appendix.....	66

TABLE OF FIGURES

Figure 1: Lithotectonic map of the Appalachian Mountains from Hibbard et al. (2010).....	5
Figure 2: Location map of the Oliverian Domes of New Hampshire from Dorais et al. (2008)....	9
Figure 3: Granit 7.5' Quadrangle map of New Hampshire from Granit.com (2005).....	9
Figure 4: Billings et al. (1946) bedrock geology map of Mt. Dartmouth 7.5' quadrangle.....	13

Figure 5: Lyons et al. (1997) bedrock geology map of the Mt. Dartmouth 7.5' quadrangle.....	14
Figure 6: Taconic 1 and 2 tectonic models by van Staal et al. (2009).....	16
Figure 7: Taconic 2 and 3 tectonic models by van Staal et al. (2009).....	17
Figure 8: Taconic orogeny model by Moench and Aleinikoff (2003).....	20
Figure 9: Western-dipping subduction zone tectonic theory for the development of the Bronson Hill Arc by Karabinos et al. (1998).....	20
Figure 10: Taconic orogeny model by Hatcher (2010).....	21
Figure 11: Tectonic model of the Taconic orogeny by Macdonald et al. (2014).....	22
Figure 12: Diamond Pacific slab saw and Lotorne Inc. Lapiday saw used for cutting thin sections.....	27
Figure 13: Olympus BH-2 microscope and Olympus DP21 camera used for transmitted light microscopy and photomicrographs.....	28
Figure 14: Diagram of the process behind generating and focusing the beam of a Scanning Electron Microscope from Perdue.edu.....	29
Figure 15: Diagram of production of x-rays and ejected electrons when using SEM from projects.exeter.ac.uk.....	30
Figure 16: Updated bedrock geologic map and cross section of the Mt. Dartmouth 7.5' quadrangle from Xiao (2015).....	33
Figure 17: Map of the spatial distribution of the variety of foliation intensities in the Mt. Dartmouth 7.5' quadrangle, modified from Xiao (2015).....	34
Figure 18: Sample mineralogies plotted on a QAP diagram, from Nesse (2012).....	35
Figure 19: Sample 175: Hand specimen photo, photomicrographs of dextral S-C fabrics and crenulations.....	36
Figure 20: Photomicrographs of sinistrally sheared quartz vein of Sample 175.....	37
Figure 21: Sample 105: Hand specimen photo, photomicrographs of weakly-developed foliation.....	39
Figure 22: Sample 132: Hand specimen photo, photomicrographs of dextral S-C fabrics, and of well-developed foliation.....	41

Figure 23: Sample 138: Hand specimen photo, photomicrographs of dextral S-C fabrics and medium-well-developed foliation.....	42
Figure 24: Sample 189: Hand specimen photo, photomicrographs of very weakly-developed Foliation.....	43
Figure 25: Sample 52: Hand specimen photo, photomicrographs of amphibolite fabric.....	44
Figure 26: Stereographic projections of the foliation of the Jefferson Dome, and steeply dipping foliations.....	46
Figure 27: Stereographic projection showing Cylindrical Best Fit test, the two limbs of the Jefferson Dome, and the axial trace of the Jefferson Dome.....	47
Figure 28: Photomicrograph of quartz vein obliquely cutting foliation plane in Sample 175.....	48
Figure 29: Outcrop photo of crenulations observed on Appleby Mountain.....	49
Figure 30: Possible explanation for the development of vertical planes of weakness along the axial trace of the Jefferson Dome.....	55
Figure 31: Three stages of deformation the Jefferson Dome has experienced.....	57
Figure 32: Map showing Location of the Ammonoosuc Fault and Northey Hill fault in relation to the Mt. Dartmouth 7.5' quadrangle from Roden-Tice et al. (2009).....	58

TABLE OF TABLES

Table 1: Unit name correlations between Billings et al. (1946) and Lyons et al. (1997).....	12
---	----

Introduction

Overview

The high summits of the Northern Appalachian Mountains and their lower associated ranges have attracted mountaineers, hikers, and nature-lovers to New Hampshire since the 1600s. Today the Appalachian peaks of New Hampshire are frequented by hundreds of thousands every year (MWOB, 2014), as the lower peaks of the Mt. Dartmouth Range lay in the shadows of Mounts Washington, Jefferson, and Madison. Variations in tectonic terranes from North to South have lead to the development of unique tectonic theories for each region and thus the mountain chain has been partitioned into two subdivisions, the Northern and Southern Appalachians (Fig. 1) (Hibbard et al., 2010). The Presidential and Dartmouth Ranges form part of the Northern Appalachians. The tectonic study of the Northern Appalachians will provide further insight to the tectonic history of North America. The purpose of this study is to gain a better understanding of the tectonic history of the Oliverian Domes, located along the Bronson Hill Anticlinorium (Fig. 2), by performing a mineralogical and structural analysis on the Jefferson Dome located in the Mt. Dartmouth 7.5' quadrangle of New Hampshire (Fig. 3).

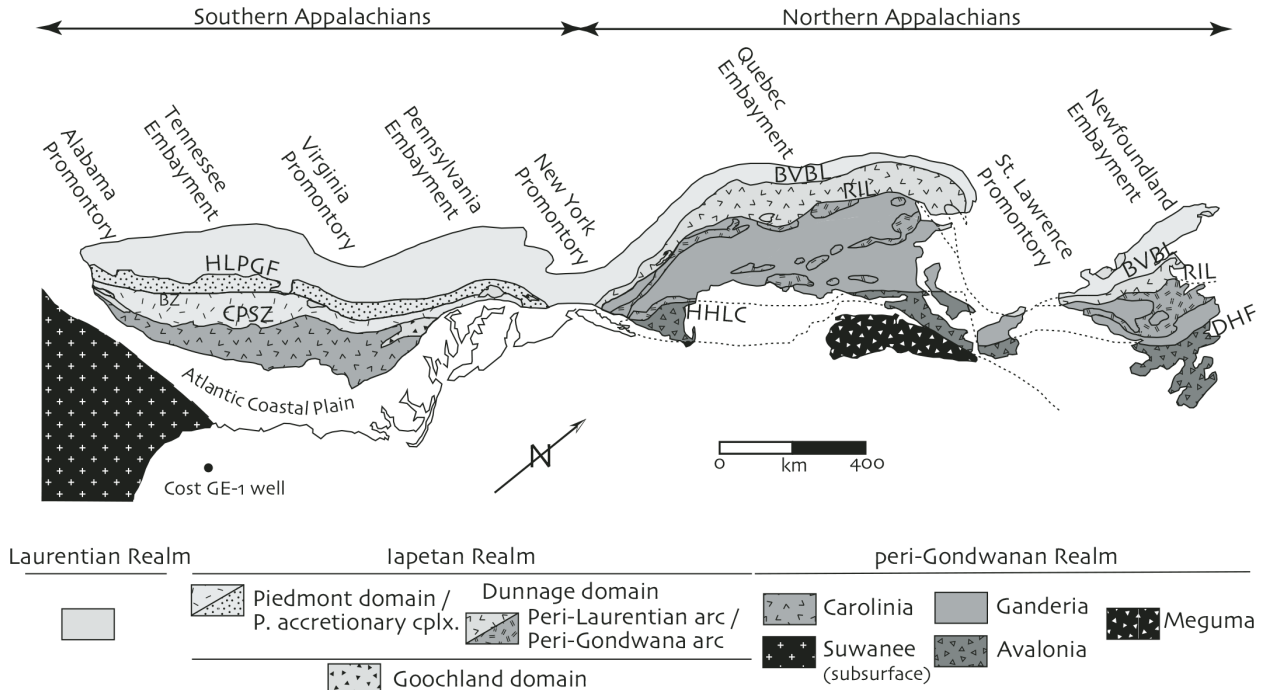


Figure 1. The lithotectonic units of the Appalachian Mountains as discerned by Hibbard et al. (2010). Variation in terranes generated the division between the Southern and Northern Appalachians, marked by the New York Promontory (Hibbard et al., 2010).

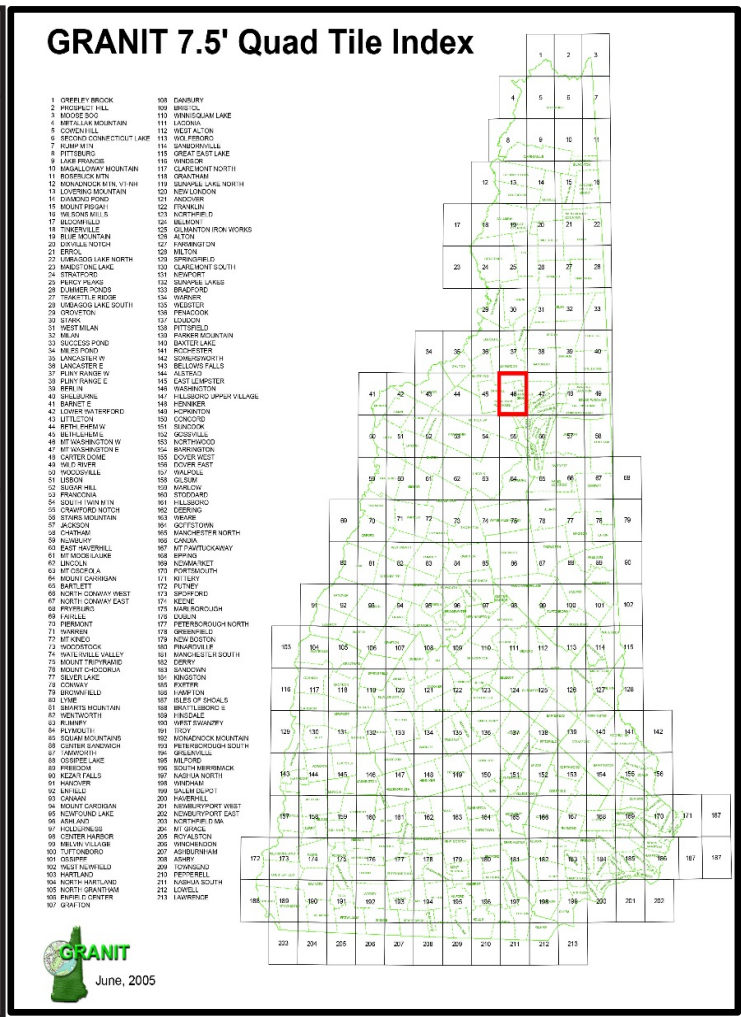
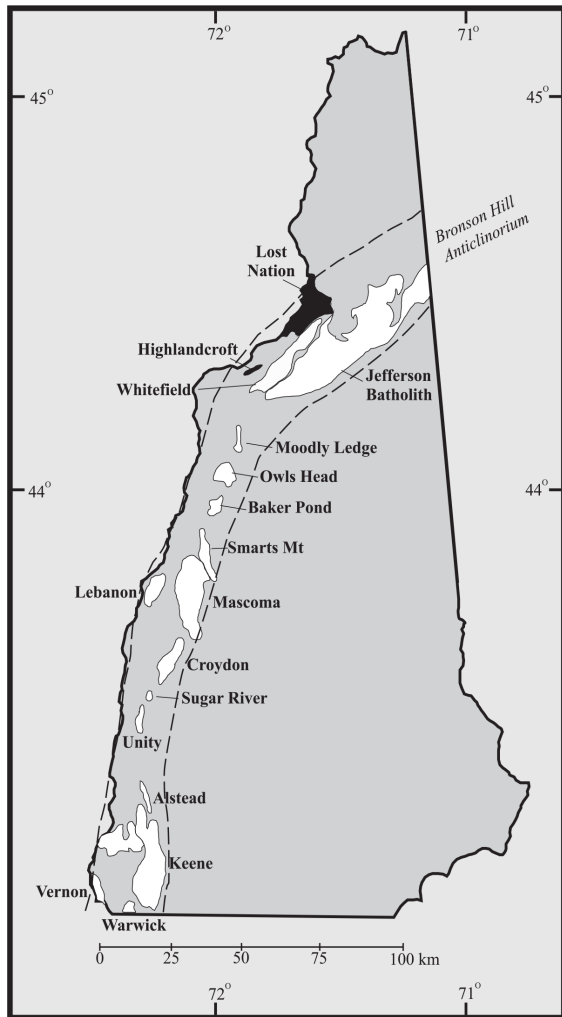


Figure 2 (left). Map of New Hampshire depicting locations of Oliverian Domes (white) along Bronson Hill Anticlinorium (Dorais et al., 2008). The Jefferson Dome, also known as the Jefferson Batholith, is the northernmost Oliverian Dome. Study area outlined in red.

Figure 3 (right). 7.5' Quadrangle map of New Hampshire. Mt. Dartmouth 7.5' quadrangle outlined in red (Modified from: Granit.com).

The complex accretionary orogenic history of the Northeast can be detailed by analyses of the igneous and metamorphic rocks of the region. The paleo-continent Laurentia and the terranes that accreted to its margins during the Paleozoic form present-day North America. When

Laurentia and Gondwana rifted from the supercontinent Rodinia 750Ma, the two paleocontinents became separated by the Iapetus and Rheic Oceans, which themselves were separated by island arcs and microterranes that had rifted from either continent. The previously passive Laurentian margin developed into a subduction zone (500 Ma) and the Iapetus began to close. Over the next 240 million years, as oceanic crust continued to subduct beneath the Laurentian margin, terranes accreted to the Laurentian margin over the course of several orogenies: the Ordovician Taconic, the Silurian Salinic, the Devonian Acadian, the Devonian to Carboniferous Neoacadian, and finally, ending with the Permian Alleghanian marked by the joining of Gondwana and Laurentia to form Pangea (Eusden et al., 2013; Hibbard et al., 2010; Hatcher, 2010).

The Bronson Hill terrane accreted to the Laurentian margin during the third phase of the Taconic orogeny (Moench and Aleinikoff, 2003; van Staal et al., 2009). The volcanism in the terrane produced magma chambers which now outcrop along the axis of the Bronson Hill Anticlinorium (Fig. 2) (Dorais et al., 2008). The anticlinorium extends 430 km south from northern New Hampshire to Long Island Sound, exposing the domes, their associated volcanic suite the Ammonoosuc Volcanics, and other Silurian and Devonian sedimentary rocks metamorphosed and deformed by the Acadian (Leo, 1991). The chain of twenty or so magma chambers compose what was called the Oliverian Magma Series by Billings et al. (1946), now the Oliverian Plutonic Suite (Lyons et al., 1997). Most of the Oliverian domes are composed of calc-alkaline granites, while a few are composed of trondjhemites chemically related to the Ammonoosuc Volcanics.

The Ammonoosuc Volcanics are found mantling, or on the surrounding flanks of, the Oliverian domes (Leo, 1991). The emplacement of the Ammonoosuc Volcanics (461 ± 8 Ma) over the Oliverian plutons (Jefferson Dome: 454 ± 5 Ma) (Moench and Aleinikoff, 2003) is still debated. The emplacement of the Oliverian domes into the Ammonoosuc Volcanics was a result differences in density between the Oliverian magma chambers and the overlying Ammonoosuc Volcanics that resulted in the diapiric rising of the domes during the Acadian orogeny. However, this doming process and the overall deformation history of the Oliverian domes is not yet clearly understood.

The purpose of this study is to investigate the deformation history of the Jefferson Dome, also known as the Jefferson Batholith, in an effort to detail the emplacement and deformation history of the Jefferson Dome. Detailed knowledge of the domes' deformation will provide a better understanding of the tectonic forces that have affected the surrounding region. The foliation of the Jefferson Dome rocks will help decipher the deformation history. Uncertainty exists around the origin of the foliation and whether it is related to the doming process or another deformational event. In this study, a mineralogical and structural analysis was conducted on the center third of the Jefferson Dome located in the Mt. Dartmouth 7.5' Quadrangle of New Hampshire (Fig. 3). The mineralogical analysis was conducted using optical identification and scanning electron microscopy-electron dispersive spectroscopy (SEM-EDS). The structural analysis was conducted using maps, cross sections, stereographic projections of foliation data, as well as microstructure analysis using thin sections in effort to relate the structure of the foliation to the tectonic history of the Jefferson Dome.

Study Area

This study was conducted in the Mt. Dartmouth 7.5' quadrangle of New Hampshire (Fig. 3), previously named the Mt. Washington East 7.5' quadrangle. The quadrangle is located to the east of Carroll, New Hampshire, and southwest of Randolph, New Hampshire. The Mt. Dartmouth 7.5' quadrangle is located in the southeastern flanks of Mt. Washington, featuring the lesser known Mt. Dartmouth Range to the southwest, and Cherry Mountain on the western boundary.

Previous Mapping

The study area was last mapped in the 1940s by Billings et al. (1946, Fig. 4). Billings et al. divided the dome rocks found in the quadrangle into three classifications: porphyritic biotite-quartz monzonite (pbqm), biotite-quartz monzonite (bqm), and coarse granite (cog). In 1997, the United States Geological Survey (USGS) published an updated bedrock map of New Hampshire (Lyons et al., 1997) using the unit contacts of Billings et al. (1946, Fig. 5). The USGS correlated the rock names created by Billings et al. (1946) with similar rocks from the domes of the Oliverian Plutonic Suite (Table 1).

Lyons et al. (1997) remapped the Ammonoosuc Volcanics of the quad as metavolcanic and metasedimentary rocks of the lower part of the Ammonoosuc Volcanics (Oal) (Lyons et al., 1997).

Table 1 . Lyons et al. (1997) rock units correlated to those of Billings et al. (1946)

Billings et al., 1946	Lyons et al., 1997
sy	J7h, Cherry Mountain Syenite
cg	J71h, Conway Granite
Dlg	Sr, Rangeley Formation
big	D1m, Bretton Woods Granite
Oam	Oal, Ammonoosuc Volcanics
bqm	Oo1b, Oliverian Dome, biotite bearing
cog	Oo1h, Oliverian Dome, hornblende bearing
pbqm	Oo1bx, Oliverian Dome, coarse-grained, biotite bearing

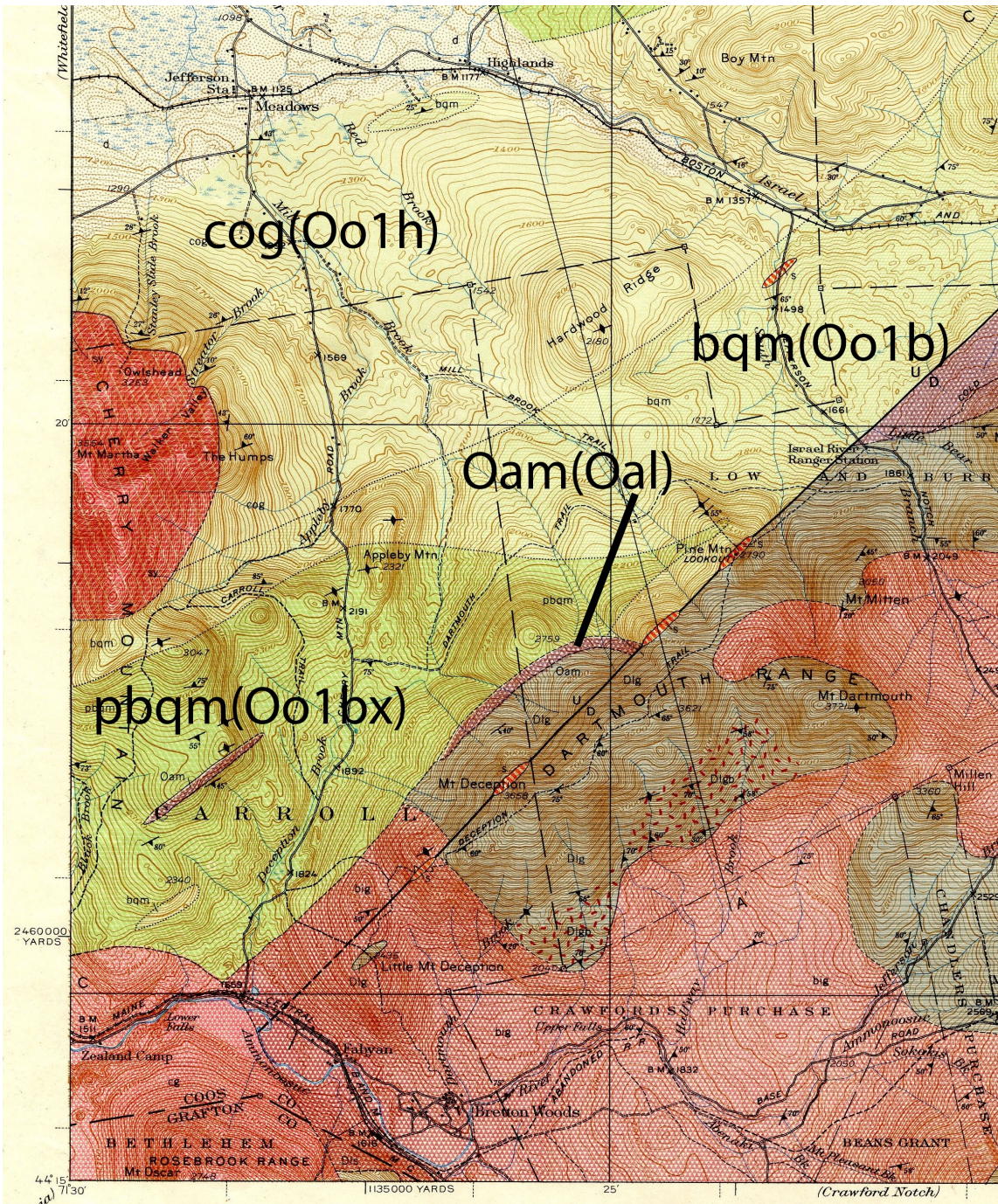


Figure 4. Billings et al. (1946) geologic bedrock map of Mt. Dartmouth 7.5' quadrangle. Oliverian dome rocks: Porphyritic biotite quartz monzonite (pbqm) shown in green; Biotite quartz monzonite (bqm) shown as yellow unit above pbqm; Coarse granite (cog) shown as yellow unit above bqm. The unit contacts have been appropriated by Lyons et al. (1997) on the current bedrock map of New Hampshire. The Lyons et al. (1997) correlative unit names are pictured in parentheses. Modified from Billings et al. (1946).

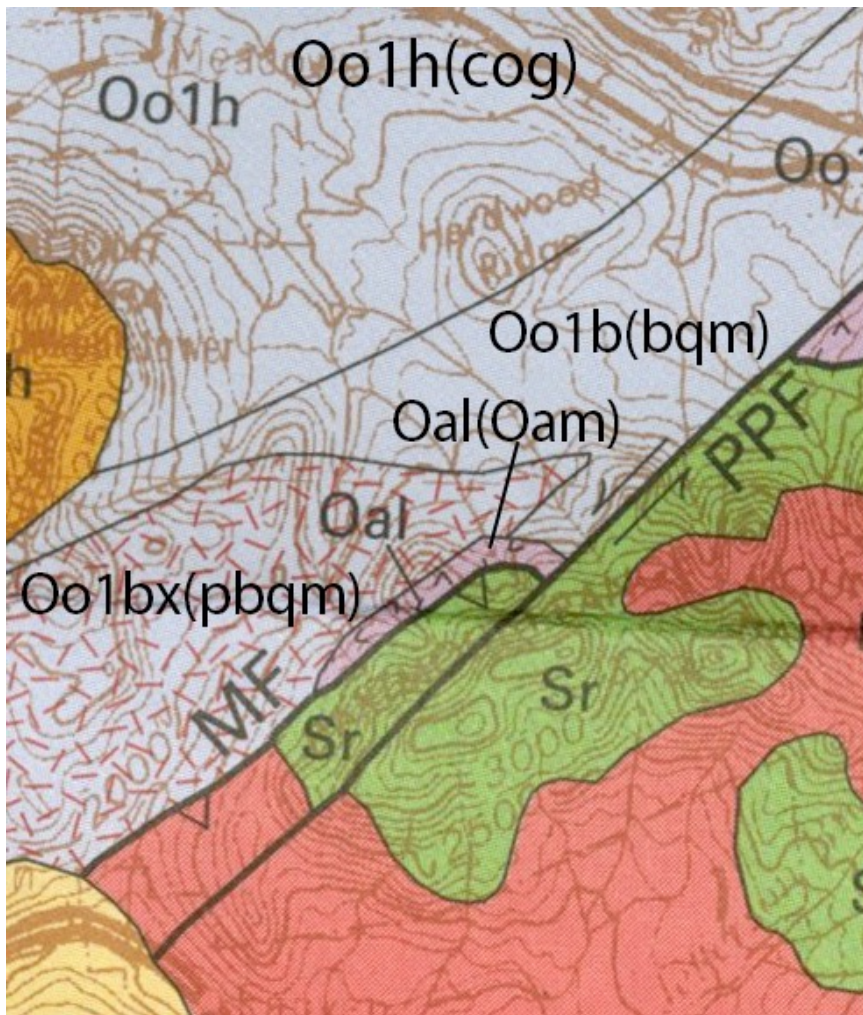


Figure 5. Appropriated Billings et al. (1946) bedrock map of Mt. Dartmouth 7.5' Quadrangle as appears on Lyons et al., (1997) map. Unit contacts have not changed between the two versions of the map, however the unit names and associated colors have changed. The Lyons et al. (1997) unit abbreviations are as follows: moderately to weakly foliated (Oo1b), porphyritic alkali feldspar biotite granite (Oo1bx), hornblende-biotite granite (Oo1h), amphibolite (Oal). The Billings et al. (1946) unit abbreviations are in parentheses (modified from Lyons et al., 1997).

Tectonic History of the Northern Appalachians

The formation and emplacement of the Oliverian Domes is just one piece of the puzzle in the grand accretionary history of the Laurentian margin. The number of existing hypothesis on its tectonic development indicates how highly complex the process was and the struggle to clearly decipher the history today.

The Appalachian mountain chain is a result of a full Wilson cycle, from the rifting of supercontinent Rodinia to the coalescence of all continents to form Pangea (Hatcher, 2010). The supercontinent Rodinia rifted and eventually formed Laurentia and Gondwana around 750Ma (Hatcher, 2010). The two newly formed continents were separated by the Iapetus ocean, there

within existed Laurentian and Gondwanan derived terranes which will later become involved in the accretionary development of the Laurentian margin. The accretionary history of the east coast of modern day North America can be divided into five orogenic events following the rifting of Rodinia: the three phases of the Taconic orogeny, the Salinic orogeny, the Acadian orogeny, the Neoacadian orogeny, and lastly the Alleghanian orogeny.

The orogenesis of the Northern Appalachians began with the Taconic Orogeny (495 Ma). The Taconic orogeny can be loosely defined as beginning with the accretion of peri-Laurentian terranes and ends with the collision of the first peri-Gondwanan terrane, the Popelogan-Victoria Arc. The Taconic orogenic events were preceded with the rifting of the Dashwoods terrane from Laurentia ~550 to 555 Ma. A small ocean basin, the Taconic or Humber seaway, separated Dashwoods from its mother continent (van Staal, 2005; van Staal et al., 2009).

During **Taconic 1** (495 Ma), the eastern edge of the Dashwoods developed an eastern-dipping subduction zone which lead to the west-directed obduction of the Lushs Bight oceanic tract onto the Dashwoods terrane (Fig. 6; van Staal et al., 2009). The Lushs Bight oceanic tract formed due to rapid hinge retreat of the eastern dipping subduction zone. During **Taconic 2**, the Humber margin developed into an eastern-dipping subduction zone (van Staal et al., 2009; Macdonald et al., 2014) and closed the Taconic Seaway, causing the collision of Dashwoods into Laurentia during the Middle Arenigian (475 Ma) (Fig. 6, Fig. 7; van Staal et al., 2009; Waldron and van Staal, 2001). The eastern dipping subduction zone generated the peri-Laurentian Notre Dame Arc possibly as early as 502 Ma. Peak igneous activity of the Notre Dame arc occurred after its accretion to Laurentia at 475 as the Shelburne Falls arc (van Staal et al., 2009; Macdonald et al., 2014). The collision of the Notre Dame arc with Laurentia is believed to have slowed down the convergence and initiated a western-dipping subduction zone, from which the Annieopsquotch ophiolite belt was generated (Fig. 6b). Annieopsquotch ophiolite belt was eastwardly obducted onto the Notre Dame Arc and formed the Late Arenig Annieopsquotch oceanic tract (480-464 Ma) (Fig. 6b). The addition of a westward-dipping subduction zone caused Molluca Sea style subduction and lead to the Late Ordovician (460-450 Ma) arc-arc

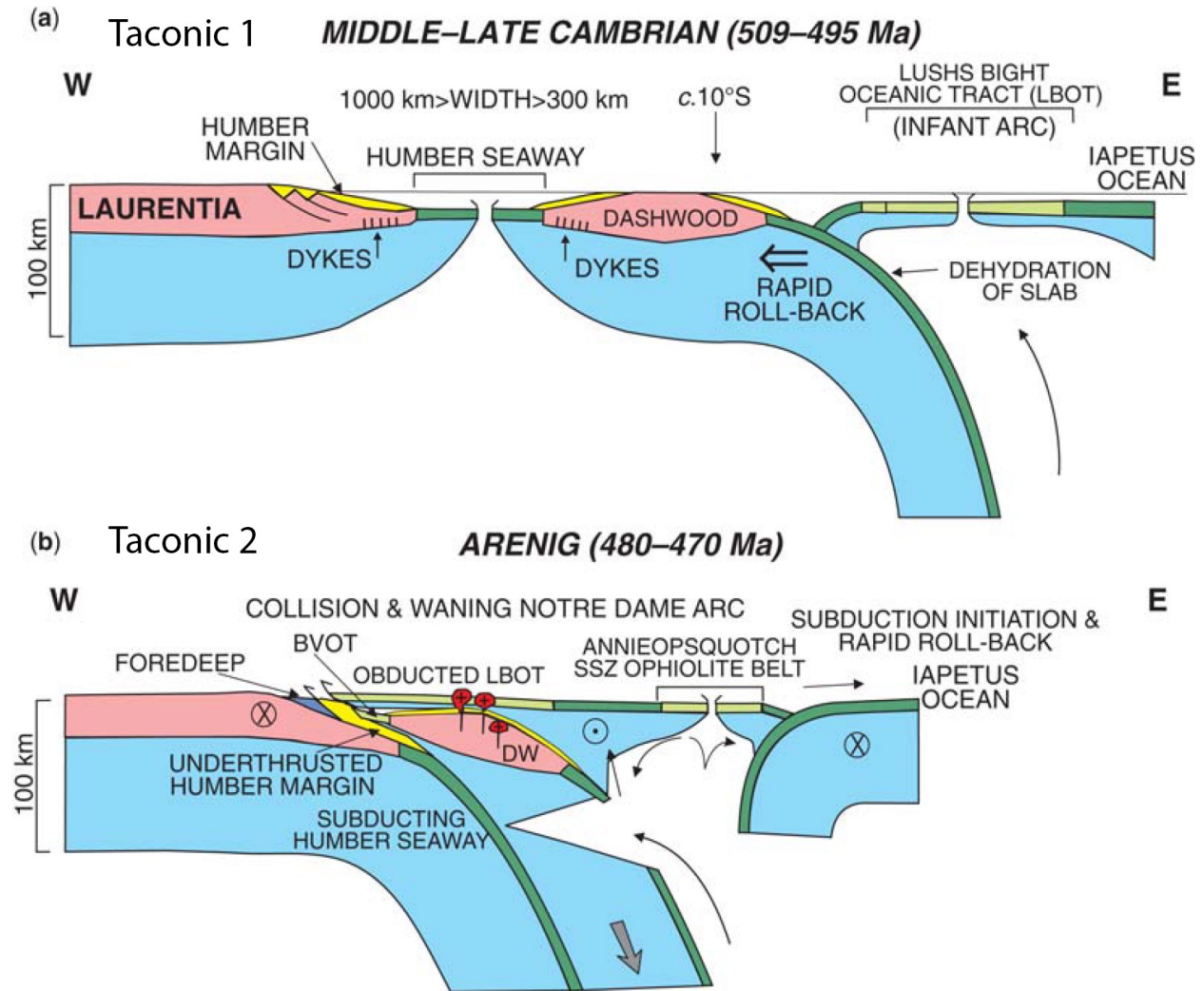
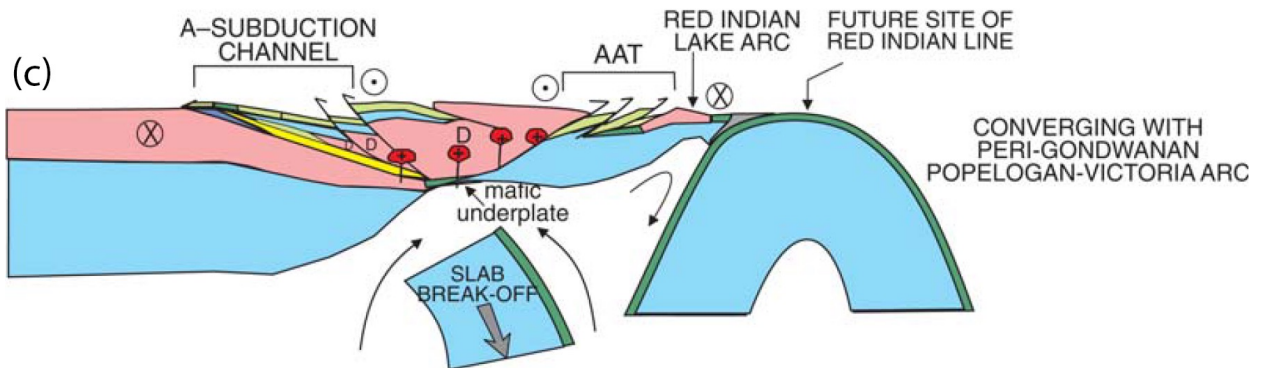


Figure 6. Tectonic model of the first and second phase of the Taconic orogeny by van Staal et al. (2009). a) Taconic 1: Initiation of eastern-dipping subduction zone off the eastern edge of Dashwoods. Rapid hinge retreat of subducting slab creates the Lushs Bight oceanic tract (LBOT). b) Subduction zone retreats into the Humber Seaway and the Baie Vert oceanic tract (BVOT) and Notre Dame arc (Shelburne Falls arc) develop. The Notre Dame Arc collides with Laurentia in the Taconic 2 arc-continent collision. The collision is believed to have slowed down convergence and as a result, the westward directed subduction zone outboard of Dashwoods. The development of the western-dipping subduction zone resulted in the formation of the Annieopsquotch Ophiolite Belt (AOB). (Modified slightly from van Staal et al., 2009).

collision of the Popelogan-Victoria Arc with the Notre Dame arc during **Taconic 3** (Fig. 7d) (van Staal et al., 2009). The western edge of Ganderia, the Popelogan-Victoria arc, is also known

Taconic 2 **LATE ARENIG–CARADOC (470–460 Ma)**



Taconic 3

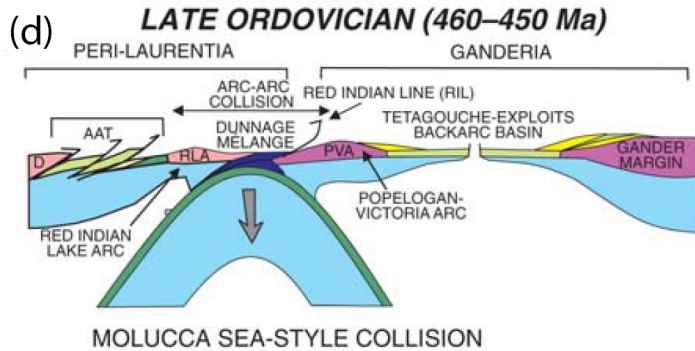


Figure 7. (c) End of Taconic 2 with the complete collision of Dashwoods with the Humber margin. Annieopsquotch ophiolite belt was thrust westward as a result and formed the Annieopsquotch oceanic tract (AAT). The western dipping subduction zone created a Molucca Sea-style subduction zone. (d) Taconic 3 occurred when the leading Ganderian edge, the Popelogan-Victoria arc (PVA), also known as the Bronson Hill Arc, collided with the Laurentian margin. (Modified slightly from van Staal et al., 2009).

as the Ammonoosuc-Popelogan arc (Reusch and van Staal, 2011). The collision of the Popelogan-Victoria arc stimulated the growth of the Bronson Hill arc along the Laurentian margin (Macdonald et al., 2014) during the Mid-Ordovician (Moench and Aleinikoff, 2003).

Following the Taconic orogeny is the Silurian Salinic orogeny. The Salinic orogeny (420–423 Ma) marks the collision of East-Ganderia and Laurentia. Ganderia was divided into West-Ganderia and East-Ganderia, separated by the Tetagouche-Exploits basin. After the western half

of Ganderia, the Popelogan-Victoria arc, accreted to Laurentia, its trailing edge, East Ganderia, followed (van Staal et al., 2009; Hibbard et al., 2010). There is little evidence of the Salinic orogeny except for Silurian metasedimentary rocks and faint structures exist (Eusden, 2015; Eusden, 2010).

The Acadian and Neoacadian orogenies followed the Salinic orogeny. The Acadian and Neoacadian orogenies began in the Late Devonian, around 410 Ma, and ended in the early Mississippian, around 345 Ma. These orogenies describe the north to south zippering of the Laurentian margin during the closing of the Rheic ocean, the ocean that separated Gander and Avalon, colliding Avalon with the Laurentian margin (Hatcher, 2010). The Acadian orogeny affected New England, and north into New Brunswick and Nova Scotia. The Neoacadian orogeny affected New England southward into the Southern Appalachians (Hatcher, 2010).

Evidence of the Devonian-Mississippian Acadian and Neoacadian orogenies can be divided into four or five deformational events (Robinson et al., 1998; Eusden et al., 1996). D0 is characterized by pre-metamorphic normal faulting from the Salinic orogeny, responsible for the development of the Moose River and Mahoosuc faults (Eusden et al., 2006; Eusden et al., 2000). Events D1 through D4 are believed to occur during the Acadian orogeny. D1, the first ductile event that produced eastern directed nappes (Eusden et al., 1996). The second event, D2, as evidenced with the Snyder Brook fault, is a thrusting event, possibly the reversal of pre-existing normal faults. D3 and D4 are late folding events that fold previous fabrics and occur post-peak metamorphism. The final event D5, possibly Neoacadian, is the doming of the Oliverian Domes, including the Jefferson Dome (Eusden et al., 2006; Eusden et al., 2009)

The final stage of the Wilson cycle was the Pennsylvanian-Permian Alleghanian orogeny, the rejoining of Laurentia and Gondwana as the Theic ocean closed (Hatcher, 2010). Hatcher (2010) proposes a rotational transpressive model for the Alleghanian orogeny. The Alleghanian marked the final orogenic event that affected the formation of the Appalachians (Hatcher, 2010; van Staal et al., 2009; Hibbard et al., 2010).

Tectonic Models: Bronson Hill Arc

Many tectonic models exist in attempt to explain the complex tectonic history of North America. In the following section, several popular models are outlined.

Moench and Aleinikoff (2003) proposed a three terrane model for the development of the Bronson Hill arc (Fig. 8). In this model, Terrane 1 (T1) includes the St. Daniel Formation mélangé and the Chain Lakes Massif. T1 is attached to T2. During the Early-Mid Ordovician, T1+T2 collided with Laurentia with the closing of a small oceanic tract found between T1+T2 and Laurentia. T1+T2 are considered peri-Laurentian terranes and together form what is known as the Notre Dame terrane. During the Late Ordovician, T3, the Exploits-Gander terrane, collided with Laurentia as the Iapetus subducted beneath Laurentia. With this collision, the Oliverian plutonic suite developed alongside the Highlandcroft plutonic series. The T3 terrane shows the Popelogan arc to the Northwest separated from Gander by the Tetagouche backarc basin (equivalent to the Tetagouche-Exploits basin, van Staal et al., 2009). The Oliverian domes and the Ammonoosuc Volcanics are considered to be part of T3 because of their formation with the collision of T3 into T1+T2 (Moench and Aleinikoff, 2003). From this model, Moench and Aleinikoff propose that the Oliverian domes were not deposited into T2 until the collision of the Exploits-Gander terrane 458Ma into Laurentia (Fig. 8). Based on uranium-lead zircon dating, the Ammonoosuc Volcanics are found to be slightly older than the Oliverian Domes, suggesting their deposition precedes the formation of the Oliverian Domes. This suggests bimodal magma development, with the Ammonoosucs developing first as a result of partial melting, followed by the Oliverian magma from crustal melting (Moench and Aleinikoff, 2003).

Karabinos et al. (1998) proposed that the Bronson Hill arc formed as a volcanic arc to a west-dipping subduction zone and then collided with Laurentia (Fig. 9). Karabinos et al. propose that the Shelburne falls arc developed on a piece of continental crust that rifted from Laurentia and were separated by a small ocean basin the Neo-Iapetus. Van Staal et al. (2009) interpret this continental fragment as the Dashwoods terrane, and the margin between Laurentia and the Neo-Iapetus is the Humber passive margin. Due to similarities between metasedimentary rocks east of the Bronson Hill Arc, Karabinos et al. suggest a west-dipping subduction zone developed and the Bronson Hill arc formed as the associated volcanic arc (Fig. 9). This resulted in the Dashwoods

terrane to dock back onto Laurentia, and eventually, due to crustal shortening, the Bronson Hill arc collided with Laurentia.

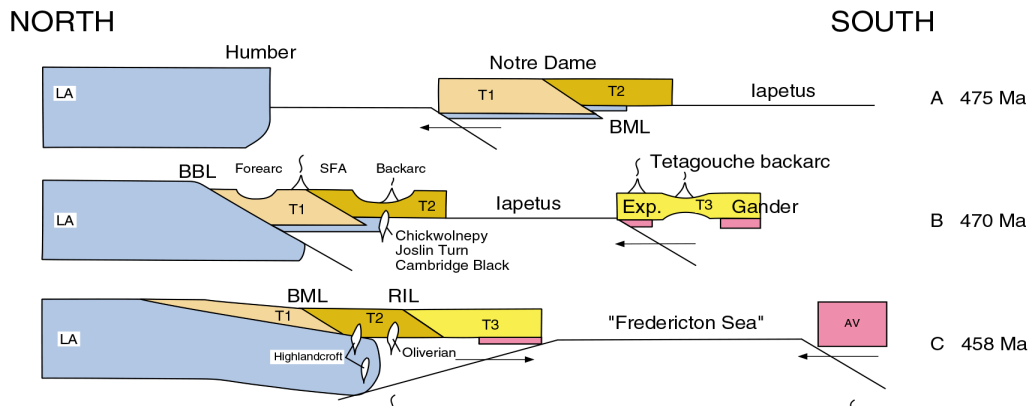


Figure 8 (above). Tectonic model of the Taconic orogeny by Moench and Aleinikoff (2003). T1 is equivalent to the Chain Lakes massif, also known as the Dashwoods terrane. T2 is equivalent to the Notre Dame arc. T3 is equivalent to Ganderia. A) Taconic 1: The collision of Dashwoods (T1) and Notre Dame arc (T2). B) West ganderia (equivalent to the Popelogan-Victoria arc) and East Ganderia, separated by the Tetagouche backarc (equivalent to the Tetagouche-Exploits basin) approach the Laurentian margin. C) Taconic 2 and 3: The collision of west ganderia (T3), the closure of the Tetagouche backarc, and the subsequent collision of east ganderia (T3). The collision of Gander with Laurentia generates the Oliverian Plutons (the Bronson Hill arc) (Modified slightly from Moench and Aleinikoff, 2003).

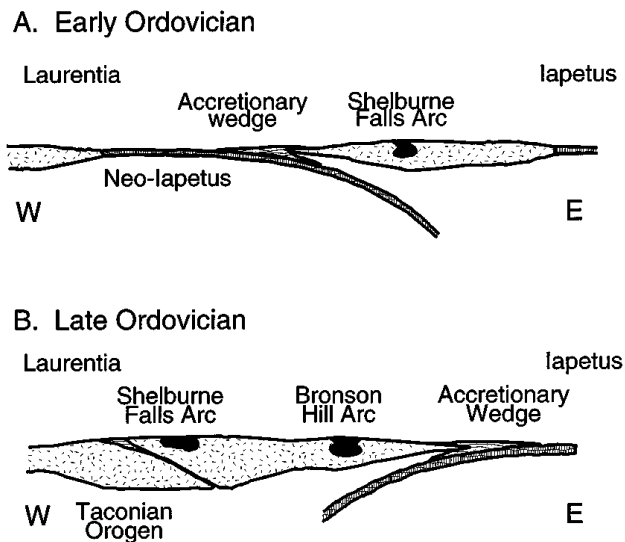


Figure 9 (left). Tectonic model by Karabinos et al. (1998) illustrating the development of the Bronson Hill arc. A) The Shelburne Falls arc forms as a result of an east-dipping subduction zone that then accretes to the Laurentian margin during the Late Ordovician with the subduction reversal. B) The Bronson Hill arc forms as a result of slab-subduction reversal from eastern-dipping to western-dipping.

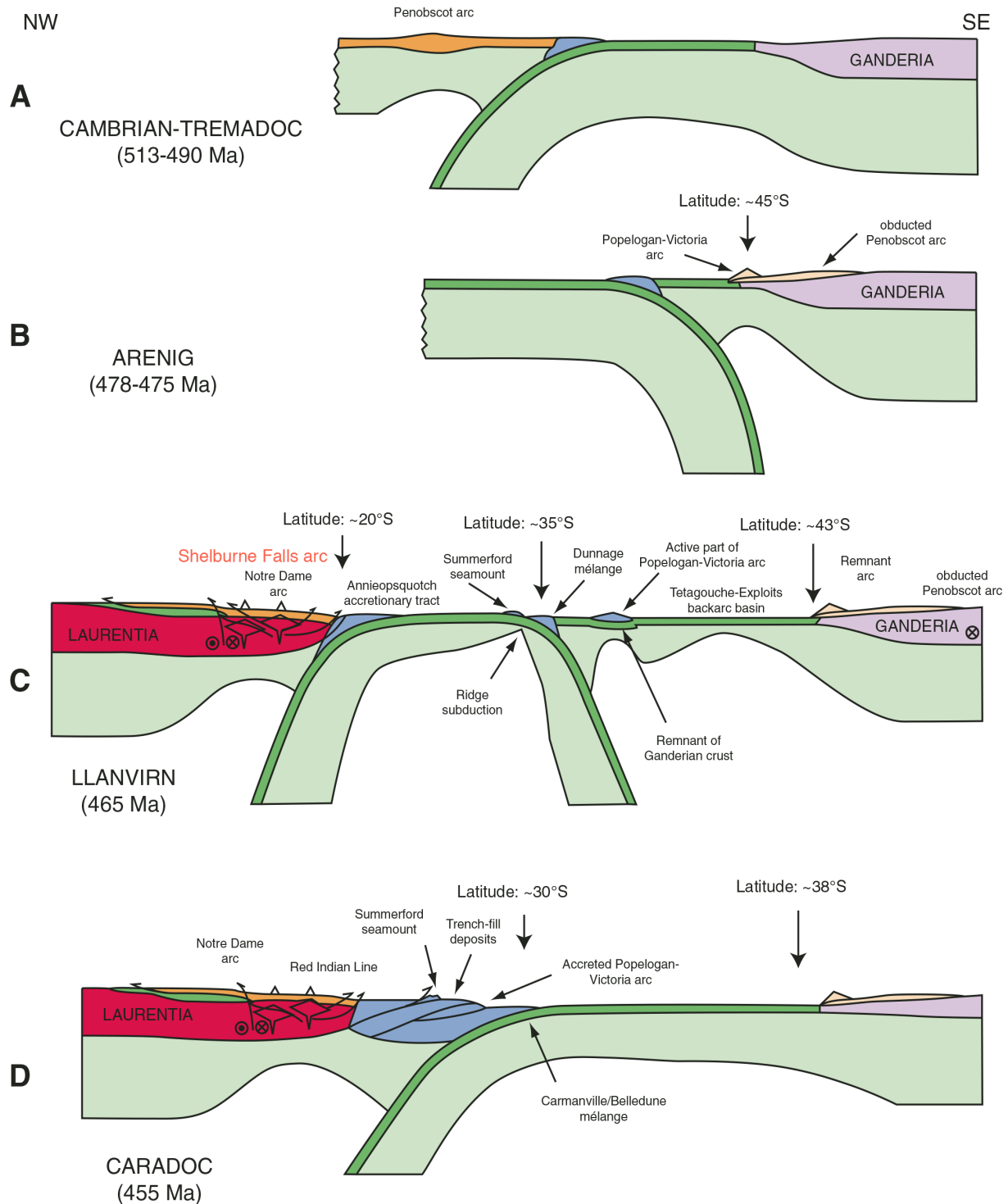


Figure 10. Tectonic model of the Taconic orogeny by Hatcher (2010). A) The Iapetus ocean separating the Laurentian margin (Penobscot arc) and Ganderia. B) The rifting of the Popelogan-Victoria arc from Ganderia. C) The Molluca Sea-style subduction zone and the formation of the Notre Dame arc (also known as the Shelburne Falls arc). D) The succession of slab subduction, ultimately resulting in a dormant east-dipping slab and a dominant west-dipping slab.

Hatcher (2010) proposed that the Bronson Hill arc occurs after the accretion of the Popelogan-Victoria Arc. Hatcher illustrates the employment of both a west-dipping subduction zone and an east-dipping subduction zone (Fig. 10) between Laurentia and Gander, similar to the tectonic model of van Staal et al. (2009; Fig. 6, Fig. 7). During the mid-Ordovician both of these subduction zones were active until the subduction of their spreading ridge. The east-dipping subduction zone was then subducted beneath Laurentia via the west-dipping subduction zone (Fig. 7d) and the Popelogan-Victoria arc accreted by 455Ma (Hatcher, 2010).

The Popelogan-Victoria arc referenced by Macdonald et al. (2014) (Fig. 11) and Hatcher (2010) is equivalent to T3 referenced by Moench and Aleinikoff (2003) (Fig. 8). To synthesize, the final phase of the Taconic Orogeny is marked by the collision of T3, or the Popelogan-Victoria arc, or west Ganderia, with the eastern Laurentian margin during the Ordovician. The collision of western Ganderia resulted in the magmatism that formed the Bronson Hill Arc and the Oliverian Domes. The method of collision is due to the ultimately west-dipping subduction

zone along the eastern Laurentian margin, after the east-dipping subduction zone becomes inactive and subducts beneath Laurentia via the west-dipping subduction zone.

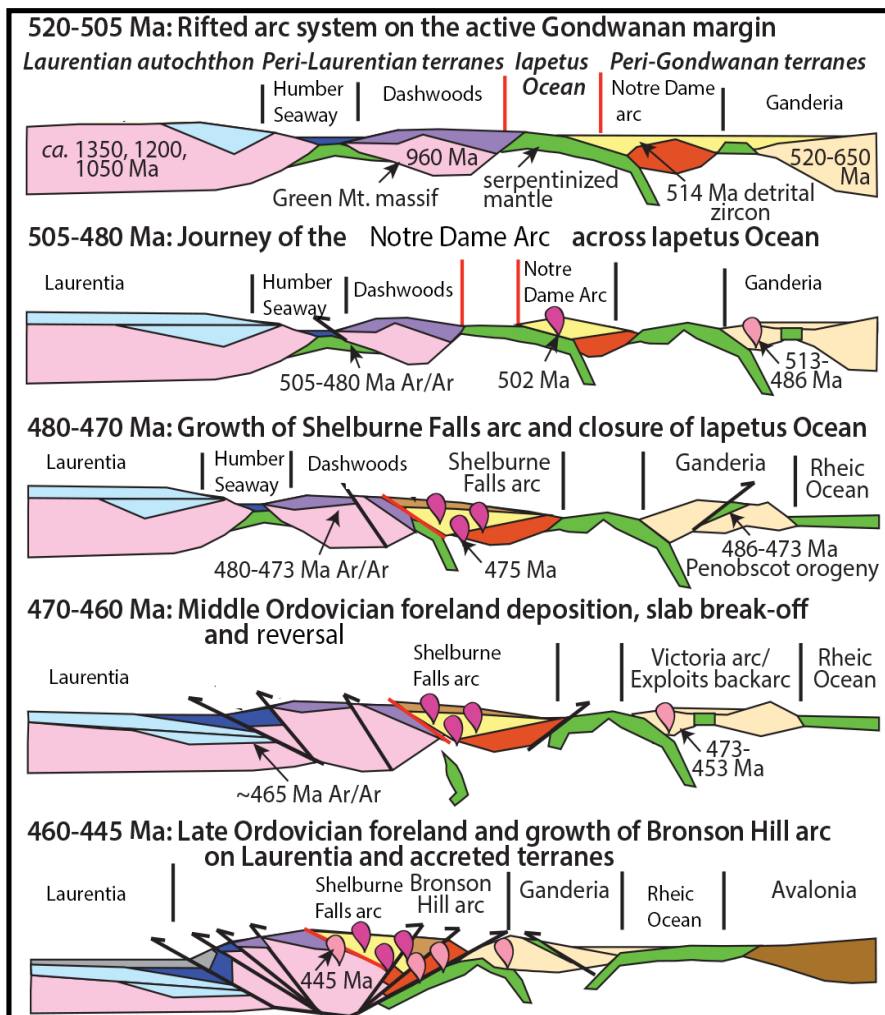


Figure 11. Tectonic model of the Taconic orogeny by Macdonald et al. (2014) demonstrating a similar theory to that of van Staal et al. (2009) and Hatcher (2010). (Modified from Macdonald et al., 2014).

Doming Theories

The formation of the Oliverian plutons is a two-stage process. Leo (1991) begins with formation of the plutons during the Late Ordovician, and ending with the rising of the plutons through the crust. The bimodality of the magma to produce the tholeiitic Ammonoosuc volcanics and the calc-alkaline plutons is proposed to be due to two different magma sources. Partial melting of the down-going ocean slab is proposed as the source of the Ammonoosuc Volcanics. Contact melting with the continental crust is proposed as the source of the calc-alkaline Oliverian plutons (Leo, 1991).

The formation of the plutons predates their doming, or uprising through the crust. A long-standing theory is that the rising of the plutons was most likely a result of two factors: the deformational forces from the Acadian Orogeny, and the density difference between the plutons and the overlying rocks, including the Ammonoosuc Volcanics (Leo, 1991; Lyons et al., 1996).

Foley (2009) suggests a faulted relationship between the Ammonoosuc Volcanics and the Oliverian Dome rocks such as the pbqm, bqm, and cog (Billings et al., 1947) which are now referred to as Oo1bx, Oo1b, and Oo1h (Table 1) (Lyons et al., 1997), is responsible for the intercalation of the units. Though strong evidence to support either an intrusive or a faulted contact is lacking, Foley uses the presence of structural fabrics to support a sheared, faulted contact. Foley proposes that the increase in intensity of structural fabrics in both units as proximity to their contact increased is most likely due to faulted-related shearing. For this reason, Foley suggests a faulted contact between the Ammonoosucs and Obqm. Foley proposes Acadian thrusting (Kohn and Spear, 1999) as a possible mechanism for the fault contact. Listric normal faults are also proposed mechanisms for the intercalation of the units.

Kinematic indicators observed supported deformation due to doming as well as deformation that predates doming. Near the contact between the Ammonoosuc Volcanics and the Jefferson Dome rocks, S-C mylonites showing both normal and reverse motion have been observed (Eusden et al., 2009). Normal fabrics in the Ammonoosucs support doming-related shearing, and reverse fabrics in the Jefferson Dome rocks support pre-doming deformation. Foley proposes the shear zone was a normal fault later reversed by doming. Eusden et al. (2009) have named the late Acadian, normal sense shear zone to be the Moose River fault.

Dupee (2002) identified several shear zones in his study area. He suggests the motion of the Mahoosuc Fault is responsible for the many shear zones identified in his study area as well as the removal of units from the stratigraphy. The mylonite shear zones at Memorial Bridge all show thrust faulting (Dupee, 2002).

Several theories attempt to explain the contact between the Ammonoosuc Volcanics and the Jefferson Dome rocks. Schumacher (1988) observed the Ammonoosuc volcanics conformably overlie the Oliverian Dome at the Quabbin Reservoir in Massachusetts, whereas Foley (2009) identified a shear zone, or normal fault, between the Ammonoosuc Volcanics and the Jefferson Dome rocks. The contact relationship between these the Jefferson Dome and the overlying Ammonoosuc Volcanics is key to understanding the emplacement of the dome, the relationship between the two units, and its deformation history.

Foliation in the field

The foliation and foliation structures of the Jefferson Dome rocks are indicative of the deformation history of the rock. The mylonites found near the contact between the Ammonoosuc Volcanics and the Jefferson Dome rocks showed shear sense, as well as lineation (Dupee, 2002; Foley, 2009). These mylonites were identified as zones. Hanmer (1981) correlated vertical ductile shear zones with areas of steeply dipping foliation in Newfoundland. Hanmer found foliations trending 015° , 075° , and 035° geometrically corresponded to the R, R', and P of a set of riedel shears from a sinistral shear zone trending 035° . Hanmer proposes the shearing is syntectonic with the plutonism of granitic domes (1981). Steeply-dipping shear structures found within the dome could be possibly vertical ductile shear zones.

Significance of Study

The doming theory of the Oliverian Domes is generally accepted, however indications of tectonic stresses affecting the domes post-doming have not yet been identified. To better understand the overall tectonic stresses that affected the development of the Appalachians, as well as to how far-reaching those stresses were, it is imperative to study the Oliverian Domes for any indications of stress. The purpose of this study is to perform a mineralogical and structural

analysis using the orientation of the entire Jefferson Dome, the orientation of its foliation, the intensity of its foliation, as well as shear indicators, to observe the possibility of tectonic stresses on the Jefferson Dome post doming, and to identify the origin of those deformed structures.

METHODS

Field Mapping Methods

Bedrock mapping of the study area was conducted over a seven-week period during the months of July-August 2014. The study area was 5-10% exposed bedrock, the remaining 95-90% was forest cover or glacial and modern deposits such as till, lake clays, and river alluvium.

As a limited number of trails existed in our study area, bushwhacking was the primary method of locating outcrop. Logging roads, skidoo paths, and old hiking trails as noted in Billings et al. (1946) were also used for traversing. Outcrop was often found in steep changes in slope ranging from 0.5m-10m in height, and was often covered by a layer of forest ground cover that, once removed, revealed bedrock. Significant boulder exposures were also mapped as float. A float stop was only mapped if float blocks were angular (unrounded), greater than 1m in all dimensions, and more than two boulders were found within a 10-20 m radius of each other.

Once an outcrop was located, several fields were recorded as well as a description of the rock unit and outcrop. Notes were recorded in a traditional field notebook as well as a Trimble Juno handheld GPS unit installed with TerraSync software. The Trimble Juno was loaded with a geo-referenced topographic map of the study area. The Trimble Juno was used to save GPS coordinates for each outcrop, as well as to locate outcrops on the topographic map. A printed copy of the topographic map was also carried in the field, and the location of each outcrop from the Trimble Juno would be marked on that map.

A total of 309 outcrop stations were mapped by the end of the field season. At each outcrop station, the fields recorded consisted of structural measurements of fractures and foliations, and lineations and folds, all measured with a Brunton Compass using the Right Hand Rule. Mineralogy and rock type were also recorded. Representative samples were taken from outcrops when possible, with emphasis on obtaining a sample collection representative of the

variety of rock types present in the field area. A GPS location for each float station was recorded, however no fields were measured, and no samples were collected from float blocks.

Laboratory Mapping Methods

Once a week, the data file from the Trimble Juno, which included the GPS station locations as well as digitized record of note fields, was transferred to a Panasonic Toughbook using GPS pathfinder Office, exported as an ESRI Shapefile, and uploaded to ArcGIS 10.1. The Shapefiles for each week were merged to form one master file. From the GPS-logged station locations, each station was plotted onto a sheet of Mylar over the field map using properly oriented strike and dip symbols corresponding to the foliation, joint, or dike data for each station. Float stations lacked structural data and were instead marked with a dot and an “F”. Contacts between rock units were drawn by hand on the Mylar and followed the overall strike of the local foliation. Rock units were differentiated by difference in texture and mineralogy. The placement of contacts was also guided with some reference to the contacts drawn by Billings et al. (1946). The contacts were scanned, uploaded to ArcGIS and its tool Arcscan was used to digitize them (Xiao, 2015).

Twenty-two outcrop locations and associated information (foliation strike and dip) from Billings et al. (1946) were added to the digitized version of the map.

If not done in the field, the foliation intensity of each collected unit sample would be determined using a foliation scale we developed. The scale is as follows: very weakly foliated: mafic minerals exist, no large aggregates and no directional alignment; weakly-foliated: mafic mineral aggregates beginning to form, no directional alignment; medium-foliated: well-formed mafic aggregates forming discontinuous planar fabric showing directional alignment; medium-well-foliated: both discontinuous and continuous planar fabrics of foliation; well-foliated: continuous planes of foliation.

Thin Section Production

Eight thin sections were made from outcrop samples, seven from igneous dome rocks and one of the Ammonoosuc Volcanics. The samples were chosen to represent the range of mineralogy and varied degree of foliation observed in the dome rocks in the field.



The samples were cut to thin section size before being sent to Spectrum Petrographics for finishing. Each sample was first cut using a Diamond Pacific TR-18 Slab Saw (Fig. 12) and then trimmed to thin section size, 27x46 mm, using a Lapidary Trim Saw FS8 from Lortone, Inc. (Fig. 12). Because the thin section analysis was not only a mineralogical analysis but also an analysis of foliation fabric, the thin section face of each sample was cut perpendicular to the planes of foliation, if present, and parallel to lineation, if present, to better evaluate kinematics of the rock. The eight samples were cut to size and sent to Spectrum Petrographics of Vancouver, Washington to be mounted onto slide glass, cut to a thickness of 30 μ m, and polished for the microprobe on one face.

Figure 12. (Top) Diamond Pacific TR-18 Slab Saw used to cut samples to a smaller size; (Bottom) Lortone, Inc. Lapidary Trim Saw FS8 used to trim cut sample to thin section dimensions

Mineralogical Analysis

Transmitted Light Microscopy

Mineralogy and microstructure analyses were conducted with transmitted light microscopy. The thin sections were viewed under plane-polarized light as well as cross-polarized light to obtain a complete understanding of the mineralogical composition, and microstructures present.

The microscope used was the Olympus BH-2 (Fig. 13). The Olympus BH-2 uses a 100-



watt Halogen-L lightbulb located in the lamphouse, connected to the base of the microscope. Between the lamphouse and the base of the microscope is a series of filters that emplace removable color, correction, heat, and neutral density filters in the optical pathway. The light travels from the lamphouse to the base and is reflected upwards by a substage mirror into a polarizing lens oriented in an East-West direction. The polarizer is composed of a doubly cut refracting material cemented to form a prism. The polarizer separates the beam of white light from the lamphouse into the ordinary ray and the extraordinary ray. The ordinary ray impacts the specimen at an angle

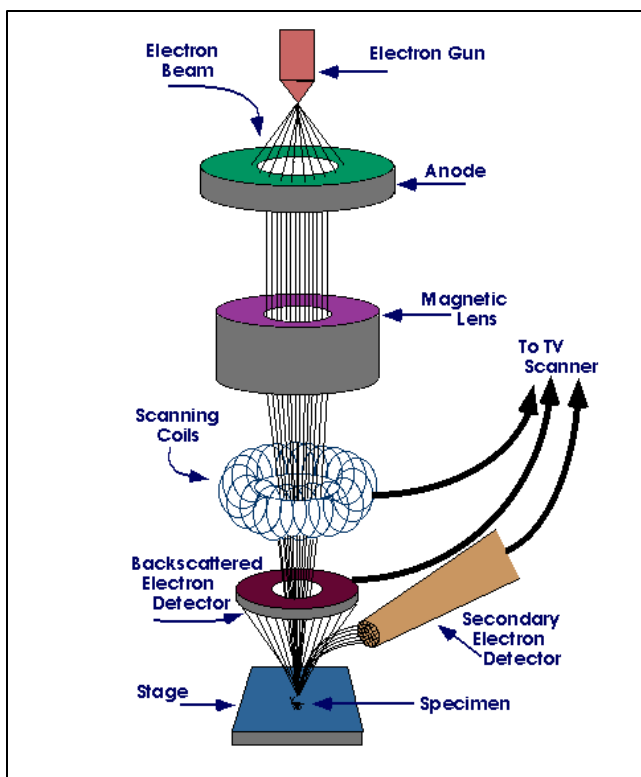
Figure 13. Olympus BH-2 microscope used for transmitted light thin section analysis. (Olympus DP21 camera used to take photo micrographs shown attached to top of microscope.)

of total internal reflection and is therefore absorbed when it hits the specimen. The extraordinary ray is a ray of linearly polarized light that passes through a strain-free condenser to the specimen on the circular rotating stage. The condenser increases the contrast between images observed

through the eyepiece. The light that passes through the specimen is received through a strain-free objective lens of magnifications ranging from 2x, 4x, 10x, 40x. For cross-polarized light, a second polarizer, or an analyzer, oriented at right angles to the first polarizer, is positioned into the light path. Cross-polarized light enables the use of the birefringence, degree of relief, and extinction angle to aid in the identification of the minerals in the slide. The light then passes through to the inclined observation tubes, passing through several prisms to redirect the beam. Finally, the light passes through the observation tubes to the eyepiece outfitted with a diopter adjustment used to achieve maximum magnification (OlympusMicro.com, 2012). Plane-polarized light was used in conjunction with cross-polarized light to analyze each slide for mineral chemistry, mineral percentages or mode, and microstructure strain analysis.

Photomicrographs of thin section were taken with an Olympus DP21 camera at various magnifications.

Scanning Electron Microscopy-Energy Dispersive Spectroscopy



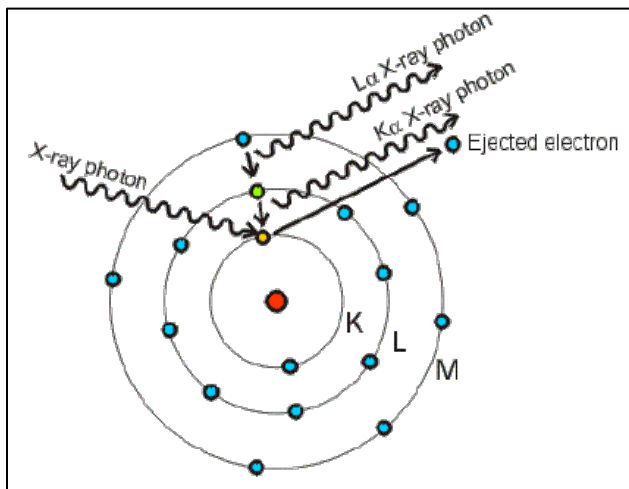
Scanning electron microscopy was used to determine mineral chemistry for individual crystals as well as overall mineral chemistry of homogeneous slides. A JEOL JSM-7100 Field Emission scanning electron microscope (SEM) was used in conjunction with the energy dispersive spectroscopy (EDS) software Thermo/Noran System 7 v7.1.x.

Each slide was coated with a sputter coat of carbon to make the slide conductive. The coated slide was then placed into the microscope for analysis. The electron gun (Fig. 14), featuring a nail of tungsten, was heated and used to produce an incident beam

Figure 14. Diagram of Scanning Electron Microscope (Source: Perdue.edu)

of excited electrons to accelerate down the vacuum chamber through an anode and magnetic lens to focus the incident beam. Scanning coils create a magnetic field using alternating voltage, and are used to manipulate the beam and direct it to the desired place.

Point specific chemical analyses were used to determine the chemical composition of desired minerals for each slide. These were conducted using an accelerating voltage of 15.0 kV, an acquisition time of 2 seconds of 5 total frames at 0.5 seconds/frame. The incident beam excites electrons of the sample (Fig. 15) and produces an energy cascade unique to the excited element. Once the beam is focused to the desired place, the incident beam (X-Ray photon in Fig. 15) then excites the electrons of the mineral beneath the beam. The electrons are thus ejected, and an energy cascade is produced as higher energy-level electrons fall down in energy levels to fill the now vacant shells (Fig. 15). The movement of each electron to a certain energy shell



emits a discrete amount of radiation. The radiation emitted is unique to each element. The X-rays emitted from the energy cascade are received by an X-ray detector attached to the SEM and the EDS software is used to produce an EDS spectrum, showing peaks of the elements present in relative abundance (Egerton, 2005). This method was used to identify the composition of the minerals in the samples.

Figure 15. Diagram of electron ejection by X-ray photon and resulting energy cascade. X-ray photon represents incident beam generated by electron gun. (Source: projects.exeter.ac.uk)

Backscatter images were obtained for each sample. To do so, the back-scattered electron detector (BSE) was emplaced into the SEM chamber. The BSE receives the ejected electrons to produce an image. Minerals composed of larger atoms, such as iron oxides, eject more electrons than minerals composed of smaller atoms, such as framework silicates. The more electrons received, the brighter the image. Therefore, minerals composed of larger atoms produce brighter

BSE images than minerals composed of smaller atoms. Therefore, an iron oxide can be expected to appear brighter on an SEM than a feldspar (Krinsley, 1998).

An x-ray compositional map was also obtained for the imaged samples. The same technology as described above for the point-specific EDS analysis applies to the scan, the only difference being the incident beam scans a larger area of the thin section. Each x-ray map was gathered with an acquisition time of 1000 seconds, 50 total frames, with each frame at 20 seconds/frame.

Structural Analysis

Stereographic Projections

Equal area lower-hemisphere stereographic projections, 1%-area contours, and a Cylindrical Best Fit test were used to analyze the 3-D structure of the foliation of the Oliverian Plutonic members. The strike and dip values of the foliation at all stations of the Jefferson Dome were plotted as planes and poles to planes on a lower-hemisphere stereographic projection using the program OSXStereonet (Cardozo and Allmendiger, 2013). One-percent-area contouring was used to determine areas of pole concentration from which the average strike and dip of each limb was derived. These averages were used in conjunction with a Cylindrical Best Fit test to determine the hinge line orientation of the Jefferson Dome.

The OSXStereonet Cylindrical Best Fit test was performed to determine the trend and plunge of the hinge line of the Jefferson Dome from the foliation data. The Cylindrical Best Fit test plotted three Eigenvectors in respect to the poles of the foliation planes. The Cylindrical Best Fit plot used a Bingham Analysis to calculate the three Eigenvectors along a girdle distribution of points. As a result of the girdle distribution, the three Eigenvectors were located at right angles to each other, depicting a perfectly cylindrical fold. The projection of a perfectly cylindrical fold was used for comparison with the actual structure of the Jefferson Dome. Over the three Eigenvectors, the two limbs of the Jefferson Dome were plotted as planes using their respective average strikes and dips derived from the 1%-area contours. The trend and plunge of the hinge line of the Jefferson Dome was derived from the intersection of these two planes. The difference

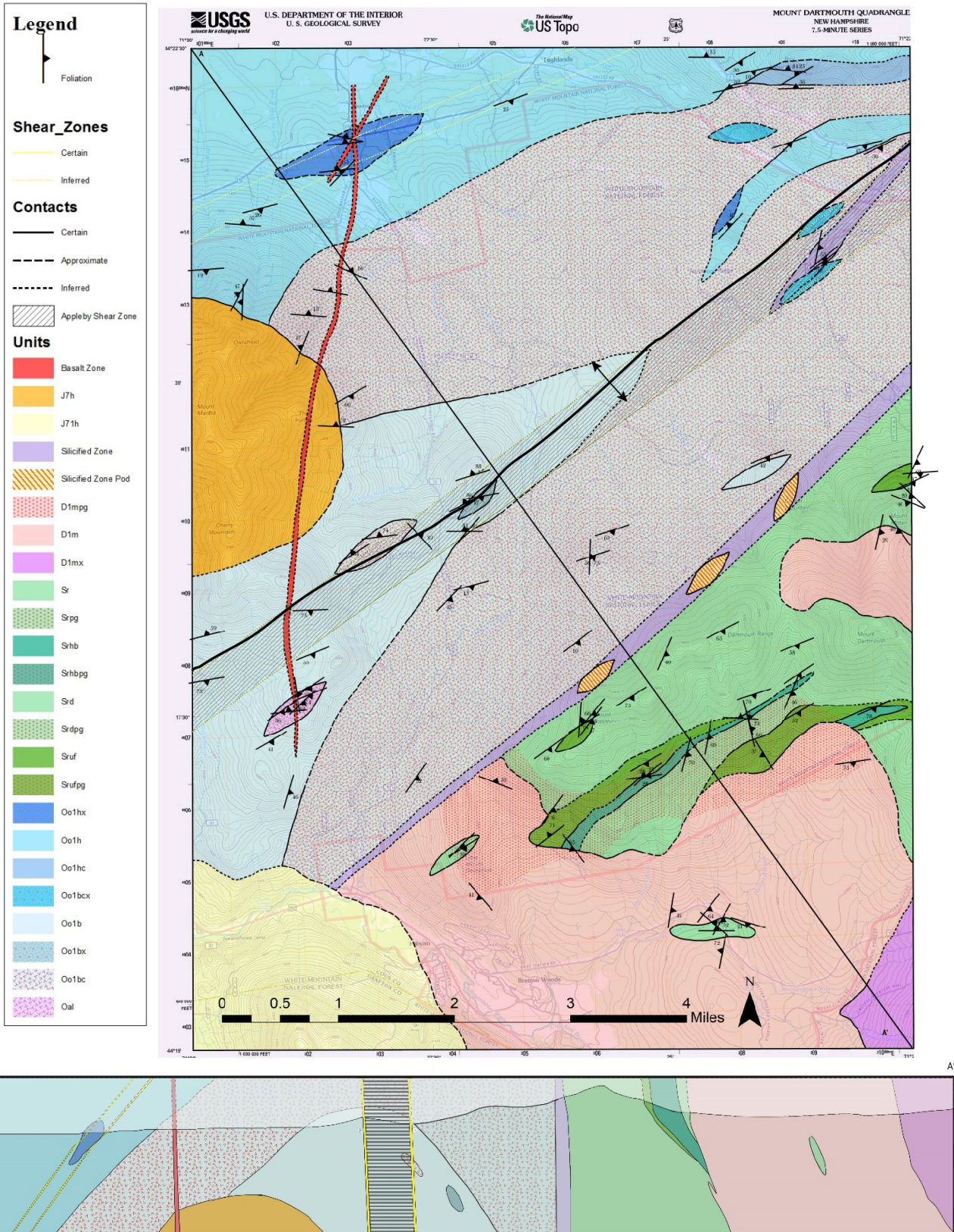
between this point of intersection and the third Eigenvector represents the deviation of the Jefferson Dome from a perfectly cylindrical fold. To determine the fold axial plane, a great circle bisecting the obtuse angle between the great circles of the two limbs was drawn by hand to intersect Eigenvector 3.

RESULTS

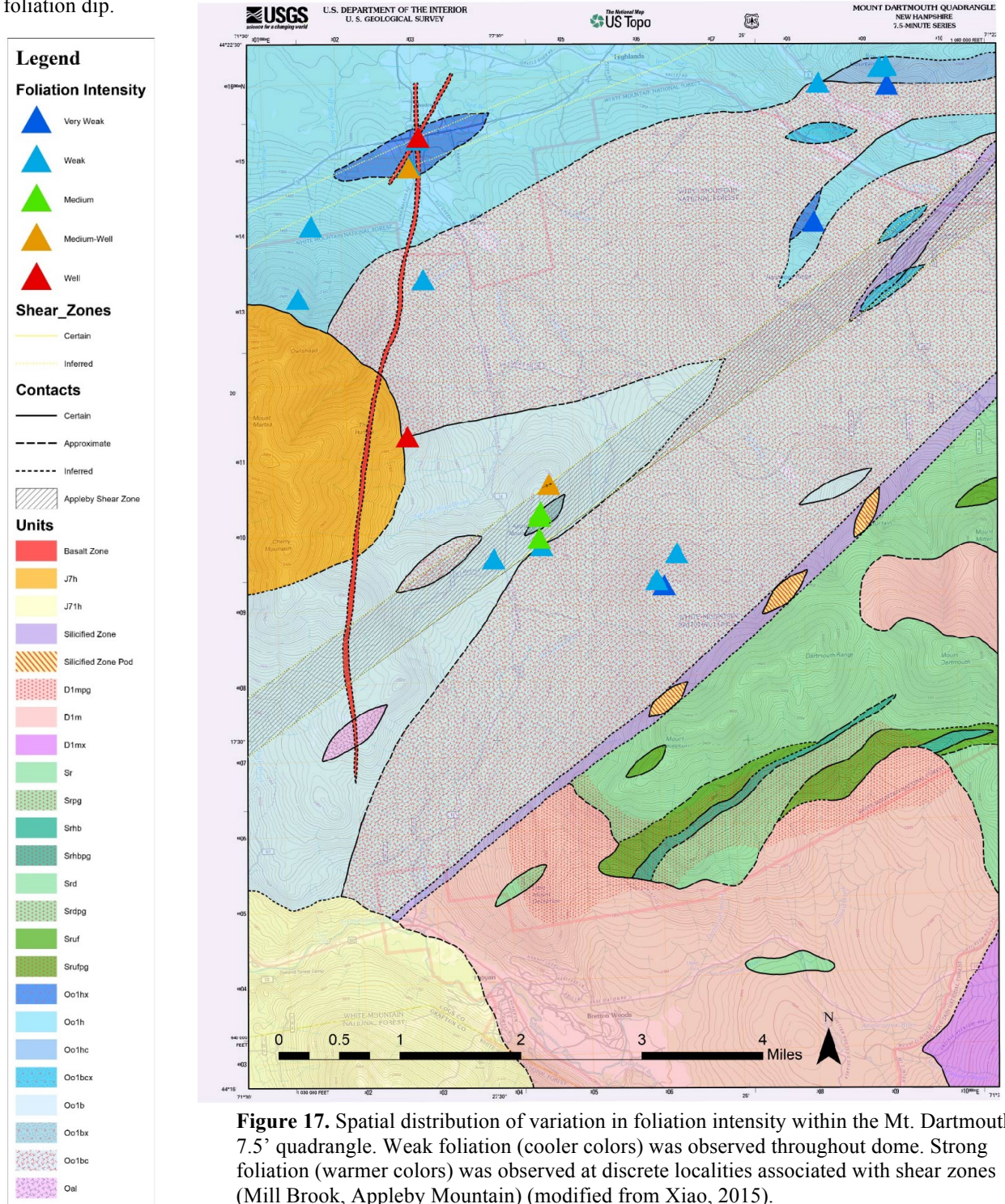
Map Contacts and Units

Overview

An updated version of the bedrock geology in the Mt. Dartmouth 7.5' Quadrangle (Fig. 16, Fig. 17) was produced by Xiao (2015) from data collected from the fieldwork of Devoe (2015), Oxman (2015) and Xiao (2015). The new map (Xiao, 2015) divides the Jefferson Dome into the Ammonoosuc Volcanics (Oal) and seven units of the Late Ordovician Oliverian Plutonic Suite: Oo1b, Oo1bx, Oo1bc, Oo1bcx, Oo1h, Oo1hx, and Oo1hc. Two new porphyritic units (Oo1bcx and Oo1hx), the names of which were created by Xiao (2015) and Devoe (2015), were added to the pre-existing dome units of Lyons et al. (1997). Each unit was initially identified using the descriptions of the correlative units from Billings et al. (1946) (Table 1). Our mineral analyses have, however, updated unit descriptions slightly based on data from transmitted light microscopy and Scanning Electron Microscopy-Energy Dispersive Spectroscopy (SEM-EDS). The overall mineralogy is rich in alkali feldspars. X-ray maps can be found in the appendix.



(continued figure caption for Fig. 16) and dip data of foliation (Xiao, 2015). On map, the dip appears as a small number next to strike symbol. Units of the Jefferson (caption for Fig. 16 continued from previous page) Dome include Oliverian Plutonic Suite (Oo1b, Oo1bx, Oo1bc, Oo1bcx, Oo1h, Oo1hx, Oo1hc) and the Ordovician Ammonoosuc Volcanics (Oal). Mill Brook shear zones illustrated as dashed yellow lines. Appleby shear zone illustrated as wide band of gray fill outlined by two dashed yellow lines. Cross section runs along line from A to A'. Mill Brook shear zones follow dip of dome, Appleby shear zone vertically cuts through the dome irrespective of foliation dip.



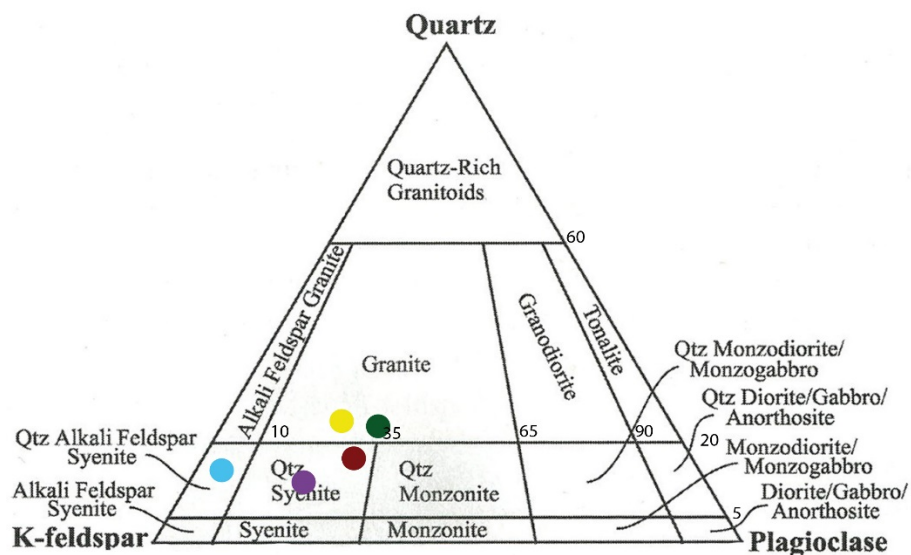


Figure 18. Quartz, Alkali feldspar, Plagioclase (QAP) diagram showing overall composition of the Oliverian Plutonic Suite of the Jefferson Dome. Mineralogy of individual samples denoted with a colored dot: Sample 309 (red), Sample 105 (purple), Sample 132 (green), Sample 138 (blue), Sample 189 (yellow). (QAP diagram modified from Nesse, 2012).

Oo1b

The Oliverian Plutonic member Oo1b forms a triangular polygon extending 7km into the center of the map from the West with a maximum width of 6km (Fig. 16). It contains lenses of Oo1bx and Oal and is intruded by a pluton of Jurassic syenite on its northern boundary (Fig. 16). One lens of Oo1b, 1km long and 225m at its maximum width, is proximal to the Pine Peak Fault silicified zone. Oo1b is a massive, light-brown to white quartz syenite with biotite aggregates (Fig. 19, Fig. 20). More intensely foliated varieties show an overall grayer coloration. Oo1b outcrops as clean ledges ranging from 0.5m to 10m in height. In hand sample, this unit retains its massive texture and light-brown coloration with a range in foliation from very weak (see map distribution on Fig. 16) to medium-well developed (Fig. 19).

Samples 175 and 309 are classified as Oo1b. Sample 175 is composed of 50% quartz, 35% of feldspars of various kinds including alkali feldspar ($K_{0.934}Ba_{0.043}Na_{0.087}Al_{0.909}Si_{3.052}O_8$), 10% of biotite and chlorite altered biotite, and 5% minerals that appear opaque through transmitted light microscopy. From here on, this undifferentiated group of minerals will be referred to as “opaque minerals”. Sample 309 is composed of 56% alkali feldspar ($K_{0.964}Na_{0.48}Al_{1.02}Si_{2.982}O_8$), 24% plagioclase ($Na_{1.046}Ca_{0.098}Al_{1.116}Si_{2.852}O_8$), 15% quartz, 3% biotite, and 2% opaque minerals and is therefore classified as a biotite quartz syenite (Fig. 18, red dot).

Dextral S-C fabrics were observed in Sample 175. Transmitted light microscopy revealed foliations planes of biotite grains oriented to show dextral shear sense (Fig. 19).

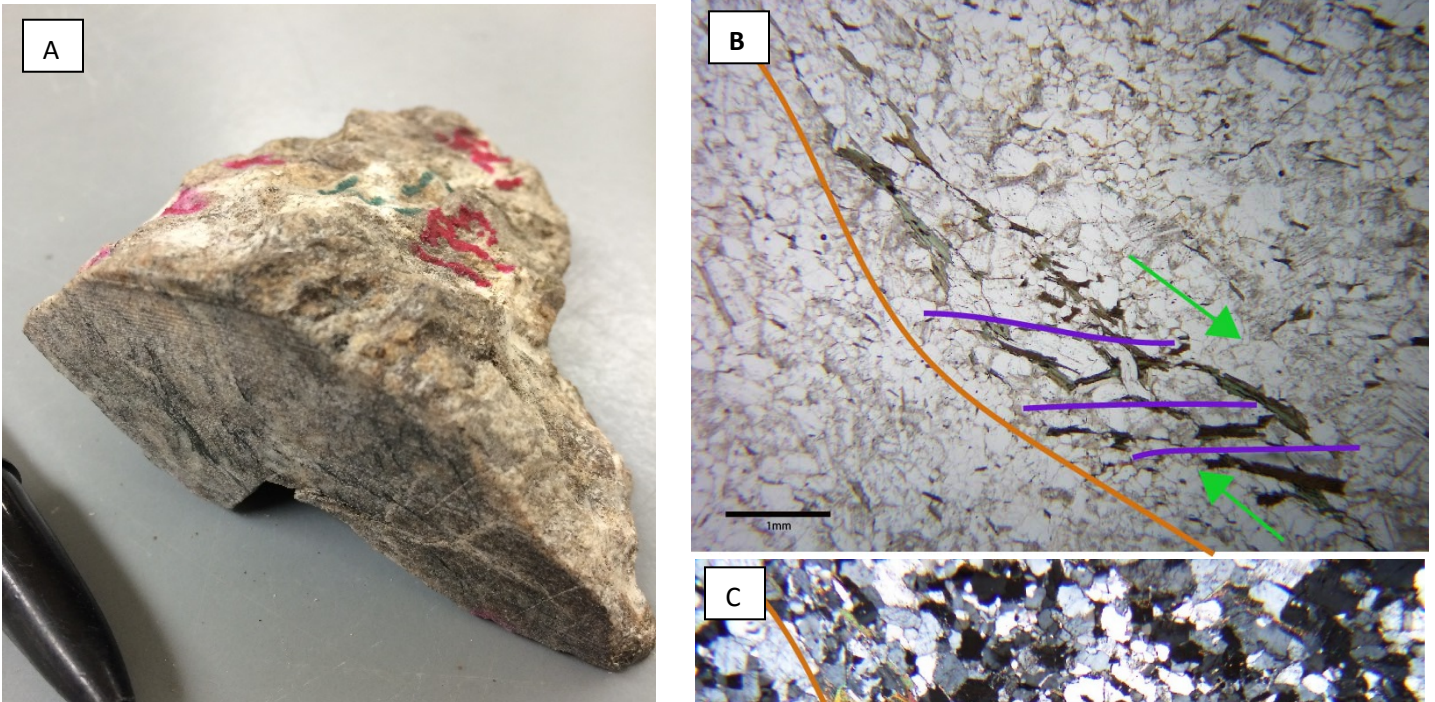
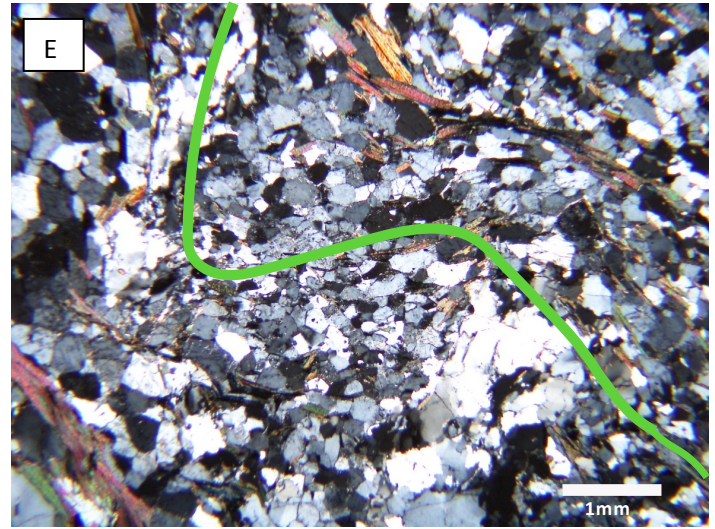
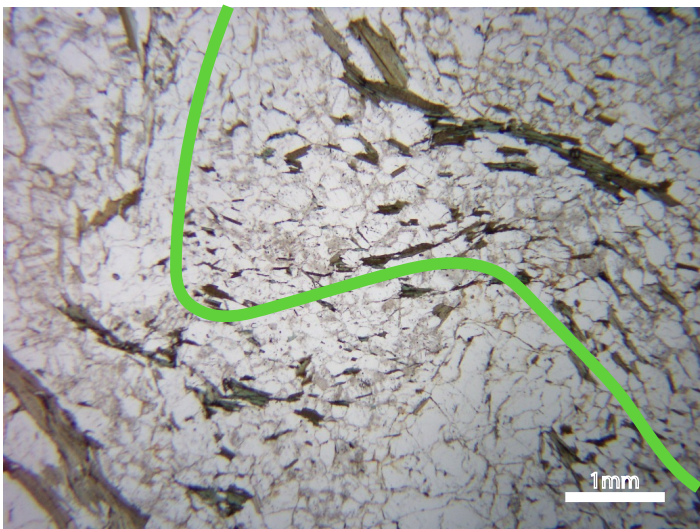


Figure 19. A) Sample 175 (Oo1b) is from the Northeast flank of Appleby Mountain and features dextrally sheared S-C fabrics (B,C). S-fabric denoted with orange line, C-fabric denoted with purple lines.

D, E) This sample is characterized by crenulations that fold the fine matrix of biotite and chlorite. Sample 175 is classified as medium-well foliated, showing both continuous and discontinuous planes of directional foliation.



Sinistrally sheared quartz veins (1mm in width) were observed in Sample 175 (Fig. 20). These quartz veins run parallel to foliation and show sinistrally sheared sigmoidal quartz subgrains (Fig. 20B).

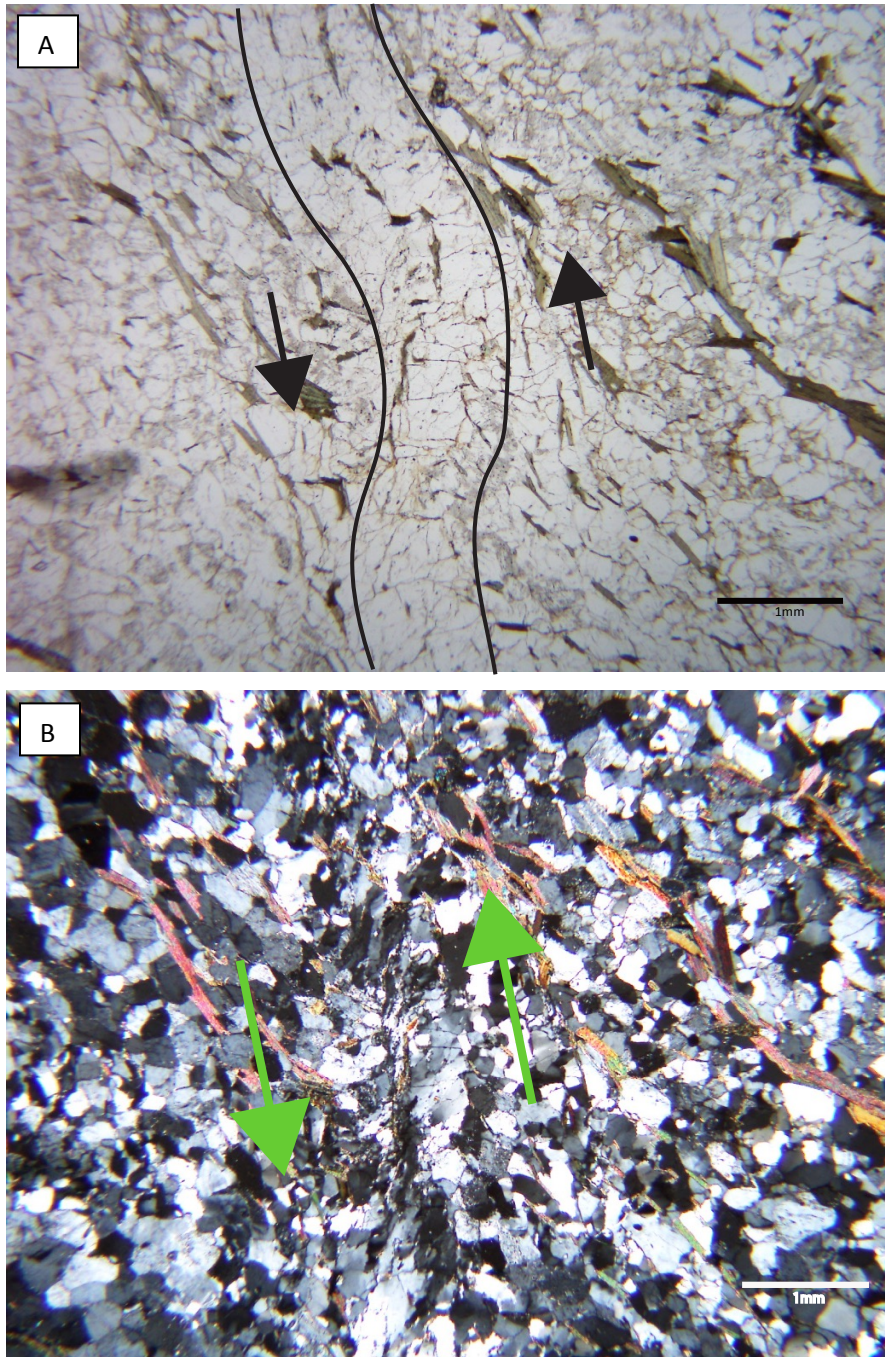


Figure 20. A) Quartz vein (outlined in black) found in Sample 175. Here quartz vein runs parallel to foliation. B) Under cross polarized light, quartz vein shows sinistrally sheared sigmoidal quartz subgrains confined to the quartz vein.

Oo1bx

There is one lens of Oo1bx, 1.3km in length with a maximum width of 2km, located in the northern portion of the Oo1b polygon (Fig. 16). Oo1bx is a porphyritic variety of Oo1b. The physical characteristics and chemical composition, as determined optically at outcrop, are the same as Oo1b.

Oo1bc

The Oliverian Plutonic member Oo1bc is the dominant unit of the 7.5' Mt. Dartmouth quadrangle, composing the middle third of the map (Xiao, 2015) as an oblong oval 11km long with a maximum width of 6km (Fig. 16). The northern boundary of Oo1bc is against the contact with Oo1h. The southern boundary of Oo1bc is formed by contact with the main silicified zone (Sz) the Pine Peak Fault. This polygon is intruded by Oo1b from the west and smaller lenses of Oo1h in the northeast corner of the quad (Fig. 16). The main polygon of Oo1bc is also cut by a late, minor silicified zone (Sz) in the northeast. A small lens of Oo1bc, 1.3km long with a maximum width of 350m, is located within the main body of Oo1b in the center west of the quadrangle (Fig. 16).

Oo1bc is the coarse-grained variety of Oo1b (Fig. 21); the two members are similar in physical characteristics and chemical composition, however Oo1bc is composed of mineral grains ranging from 0.5cm-1cm in diameter. In hand sample, this unit retains its massive texture and light-brown to pink coloration with a weakly developed foliation (Fig. 21).

Sample 105 is classified as Oo1bc and is composed of 60% alkali feldspar, 15% plagioclase ($\text{Ca}_{0.223}\text{Na}_{0.867}\text{Al}_{1.225}\text{Si}_{2.753}\text{O}_8$), 15% quartz, 4% biotite, 4% opaque minerals including hematite, and 2% sphene. Therefore, Sample 105 is classified as a quartz syenite (Fig. 18, purple dot).

Oo1bcx

Oo1bcx is a coarse-grained, porphyritic variety of Oo1b, similar to Oo1b in physical characteristics as well as chemical composition. Three oval-shaped lenses of Oo1bcx are in the northeastern corner of Oo1bc (Fig. 16). These lenses are all ~1km long and their widths vary from 160m to 320m.

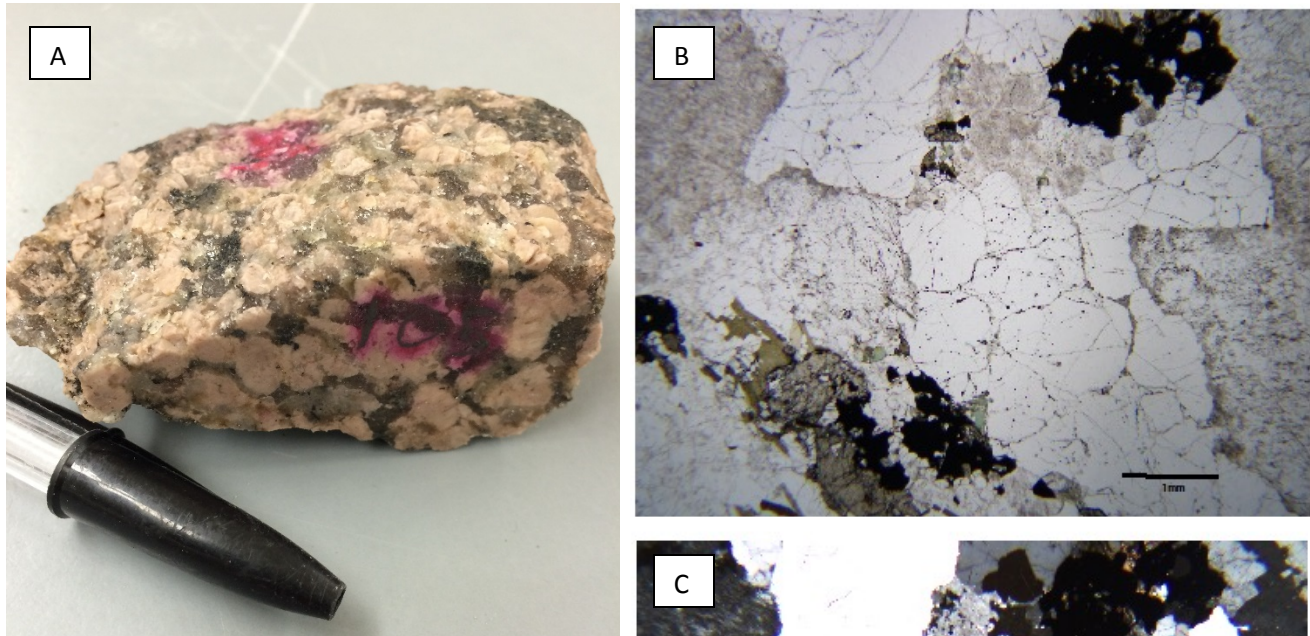


Figure 21. Sample 105 (Oo1bc) is a quartz syenite from Streator Brook on the Northeast flank of Cherry Mountain. Sample 105 is characterized by its coarse texture of quartz and feldspar, with smaller clasts and aggregates of biotite, chlorite, and sphene. Hand sample shows weak foliation, or aggregates of biotite, chlorite, and sphene that show no directional pattern; B) Weakly-developed foliation is observed in thin section under plane polarized light as well; C) Fig. 21B under cross polarized light.

Oo1h

Oo1h is the hornblende-bearing member of the Oliverian Plutonic series. Oo1h appears as a polygon extending 10km across the northern boundary of the map and 2.4 miles to the south at its greatest width (Fig. 16). Its contact with Oo1bc forms its southern boundary. Another pluton of Oo1h forms a southward-bending oblong oval in the northeast corner of the map cutting through the main pluton of Oo1bc. This pluton is 4km in length and 5km at its greatest width (Fig. 16)

Oo1h is similar to Oo1b and Oo1bc in physical characteristics and chemical composition, however Oo1h additionally contains hornblende. In Oo1h, hornblende forms aggregates with biotite. Its presence is verified using a hand lens in field and a microscope in lab. The foliation of Oo1h ranges from weakly foliated (Fig. 17) to well-foliated (Fig. 22).

Samples 10 and 132 are classified as Oo1h. Sample 10 is composed of 60% of various feldspars including alkali feldspar ($K_{0.939}Na_{0.081}Al_{1.020}Si_{2.980}O_8$) and plagioclase ($Na_{1.004}Ca_{0.100}Al_{1.109}Si_{2.287}O_8$), 35% quartz, 3% biotite and chlorite altered biotite, 1% sphene, 1% opaque minerals. Sample 132 is composed of 39% alkali feldspar ($K_{0.929}Na_{0.077}Al_{1.021}Si_{2.982}O_8$), 21% plagioclase, 25% quartz, and 15% hornblende and biotite. Sample 132 is classified as a hornblende granite, on the boundary between a syeno-granite and monzo-granite (Fig. 18, green dot).

Dextral S-C fabrics were observed in Sample 132 (Fig. 22.). Transmitted light microscopy revealed biotite oriented to show a dextral shear direction.

Oo1hx

Oo1hx is a porphyritic variety of the Oliverian Plutonic member Oo1h. There are two plutons of Oo1hx. The first is an oval, 2km long and 600m at its maximum width, located within the main body of Oo1h in the northwest of the quadrangle (Fig. 16). The other lens is an oval, 800m long and 160m at its maximum width, located within the oblong oval-shaped lens of Oo1h in the northeast corner of the quadrangle (Fig. 16).

Oo1hx is similar to Oo1h in physical characteristics as well as chemical composition, however Oo1hx is also composed of various porphyroclasts. Samples 138 (Fig. 23) and 189 (Fig. 24), both classified as Oo1hx, exhibit feldspar porphyroclasts 2.5mm-5mm in diameter (Fig. 23), and pyrite porphyroclasts ranging 2mm-5mm in diameter (Fig. 24), respectively. Oo1hx ranges from very weakly (Fig. 24) foliated to well-foliated (Fig. 23).

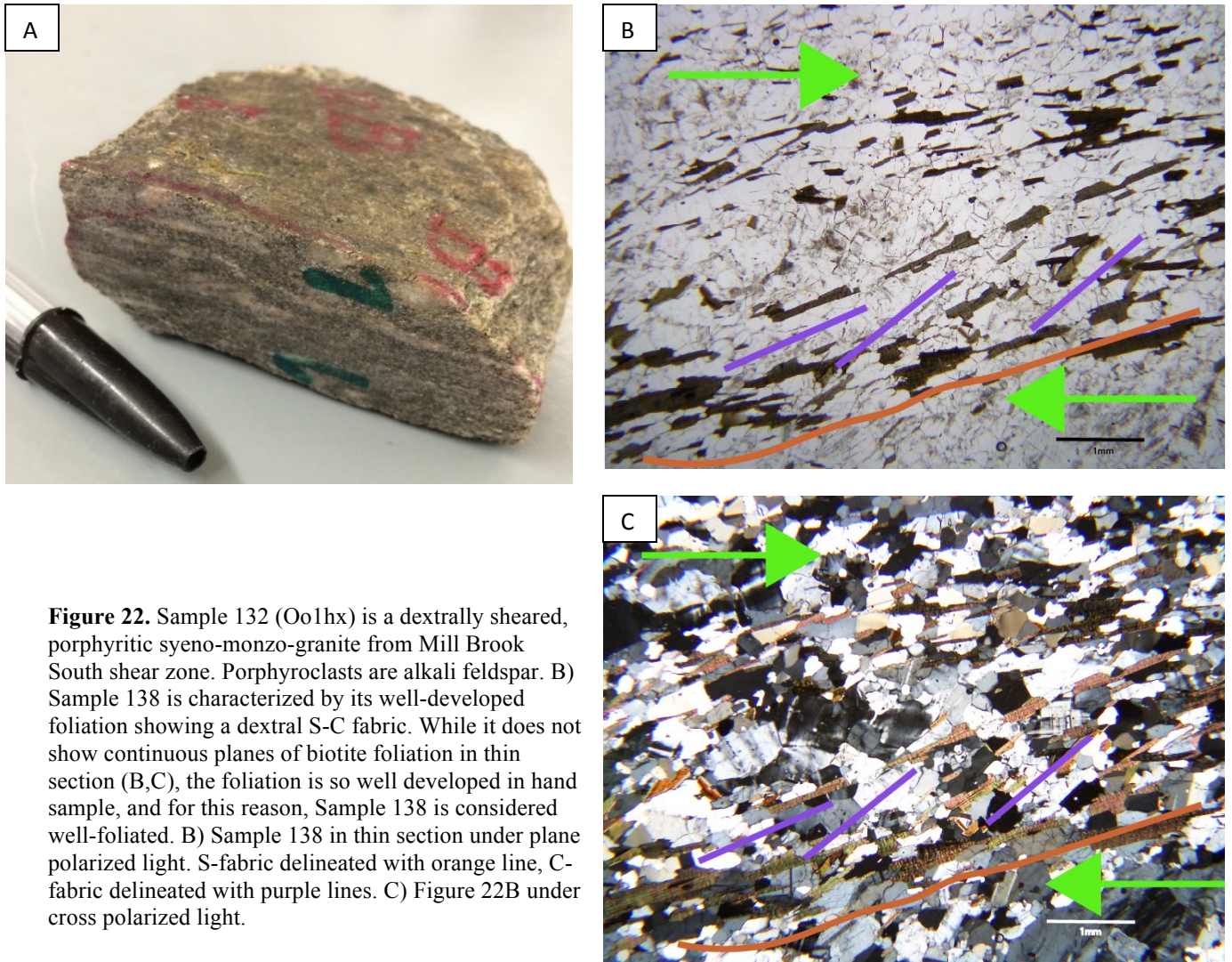


Figure 22. Sample 132 (Oo1hx) is a dextrally sheared, porphyritic syeno-monzo-granite from Mill Brook South shear zone. Porphyroclasts are alkali feldspar. B) Sample 138 is characterized by its well-developed foliation showing a dextral S-C fabric. While it does not show continuous planes of biotite foliation in thin section (B,C), the foliation is so well developed in hand sample, and for this reason, Sample 138 is considered well-foliated. B) Sample 138 in thin section under plane polarized light. S-fabric delineated with orange line, C-fabric delineated with purple lines. C) Figure 22B under cross polarized light.

Sample 138 is composed of 75% alkali feldspar, 4% plagioclase ($\text{Na}_{0.932}\text{Ca}_{0.012}\text{Al}_{0.794}\text{Si}_{3.165}\text{O}_8$), 15% quartz, 5% hornblende and biotite, and 1% opaque minerals. Sample 138 is classified as a quartz alkali feldspar syenite (Fig. 18, blue dot).

Sample 189 is composed of 49% alkali feldspar ($\text{K}_{0.04}\text{Na}_{1.05}\text{Al}_{1.05}\text{Si}_{2.9}\text{O}_8$), 16% plagioclase, 25% quartz, 5% hornblende and biotite, 5% opaque minerals including pyrite. Sample 189 is classified as a hornblende-bearing syeno-granite (Fig. 18, yellow dot).

Dextral S-C fabrics were observed in Sample 138 (Fig. 23). Transmitted light microscopy revealed foliation planes with biotite grains oriented to show dextral shear sense (Fig. 23).

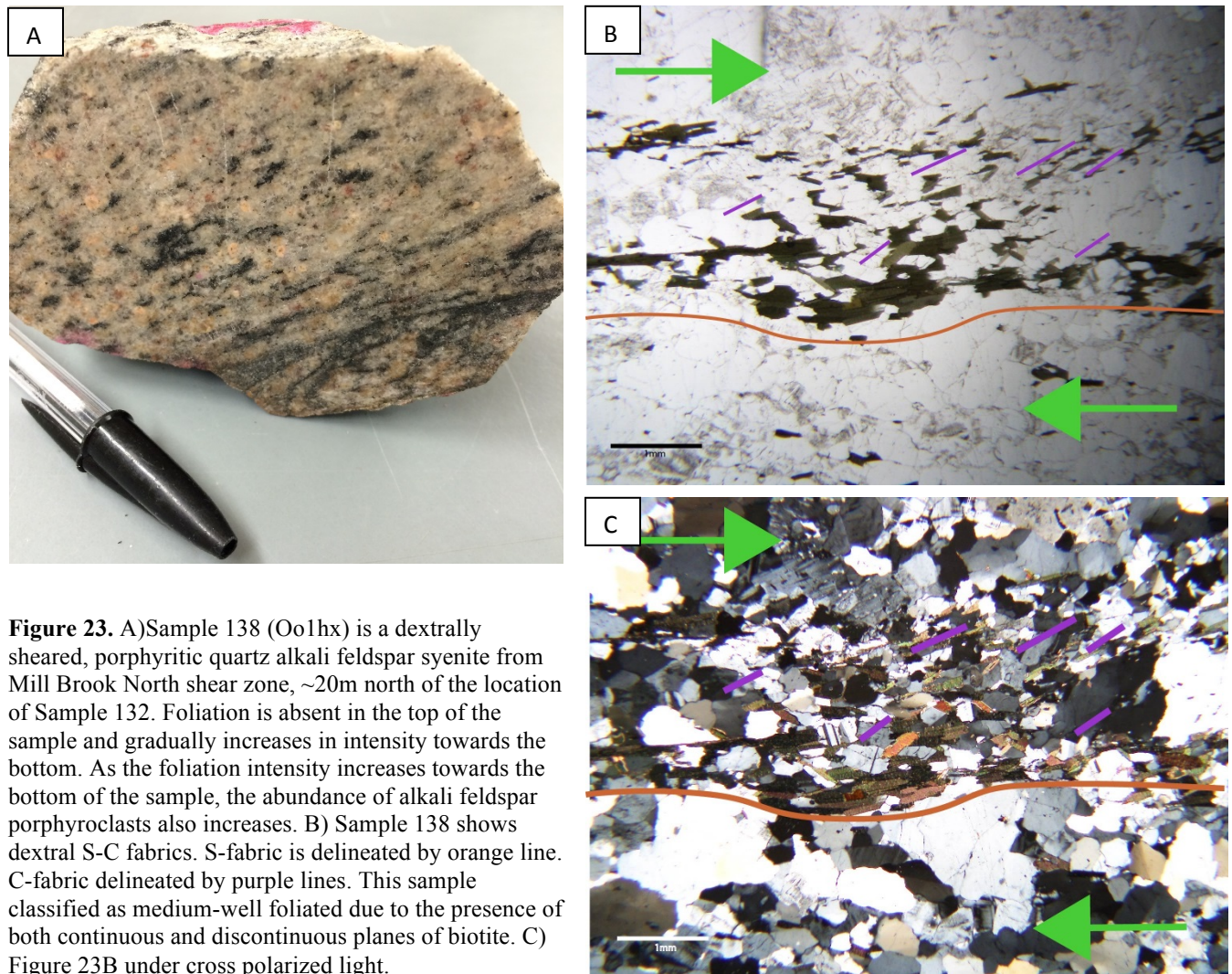


Figure 23. A) Sample 138 (Oo1hx) is a dextrally sheared, porphyritic quartz alkali feldspar syenite from Mill Brook North shear zone, ~20m north of the location of Sample 132. Foliation is absent in the top of the sample and gradually increases in intensity towards the bottom. As the foliation intensity increases towards the bottom of the sample, the abundance of alkali feldspar porphyroclasts also increases. B) Sample 138 shows dextral S-C fabrics. S-fabric is delineated by orange line. C-fabric delineated by purple lines. This sample classified as medium-well foliated due to the presence of both continuous and discontinuous planes of biotite. C) Figure 23B under cross polarized light.

Oo1hc

Oo1hc is a coarse-grained variety of Oo1h, similar in physical characteristics and chemical composition. Oo1hc forms one lens, 2km long and a maximum width of 3km, in the northeastern corner of the quadrangle (Fig. 16)

Oal

The Ammonoosuc Volcanic unit Oal appears as a small lens, 1km long and 300m at its greatest width, in the southern portion of the main polygon of Oo1b (Fig. 16). The lens is intruded by the north-south striking Mill Brook Dike Zone (Oxman, 2015). Oal is an amphibolite with a fine-grained green to black matrix and hornblende grains 1mm in length (Fig. 25).

Sample 52 is classified as Oal. Sample 52 is composed of 50% hornblende, 30% biotite, 15% feldspar, 5% quartz, and minor amounts of titanite and apatite. The feldspars are anhedral, and sericite alteration is present.

Sample 52 has a weak foliation with a strike and dip 351° , 74° , an orientation incongruent with the surrounding foliation of the Oo1b pluton (average is 57° , 37°) (Fig. 16).

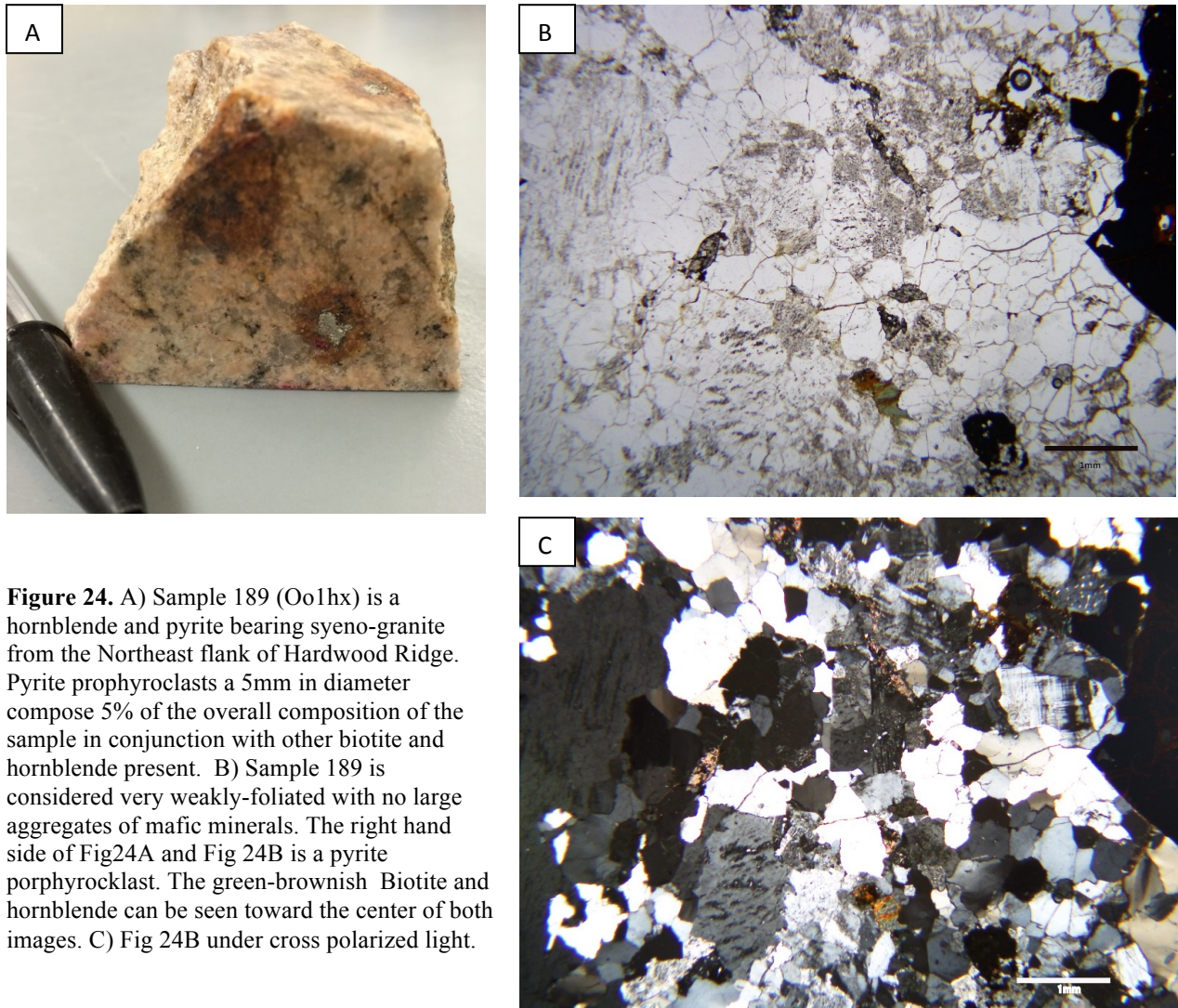


Figure 24. A) Sample 189 (Oo1hx) is a hornblende and pyrite bearing syeno-granite from the Northeast flank of Hardwood Ridge. Pyrite porphyroclasts a 5mm in diameter compose 5% of the overall composition of the sample in conjunction with other biotite and hornblende present. B) Sample 189 is considered very weakly-foliated with no large aggregates of mafic minerals. The right hand side of Fig24A and Fig 24B is a pyrite porphyroclast. The green-brownish Biotite and hornblende can be seen toward the center of both images. C) Fig 24B under cross polarized light.

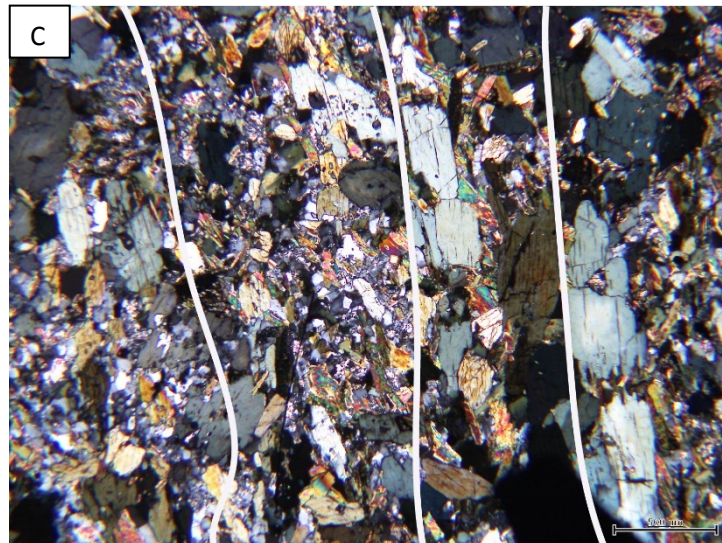
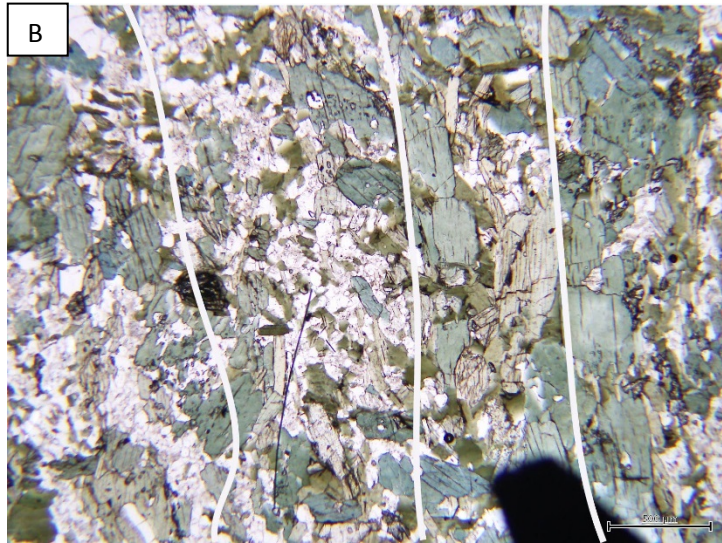
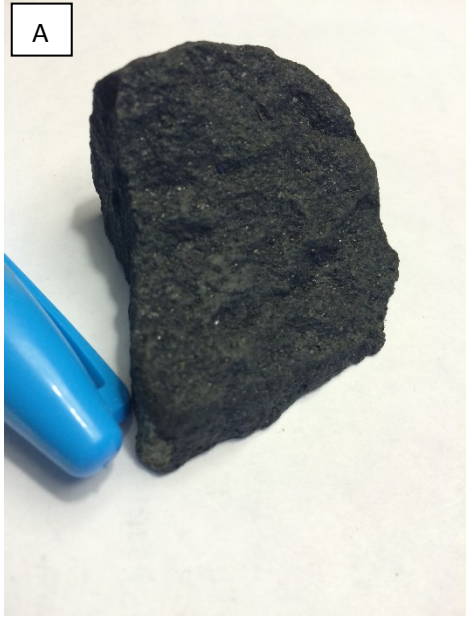


Figure 25. A) Sample 52 (Oal) is a fine-grained amphibolite from the lens of Oal in the southwestern portion of the quadrangle. B) Sample 52 forms a weak fabric of aligned hornblende and biotite delineated with white lines. C) Fig. 24B under cross polarized light. This sample was not oriented so the direction of fabric is indiscernible. The black rhombus in the bottom right corner of A and B is a piece of aluminum tape.

Structural Analysis

Using Foliation to Construct the Shape and Orientation of the Dome

Foliation intensity varied throughout the mapped portion of the Jefferson Dome (Fig. 17). The expected, well-foliated dome margin and weakly or non-foliated dome interior, commonly seen throughout the Bronson Hill Anticlinorium, was not found. Rather, areas of stronger foliation intensity were found in the interior of the dome and many of these were related to the presence of shear zones. Some, but not all, of these shear zones have steeply dipping foliations classified by dips greater than 74° (Fig. 17) Shear zones will be discussed in *Structural analysis: Shear Zones*.

The foliation scale (see *Methods*) was used to classify the range in foliation from very weakly-foliated to well-foliated. Out of the 37 samples collected from the quad, 16% showed very weak foliation (Fig. 24); 46% were classified as weakly foliated (Fig. 21); 6% were classified with medium-developed foliation; 8% show mid-well developed foliation (Fig. 23); and 24% with well-developed foliation (Fig. 22). Descriptions of foliation intensity as observed in hand sample agreed with foliation observed using transmitted light microscopy.

An equal area projection of the dome foliation shows two major sets (Fig. 26A). The two major sets yield average strikes and dips of 50° , 42° SE and 273° , 22° NW, respectively. These two sets are interpreted as the two limbs of the Jefferson Dome and resemble limbs on the map. Steeply dipping foliation, classified as foliation with a dip greater than 74° , were plotted separately (Fig. 26B). The steeply dipping foliation were plotted separately because a correlation between steeply dipping foliation, well-developed foliation, and evidence of shearing was observed. For this reason, the steeply dipping foliation is most likely related to a shear zone that occurred post-doming and is unrepresentative of the overall anticlinal, dome-like foliation structure.

The Dome

The limbs of the dome, represented by the two major sets, dipping north and southeast, respectively (Fig. 26A). Using the average strike and dip of each limb, a Cylindrical Best Fit test generated the trend and plunge of the hinge line as 63° , 11° with an interlimb angle of 120° (Fig. 27). The axial plane of the fold was determined to be 245° , 76° and runs along the center of the Oo1b polygon (Fig. 27, Fig. 16) Taken together, the dome can be classified as a gently plunging, steeply inclined anticline (Fleuty, 1964).

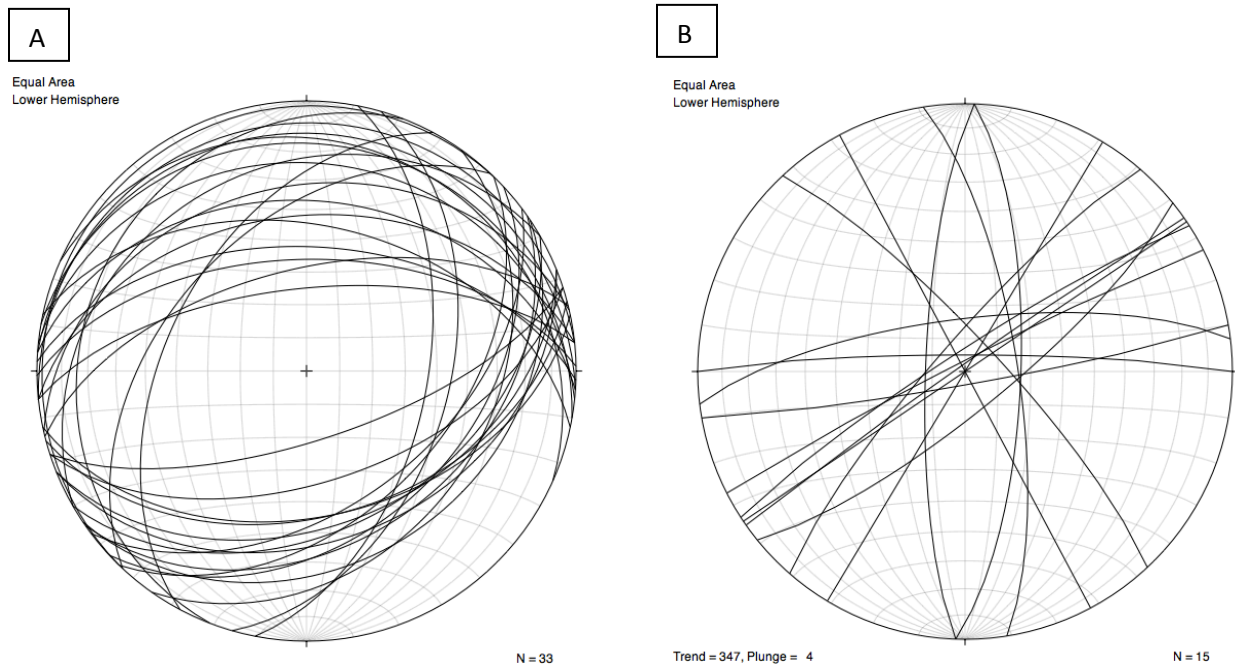


Figure 26. Equal area southern hemisphere stereographic projections of biotite foliation found in the Oliverian Plutonic Suite of the Jefferson Dome. A) The beta diagram of the Oliverian Plutonic Suite shows two dominant sets of orientations: 1) a northeast-southwest striking set dipping to the southeast and 2) an east-west striking set dipping to the north. These two foliation orientations are interpreted as the north and southeast dipping limbs of the Jefferson Dome. B) An equal area projection of the fifteen recorded steeply dipping foliations. The steeply dipping foliations are separated from those in figure 26A due to the correlation between steep dip, the high intensity foliation, and the presence of shearing. Therefore, steeply dipping foliations are likely related to shear zones that occur post-doming and therefore are unrelated to the overall dome structure. Foliation was classified as “steep” with a dip between 74° to 90° . The north-south striking planes are from Sample 52, and are most likely a roof pendant, also unrelated to the overall dome-like foliation structure.

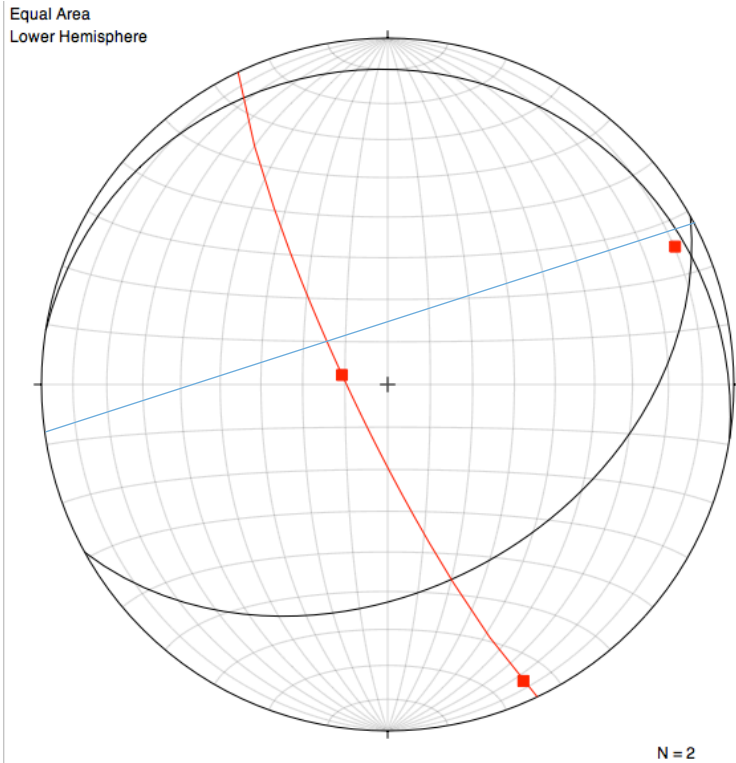


Figure 27. Using the average strike and dip of both limbs of the Jefferson Dome, a cylindrical best fit test, generated by OSXStereonet (Cardozo and Allmendinger, 2013), was performed. The trend and plunge of the hingeline of the dome was calculated to be 63°, 11° with an interlimb angle of 120°. The axial trace is illustrated on the stereographic projection with a blue line. This classified the Jefferson dome as a gently plunging, steeply inclined, gentle fold (Fleuty, 1964).

Shear Zones

Two discrete shear zones and one wide shear zone were inferred based on the evidence of shearing, well-developed foliation, and in some cases, steeply dipping foliation. The northernmost shear zone, Mill Brook North, is evidenced by the dextrally oriented S-C fabric of Sample 138 (Fig. 23). Just south of Mill Brook North is the Mill Brook South shear zone which is evidenced by the dextrally oriented S-C fabric of Sample 132 (Fig. 22). Samples 132 and 138 also show high foliation intensity (medium-well to well-developed) as well as shallowly dipping foliation (45° and 65°, respectively.) It appears that high intensity foliation is associated with shearing. Therefore, because the sampling locations of Samples 132 and 138 are surrounded by weakly foliated rock which is most likely absent of shearing, the Mill Brook shear zones are represented as two narrow shear zones rather than the northern and southern limits of one wider shear zone (like Appleby shear zone).

The dextrally oriented S-C fabric in Sample 175 (Fig. 19B, 19C) evidences the existence of the Appleby shear zone, a shear zone 0.4 miles in width, located south of Mill Brook South striking at 237°.

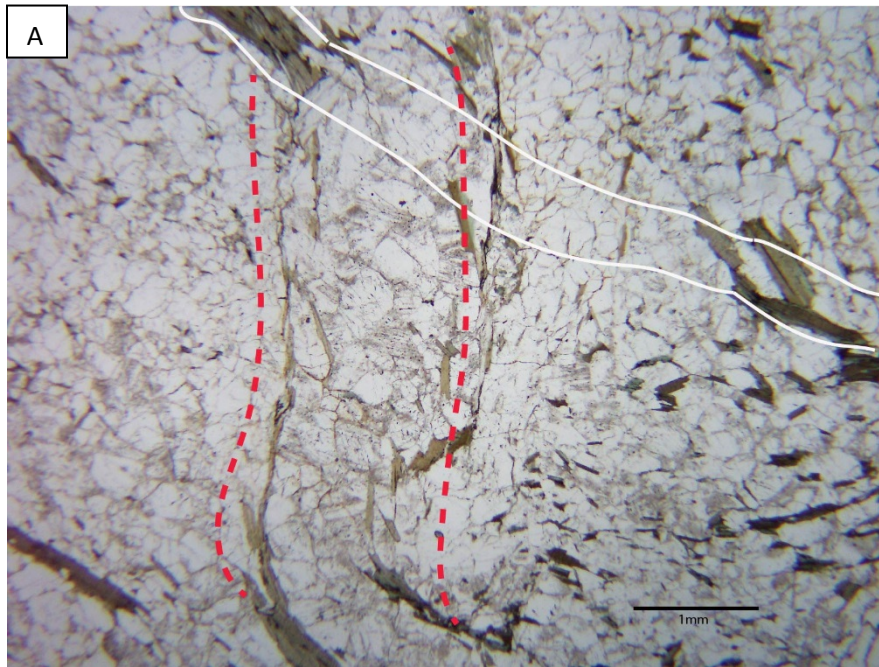
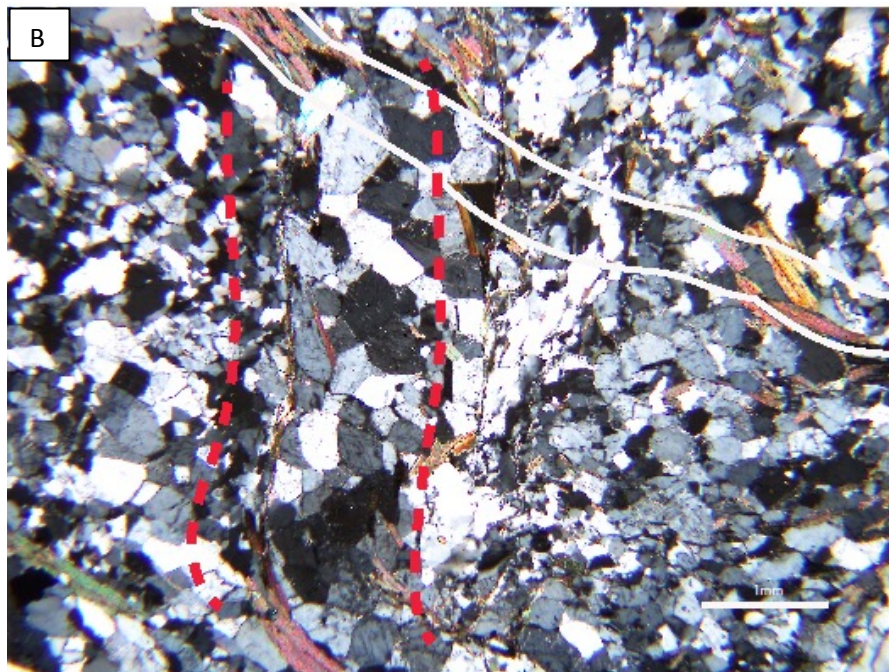


Figure 28 . A) Quartz vein (outlined by red dashed line) in Sample 175 shown obliquely cutting through plane of foliation (outlined in white). This cross-cutting relationship suggests the formation of foliation predates that of the quartz veins. B) Fig 28A under cross polarized light.



High intensity foliation (medium to well-foliated) appears to be associated with the presence of shearing, as seen in Samples 132, 138 and 175. Sample 175 and the other locations of high intensity

foliation in the area (Fig. 17) also have steeply dipping foliation (Fig. 16). Steeply dipping foliation seems to be associated with shearing unique to the Appleby area as supported by Sample 175. Therefore, Appleby shear zone encompasses locations identified with high intensity and steeply dipping foliation as those areas most likely have been sheared. The northern limit of the Appleby shear zone is the sampling location of Sample 175, the northernmost sampling location demonstrating shear sense, high intensity foliation, and steep dip. The shear zone extends as far south as the sampling location of Sample 180, the southernmost sample with high intensity and steeply dipping foliation (Fig. 16).

Sample 175 also contains quartz veins composed of sinistrally sheared sigmoidal quartz subgrains that reveal sinistral shearing (Fig. 20). Within the same sample, quartz veins are observed to obliquely cut the foliation (Fig. 28).



Crenulations on Appleby Mountain

Crenulations were observed on Appleby mountain at the location of Sample 175 (Fig. 29). An S-shaped fold in the S-C fabric was observed in Sample 175 (Fig. 19D, 19E). No cross-cutting relationships between the folded S-C fabric and shear planes or quartz veins were observed.

Figure 29. Crenulations as observed in outcrop on Appleby Mountain. Crenulations can be easily seen below index finger. (Photo credit: J. Dykstra Eusden).

DISCUSSION

Overview

Several structural features observed in the Jefferson Dome reveal the complex tectonic history of the Dome and the surrounding area. The dome-like structure of the foliation, presence of shear zones, and crenulation folds in foliation, detail the tectonic story of the Dome's formation and the tectonic forces that acted on it post-doming and in its current lithified state.

The development of the Jefferson Dome can be divided into three parts: the rising and doming of the lithified magma chamber toward the surface of the earth's crust creating the dome-shaped foliation structure, the shearing of the foliation to produce S-C fabrics, and the local crenulation folding of the S-C fabrics. A late stage of quartz veining seen in some thin sections and outcrops is thought to occur after the development of foliation and possibly part of the Pine Peak Fault.

Origin of the Oliverian Suite and Ammonoosuc Volcanics

Controversy surrounds the origin of the Oliverian Domes. Lyons et al. (1996) suggest an autochthonous origin of the Oliverian Domes based on mushroom-shaped gravity models. The presence of the "mushroom stem," or trail of magma from the plume head to the base of the melt, suggests an autochthonous Laurentian magmatic origin, rather than being floored by a thrust fault. Dorais et al. (2008) identified continental arc signatures in the Oliverian suite, in contrast to the island arc tholeiite signature of the Ammonoosuc Volcanics. However, Dorais et al. (2008) have identified the presence of both Laurentian and Gondwanan isotopic signatures within the Oliverian suite. Dorais et al. (2008) suggest magma mixing and assimilation of both Gondwanan and Laurentian derived crust due to the proximity of the Bronson Hill arc to Laurentia during the time of magma mixing and suggests an autochthonous development of the Oliverian plutons.

The current emplacement model of the Ammonoosuc Volcanics suggests a faulted contact between the Ammonoosucs and the Oliverian plutons. Dorais et al. (2012) identifies a peri-Gondwanan signature and proposes the obduction of the Ammonoosuc Volcanics onto Laurentia. Robinson et al. (1998) propose that a low-angle detachment fault emplaced the

obducted Ammonoosuc Volcanics over the Oliverian plutons, and Foley (2009) found mylonitic evidence of a faulted contact between the Ammonoosuc Volcanics and the Jefferson Dome. The Moose River Fault, a low angle fault located in the region, could be responsible for the emplacement of the Ammonoosuc Volcanics over the Jefferson Dome (Eusden, 2010).

Magmatic Differentiation and Timing of Intrusion

Because the source of the Oliverian magmatic suite remains unclear, it is difficult to postulate the reason for compositional variation within the Oliverian Suite. Continental arcs most often generate a granodiorite magma (Nesse, 2012). However, our mineralogical analyses revealed compositions were majorly alkali feldspar rich rather than plagioclase. The nature of these melts are not yet well understood (Nesse, 2012).

The differentiation of the mineral compositions and textures remains unclear. Hornblende has a greater density than biotite (Nesse, 2012) and therefore would be expected to form at the center of the dome rather than along the edges. It is strange that a coarse-grained unit (Oo1bx) is surrounded by two finer grained units (Oo1h, Oo1b) (Fig. 1). It is possible that the variation in texture is due to a variation in amount of water present, possibly due to a multi-stage doming event. It could be possible that the metamorphism that occurred during doming and the development of foliation affected the texture of the rocks as well as their water content. Alternatively, the finer grained units may have chilled against the coarser grained unit indicating multiple ages of magmatism. However, no field relations were found that support different ages of magmatism within the Dome.

Asymmetry and orientation of the Jefferson Dome

The anticlinal structure of Oliverian Plutonic Suite foliations is critical in the development of a model of formation for the Jefferson Dome. The Jefferson Dome pluton is Mid-Ordovician in age (456 ± 3 Ma; Moench and Aleinkoff, 2003), yet dome-related deformation of Devonian rocks, as well as D1, D2, and D3 structures from the Acadian orogeny indicate that the doming process is younger than the Acadian emplacement of the deformed units and structures (Eusden, 2010).

Due to a combination of transpressive tectonics and density difference, the Oliverian plutons diapirically rose through the overlying sequence, forming the Oliverian Domes outcropping along the axis of the Bronson Hill Anticlinorium. The Jefferson Dome rose through the crust to produce an anticlinal, gently plunging, steeply dipping, gentle fold (cross section, Fig. 16; Fig. 27). Other Oliverian Domes also show an asymmetrical limb structure and a northern plunge (Lyons et al., 1996). Indicators of non-uniform dome-emplacment kinematics have been found in the Ammonoosuc Volcanics at the Croydon Dome by Killam (2015). The Ammonoosuc Volcanics at the Croydon Dome show moderately plunging north-trending lineations indicating deformation during the emplacement of the dome (Killam, 2015). In addition to lineation orientations, the Ammonoosuc Volcanics of the Croydon Dome also show asymmetric porphyroclasts of plagioclase that indicate top-to-South shear sense as well as sinistral shear along the western boundary. These structures suggest the northward movement of the overlying Ammonoosuc Volcanic cover relative to the southerly-moving dome (Killam, 2015). The asymmetrical limbs and plunging quality of the Oliverian Domes suggest non-uniform stresses during the doming process and could be due Early Devonian oblique convergence during the Acadian orogeny which has resulted in asymmetric structures representative of dextral-SE-side-up kinematics (Solar and Brown, 2001). The northeastern strike, plunge, and asymmetrical limbs of the Oliverian Domes indicate transpressive, non-uniform forces were acting on the dome during the doming process and resulted in asymmetrical, plunging structures. The activation of the Pine Peak Fault could have also modified the dome shape to have produced a more steeply dipping southeastern limb as seen on cross section A-A' (Fig. 16).

The Expected Ammonoosuc Volcanic Mantle

The expected mantle of Ammonoosuc Volcanics (Oal) surrounding the dome, as is typical throughout the Bronson Hill Anticlinorium, was not observed in the study area. Billings et al. (1946) mapped two lenses of Oal in the quad, one along the southern portion of the dome in contact with the Pine Peak Fault and another within the Oo1b (Fig. 16). Our remapping of the area did not find any evidence of the lens adjacent to the Pine Peak Fault but did find the lens internal to the Oo1b (described below). The absence of the Oal lens along the Pine Peak Fault suggests that it was cut out by the fault. Because the Pine Peak Fault also cuts the Carboniferous-

Devonian Bretton Woods granite (Tmg) (Fig. 1), the motion of the fault must be younger the age of the Bretton Woods granite. Silicified zones elsewhere in the region are most often interpreted as Mesozoic structures as well (Lyons et al., 1997). Our mapping shows the Pine Peak Fault terminating against the Jurassic Conway Granite (J71h) (Fig. 1), suggesting motion sometime between the Jurassic and Carboniferous.

The one lens of Oal in Oo1b (Fig. 16) can be explained by the doming of the Oliverian pluton into the overlying Ammonoosuc Volcanics, or also by the subsequent rising of the dome through the Ammonoosuc Volcanics. It is possible that this lens of Oal is a roof pendant-- a remaining piece of the overlying Ammonoosuc Volcanics left over after the intrusion of the Oliverian pluton into the Ammonoosuc Volcanics and the doming of the pluton through the overlying sequence. The incongruity of the strike and dip of Ammonoosuc fabric (351°, 74°) with the surrounding Oliverian foliations (average is 57°, 37°) suggest that the lens of Oal is a rotated block within the dome with fabric that is unrelated to the overall structure of the Oliverian dome.

Appleby and Mill Brook Shear Zones

The three dextral shear zones were mapped in the quadrangle based on the presence of higher intensity foliation. Transmitted light microscopy revealed S-C fabrics indicating dextral shear sense for samples with strong foliation (Fig. 19, Fig.22, Fig. 23).

The Appleby shear zone was inferred using a correlation between evidence of shearing, high intensity foliation, and steep dip. Sample 175 from this region was made into thin section and revealed a dextrally sheared S-C fabric. High intensity foliation appeared in the South Branch of the Israel River, outcropping to the northeast of Sample 175 and exhibiting the same foliation orientation as the samples from Appleby. There appears to be a correlation between strongly foliated rocks and evidence of shearing. Therefore, the sheared sample location from Appleby Mountain was connected to the locations of strong foliation in the Israel River following the strike of the foliation.

The width of Appleby Shear zone as shown on Figure 16 is to encompass all similar sample locations exhibiting the same strike and dip. Locations of high intensity foliation were observed near Sample 175 near Appleby Mountain. All of these locations also exhibited a steep dip ($>74^\circ$). For this reason, shearing at Appleby Mountain was determined to be associated with high intensity foliation as well as steep dip. Therefore, Appleby shear zone, at $\sim 600\text{m}$ in width, encompasses all strongly foliated locations that also exhibit steep dip, with the northernmost and southernmost lines of the shear zone shown on the map (Fig. 16) marking the boundaries of the shear zone.

The Mill Brook North and South shear zones exhibit very different dip and distributions than those of Appleby shear zone. Again, like Appleby, the strong foliation observed at Samples 132 and 138 were associated with the presence of dextrally sheared S-C fabrics. However, the Mill Brook shear zones are depicted as narrow zones 0.4% the width of Appleby. This is because each sample with an S-C fabric from the Mill Brook area (Samples 132 and 138) were proximal to localities of very weak foliation. This indicates that the shearing at Mill Brook is much more localized and forms much narrower zones of deformation. The Mill Brook shear zones also exhibit a dip about half as steep (45° and 65°) as those of Appleby shear zone (74° - 90°).

The difference between the Appleby shear zone and the Mill Brook shear zones could be reasoned a few ways. Even though both shear zones exhibit the same shear sense and are oriented at generally the same strike, the difference in dip angle could suggest that these two shear localities were created by separate events of differing stress orientations. However, due to the similarity in shear sense, it could also be possible that the two shear zones were are resulting structures from the same deformation event, yet formed along pre-existing planes of weakness, such as the foliation of the dome or doming-related planes of weakness, that were oriented differently.

Appleby shear zone occurs along or near the axial surface of the Jefferson Dome. It could be possible that vertical zones of weakness parallel to the axial plane formed during the doming of the Oliverian pluton (Fig. 30). After the Dome was formed, the dextral shearing occurred along these planes of weakness and formed the Appleby shear zone. The difference in rock compositions could also influence shear zone orientation and shear zone width. The Mill Brook

shear zones seem to be more influenced by the existing foliations on the shallow dipping NW limb of the dome rather than the axial planar fabric as postulated for the Appleby shear zones.

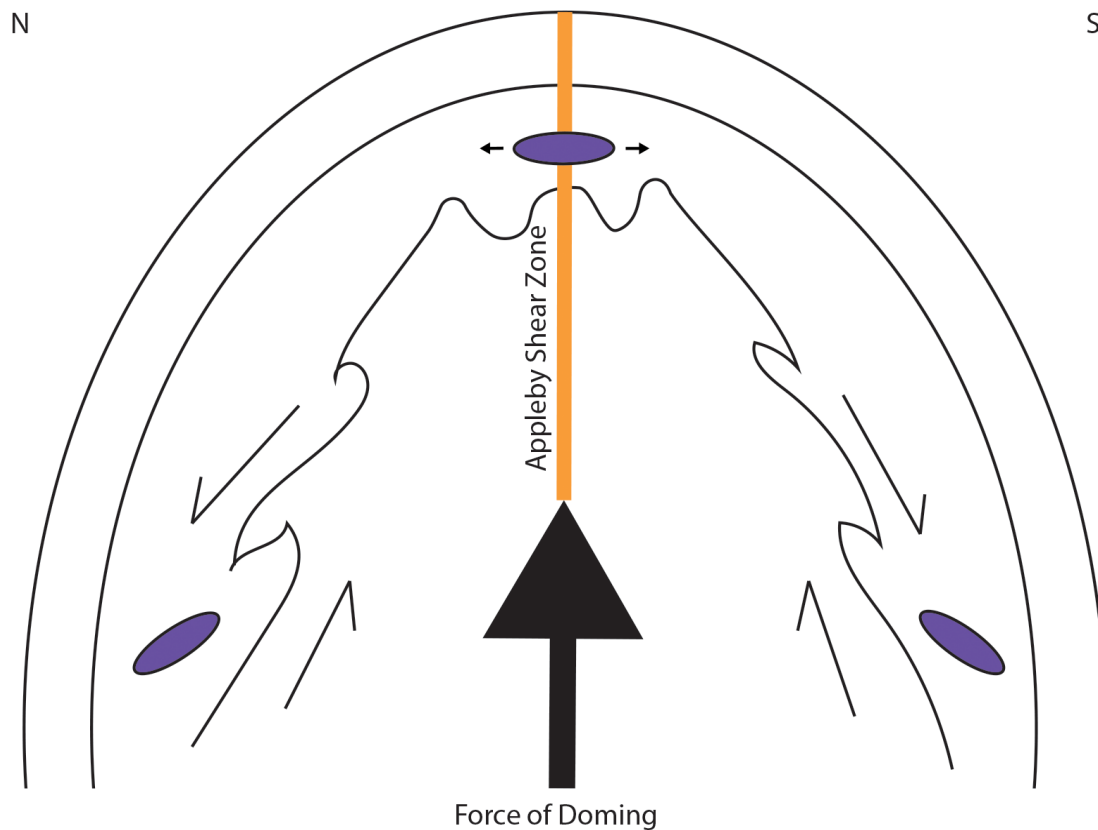


Figure 30. The formation of a vertical plane of weakness along the axial plane that could later become the Appleby Shear zone. Due to the upwards force of doming, the pluton could have created a S-M-Z style fold in the diapiric sense but not the traditional, compressional fold model sense (Fossen, 2010). Along the top of the dome, the strain ellipse (purple) shows the direction of maximum extension along the horizontal axis. The horizontal extensional forces at the top of the dome could have produced vertical planes of weakness that could have been exploited during the Alleghanian to produce the dextral Appleby Shear Zone. The Mill Brook Shear zones, which unlike the Appleby shear zone, exhibit a shallower dip, exploited the foliation planes formed along the limbs of the dome and formed along shallow dip angles of 45° and 65°.

Dextral Shear Sense

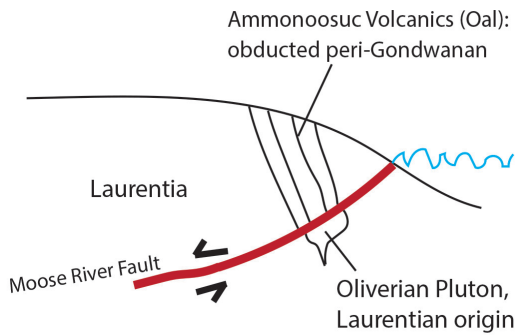
The dextral shear sense observed in the three shear zones indicates, for the first time in the region, a significant period of transpressional tectonism post doming. The Norumbega Fault, a fault system stretching 400km from New Brunswick to Southern Maine (Ludman et al., 1999), nucleating in the late middle Paleozoic (Hooke and Winski, 2014), is an Alleghanian structure with dextral motion. Ludman et al. (1999) have partitioned the activity of the Norumbega into four events, the first three of which produced dextral structures. Because the Mill Brook and

Appleby and shear zones are both ductile, dextral shear structures, it could be possible that they are part of a regional Alleghanian deformation similar to that of the Norumbega Fault.

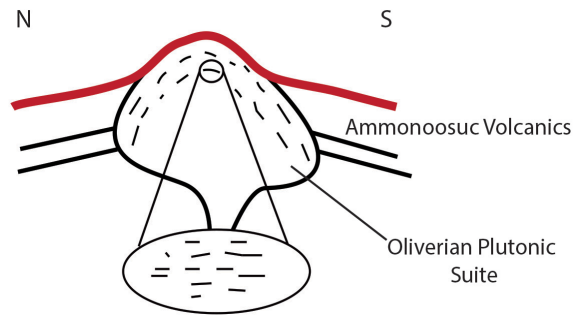
The Dome: Three Stages of Deformation

The evidence of sheared, folded, foliations illustrate a three-stage deformation history of the dome (Fig. 31). The story of the dome began during the Ordovician with the formation of the Oliverian Plutonic Suite (Moench and Aleinikoff, 2003). Evidence of Gondwanan and Laurentian provenance has been found in the isotopic signatures for the Oliverian plutons (Dorais et al., 2012). Popular tectonic models propose that the Bronson Hill arc is located on West Ganderia and therefore of Gondwanan provenance. Therefore, the presence of Laurentian isotopic signature suggests the Oliverian magma was generated very near to Laurentia, or that the plutons picked up a Laurentian signature as the plutons rose through the Laurentian crust (Dorais et al., 2012; Karabinos, 2015). Based on the sequence of deformation proposed by Eusden (2010) in the adjacent Presidential Range, the Jefferson Dome rose through the overlying Ammonoosuc Volcanics as well as Silurian and Devonian metasedimentary rocks during the late Acadian or possibly NeoAcadian Orogeny (Stage 1). The doming process produced the dome-like structure of the entire suite of foliations for the Mt. Dartmouth 7.5' quadrangle. Following the Acadian and Neoacadian orogenies, the dextral shearing during the Alleghanian Orogeny is proposed to be responsible for the Mill Brook and Appleby shear zones during the Carboniferous to Permian (Ludman et al., 1999). The dextral shearing is responsible for producing the S-C fabric of the sheared rocks. The third and final stage occurred during the Mesozoic (Triassic?) with the activation of the Pine Peak Fault (Hardcastle and Albaugh, 1990). The motion along the Pine Peak Fault not only truncated the SE edge of the Dome, cutting out all evidence of the Ammonoosuc Volcanics, but it produced a more steeply dipping southeastern limb of the Jefferson Dome. This is significant enough to have imparted strain to the surrounding rocks. Motion along the Pine Peak Fault could have produced the rare crenulations seen folding the Appleby shear zone fabrics.

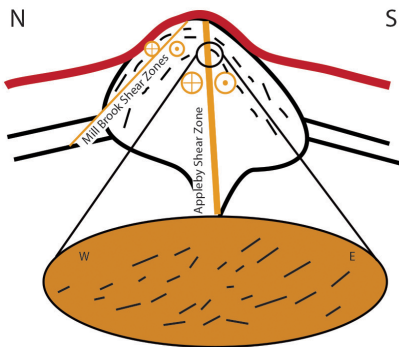
Moose River Fault develops, emplaces Ammonoosuc Volcanics on top of Oliverian Pluton (Salinic or Earliest Acadian) (Dorias et al., 2012; Eusden, 2010)



Stage 1: Doming occurs during Late Acadian/ Neoacadian. Creates dome-shaped foliation.



Stage 2: Alleghenian Orogeny creates dextral shear zones and develops S-C fabrics.



Stage 3: Ammonoosuc Fault or Pine Peak Fault crenulates S-C fabrics (Mesozoic) (Roden-Tice and Tice, 2005)

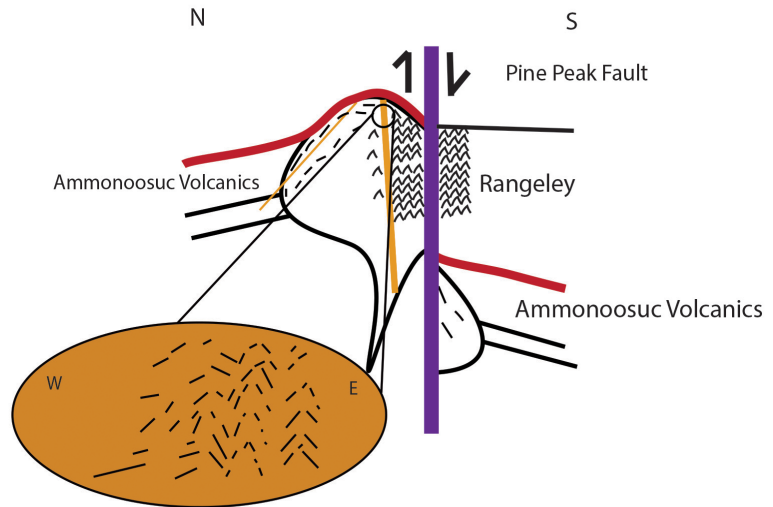
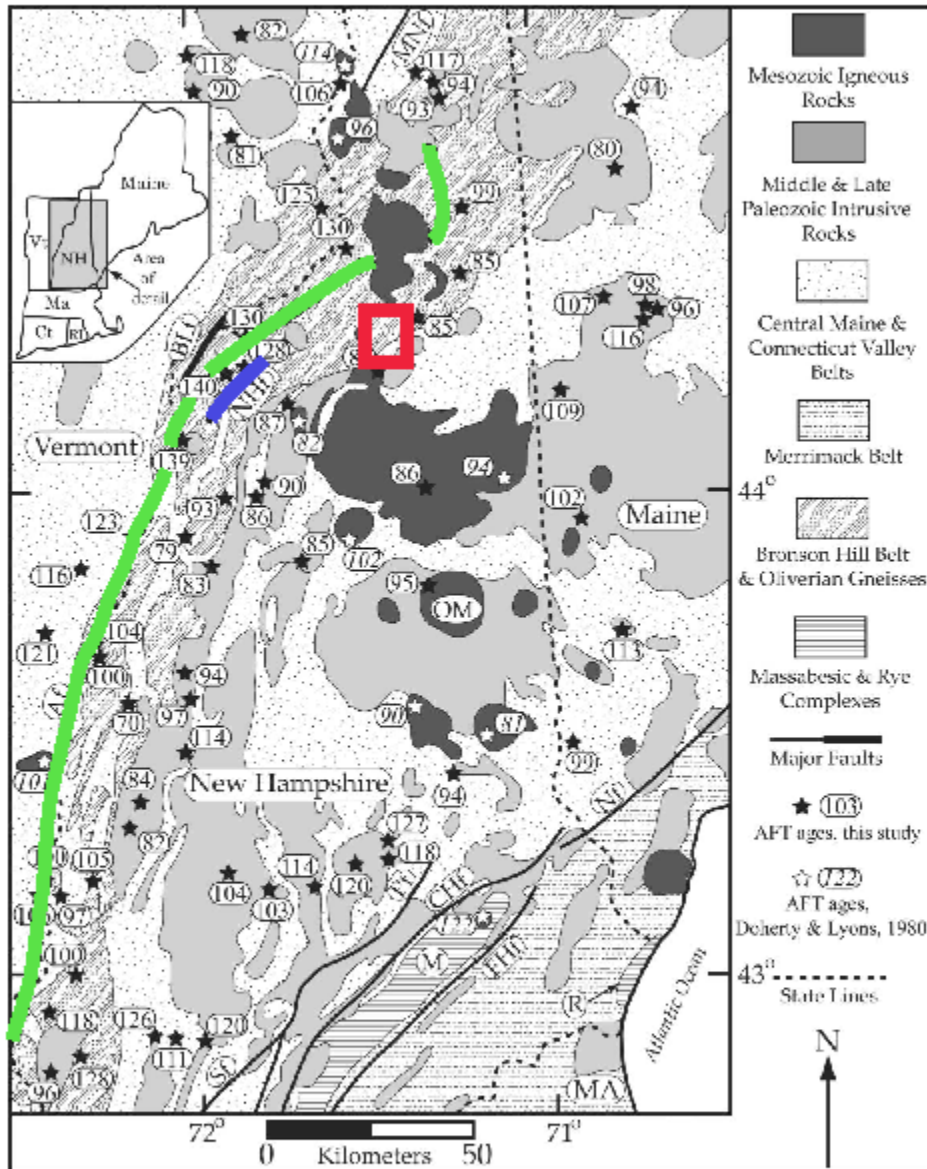


Figure 31. Three stage deformation process of the Jefferson Dome to produce the observed structures. After the formation of the magma dome during the Ordovician (Moench and Aleinikoff, 2003), the magma chamber domed through the overlying Ammonoosuc Volcanics to produce the dome-like structure of the foliation to produce two limbs, one dipping to the northwest, the other to the southeast (Stage 1). This happened during the late Acadian or Neoacadian after the refolding of the nappes the Early Acadian. This was followed by the emplacement of two shear zones via dextral motion during the Alleghanian orogeny along planes of weakness within the dome (Hooke and Winksi, 2014; Ludman et al., 1999) to produce S-C fabrics in the affected rocks. Stage 3, motion along the Pine Peak Fault during the Mesozoic (Hardcastle and Albaugh, 1990; Roden-Tice and Tice, 2005) crenulated the S-C fabrics of the nearby rocks, as far-reaching as Appleby shear zone.

The Silicified Zone and Quartz Veins

The presence of the quartz veins observed in Sample 175 are most likely related to Mesozoic silicification. The quartz veins are observed cutting through planes of foliation (Fig. 28) Though no cross-cutting relationships between the quartz veins and crenulations exist, both the activation



of the Pine Peak Fault that possibly created the crenulations, and silicification of the fault appear to me Mesozoic in age (Roden-Tice et al., 2009). The quartz vein in Sample 175 that runs parallel to foliation is sinistrally sheared (Fig. 20). It is possible that the reactivation of the Ammonoosuc fault of <80Ma (Roden-Tice et al., 2009) could have created sinistral as well as dip slip structures within the older silicified veins. It is also equally possible that the quartz veins

were sheared while the veins were opening, suggesting a simultaneous development.

Figure 32. The proximity of Ammonoosuc Fault (green) and Northey Hill Fault (blue) in relation to the Mt. Dartmouth 7.5' quadrangle (red). Reactivation of the Ammonoosuc fault <80Ma could be responsible for the sinistrally sheared quartz veins observed in Sample 175. (Modified from Roden-Tice et al., 2009).

Deformation History of the Northeast

The doming of the Jefferson dome plays a key role in deciphering the deformation history of the surrounding area. The story begins with the formation of the pluton during the Ordovician (Moench and Aleinikoff, 2003; Dorais et al., 2008). To follow, the Central Maine Trough (CMT) was deposited during the Silurian and Devonian, depositing units including the Rangeley formation (Src) and followed by the deposition of the Littleton (Dl) formation (Fig. 5). The Acadian orogeny resulted in four deformational events beginning 400 Ma, with the development of the Mahoosuc and Moose River faults develop (D0). Early recumbent folds, or nappes, develop at the beginning of the Acadian orogeny (D1) (Thompson et al., 1968; Bradley et al., 2000; Bradley and Tucker, 2002; Eusden et al., 2009). Because both the Silurian and Devonian units show recumbent folding, the nappes must be at least Devonian in age (Thompson et al., 1968; Bradley and Tucker, 2002; Eusden et al., 2009).

The extent of the Oliverian doming that tilted the Rangeley and Littleton formations has been documented by a reversal in dip direction in a band 1-3 km wide parallel to the dome's SE contact in the Presidential Range (Eusden, 2010). Northwest of the limit of doming, the dips of the Littleton formation demonstrated a southeasterly dip following the dip direction of the Jefferson Dome. Similar southeast dips are seen in the Rangeley Formation within the study area indicating that before the Pine Peak Fault developed, the doming had already reversed the dip in the Mt Dartmouth Range.

CONCLUSIONS

The Bronson Hill terrane remains a piece of the tectonic puzzle for the formation of the Appalachian mountain belt in the Northeast. The study of the Oliverian Domes, igneous intrusions occurring later in the development of the Bronson Hill Anticlinorium, reveals a previously unknown period of significant post-doming deformational history. With continued studies of the Oliverian Domes, the placement, timing, and origin of Bronson Hill terrane and its Oliverian Plutons continues to be better understood.

The Jefferson Dome has not been studied to the same extent as the southern Oliverian Domes. However, despite the intensity of study on the southern Oliverian Domes, shear zones and crenulated S-C fabrics have not been previously identified in any of the other Oliverian Domes. The relationship between the foliation structure of the dome, shear zones, and crenulated S-C fabrics is key in understanding the sequence of deformation of the Jefferson Dome, and in deciphering the tectonic forces that produced such structures that may influence the other parts of the Bronson Hill Anticlinorium.

This study identifies three stages of deformation for the Jefferson Dome. The first stage is the Late Acadian or Neocadian doming of the Oliverian pluton through the overlying sequence, including at least the overlying Ammonoosuc Volcanics, to produce the anticlinal, dome-like structure resembled in the foliation. This was followed by the development of three dextral shear zones during the Alleghanian orogeny, which is known to have produced other dextral structures such as the Norumbega fault (Swanson, 1999). The third stage of deformation crenulated the S-C fabrics of the Appleby shear zone and is most likely due to motion along either the Pine Peak Fault, the southern boundary of the Jefferson Dome in the quadrangle, or the Ammonoosuc Fault, both moving during the Mesozoic (Hardcastle et al., 1990; Roden-Tice et al., 2009).

Future studies should be performed on the REE and trace element geochemical analyses of the Jefferson Dome rocks to verify the tectonic setting and origin of the pluton. Modern geochronology of the dome rocks and the shear zones could also be a focus of future studies to gather a more precise understanding of the timing of these features.

REFERENCES

- Billings, M.P., Chapman, C.A., Chapman, R. W., Fowler-Billings, K., and F.B. Loomis Jr, 1946, Geology of the Mt. Washington Quadrangle, New Hampshire: Geological Society of America, v. 57, p. 261-274.
- Bradley, D., and Tucker, R., 2002, Emsian Synorogenic Paleogeography of the Maine Appalachians: *Journal of Geology*, v. 110, p. 483-492.
- Bradley, D.C., Tucker, R.D., Lux, D.R., Harris, A.G., and McGregor, D.C., 2000, Migration of the Acadian Orogen and Foreland Basin Across the Northern Appalachians of Maine and Adjacent Areas: USGS professional paper 1624.
- Cardozo, N., and Allmendinger, R., 2013, OSXStereonet: A computer program that plots lines and planes in spherical, equal angle or equal area, projections.
<http://www.geo.cornell.edu/geology/faculty/RWA/programs/stereonet.html>.
- Dorais, M.J., Atkinson, M., Kim, J., West, D.P., and Kirby, G.A., 2012, Where is the Iapetus suture in northern New England? A study of the Ammonoosuc Volcanics, Bronson Hill terrane, New Hampshire: *Canadian Journal of Earth Sciences*, v. 49, p.189-205.
- Dorais, M.J., Workman, J., and J. Aggarwal, 2008, The Petrogenesis of the Highlandcroft and Oliverian Plutonic Suites, New Hampshire: Implications for the Structure of the Bronson Hill Terrane: *American Journal of Science*, v. 308, p. 73-99.
- Dupee, M.E., 2002, A stratigraphic and kinematic analysis of the Ordovician Ammonoosuc volcanics, Northern Presidential Range, New Hampshire [Undergraduate thesis]: Bates College, 93 p.
- Egerton, R.F., 2005, Physical principles of electron microscopy: an introduction to TEM, SEM, and AEM: Springer, 202 p.
- Eusden, J.D., 2015, Silurian stratigraphy revisited: Extensions from New Hampshire!: Geological Society of America Northeastern Section, 50th, New Hampshire, Abstracts, vol. 47.3, p. 61.
- Eusden, J. D., 2010, The Presidential Range: Its Geologic and Tectonic History: Durand Press, Lyme, New Hampshire, 62 p. and 1:20,000 map.
- Eusden, D., Anderson, K., Beaudry, E., Dupee, M., Larkin, R., Minor, J., and Welling, D., 2006, Domes, volcanics, migmatites, refolded folds and granites: a transect from the Bronson Hill Arc inot the Central Main cover, Northern Presidential Range, New Hampshire, *in* NEIGC 2006 Guidebook, p. 1-14.
- Eusden, J.D., Foley, M., Roden-Tice, M., 2009, The Ordovician to Carboniferous bedrock geology and cooling history of the Bronson Hill and Central Main Belts, Presidential Range, New Hampshire, *in* NEIGC 2009 Guidebook, p. A3-3 to A3-8.

- Eusden, J.D., Garesche, J.M., Johnson, A.H., Maconochie, J-M, Peters, S.P., O'Brien, J.B., Widmann, B.L., 1996, Stratigraphy and ductile structure of the Presidential Range, New Hampshire: Tectonic implications for the Acadian Orogeny: Geological Society of America Bulletin, v. 108.4, p. 417-436.
- Eusden, J.D., Thompson, W.B., Fowler, B.K., Davis, P.T., Bothner, W.A., Boisvert, R.A., Creasy, J.W., 2013, The Geology of New Hampshire's White Mountains, Lyme New Hampshire: Durand Press, 175 p.
- Fleuty, M.J., 1964, The descriptions of folds: Proceedings of the Geologists' Association, v. 75, p. 461-492.
- Foley, M.B., 2009, Contact relationships between the Ammonoosuc Volcanics and the Jefferson Dome, Northern Presidential Range, New Hampshire [Undergraduate thesis]: Bates College, 118 p.
- Granit, 2005, GRANIT 7.5' Quad Tile Index, <http://Granit.unh.edu>.
- Hanmer, S., 1981, Tectonic significance of the northeastern Gander Zone, Newfoundland: an Acadian ductile shear zone: Canadian Journal of Earth Sciences, v. 18(1), p. 120-135.
- Hardcastle, K., and Albaugh, D.S., 1990, Stress and timing relationships of a fault-related, paleohydrothermal system in central New Hampshire: Record of a Mesozoic stress change in New England?: Tectonics, v. 9.4, p. 623-639.
- Hatcher, Jr., R.D., 2010, The Appalachian orogeny: A brief summary: Geological Society of America Memoir, v. 206, p. 1-19.
- Hibbard, J.P., van Staal, C.R., and D.W. Rankin, 2010, Comparative analysis of the geological evolution of the northern and southern Appalachian orogeny: Late Ordovician-Permian: Geological Society of America Memoirs, v. 206, p. 51-69.
- Hooke, R.L., and Winski, D.A., 2014, Unroofing Maine: Relating pressure of crystallization, thermochronological data, tectonics, and topography: Geomorphology, v. 210, p. 36-47.
- Karabinos, P., Samson, S.D., Hepburn, J.C., and H.M. Stoll, 1998, Taconian orogeny in the New England Appalachians: Collision between Laurentia and the Shelburne Falls arc: Geology, v. 26.3, p. 215-218.
- Karabinos, P., 2015, Was the Early Ordovician Shelburne Falls Arc built on Gondwanan crust close to Laurentia?: Geological Society of America Northeastern Section, 50th, New Hampshire, Abstracts, v. 47.3, p. 81.
- Killam, M., 2015, Emplacement of the Croydon Dome in Southwestern New Hampshire using microstructures from the northern dome margin: Geological Society of America Northeastern Section, 50th, New Hampshire, Abstracts, v. 47.3, p. 90.

- Kohn, M.J., and F. Spear, 1999, Probing the depths of Oliverian magmas: Implications for Paleozoic tectonics in the northeastern United States: *Geology*, v. 27.9, p. 803-806.
- Krinsley, D.H., 1998, Backscattered scanning electron microscopy and image analysis of sediments and sedimentary rocks: Cambridge University Press.
- Leo, G.W., 1991, Oliverian domes, related plutonic rocks, and mantling Ammonoosuc Volcanics of the Bronson Hill Anticlinorium, New England Appalachians: U.S. Geological Survey.
- Ludman, A., Lanzirotti, A., Lux, D., and Chunzeng, W., 1999, Constrains on timing and displacement of multistage shearing in the Norumbega fault system, eastern Maine: Geological Society of America Special Paper, no. 331.
- Lyons, J.B., Bothner, W.A., Moench, R.H., and J.B. Thompson Jr., 1997, Bedrock Geologic Map of New Hampshire: U.S. Geological Survey, scale 1:250,000, 2 sheets.
- Lyons, J.B., Campbell J.G., and Erikson, J.P., 1996, Gravity signatures and geometric configurations of some Oliverian plutons: Their relation to Acadian structures: Geological Society of American Bulletin, v. 108.7, p. 872-822.
- Macdonald, F.A., Ryan-Davis, J., Coish, R.A., Crowley, J.L., and Karabinos, P., 2014, A newly identified Gondwanan terrane in the northern Appalachian Mountains: Implications for the Taconic orogeny and closure of the Iapetus Ocean: *Geology*, v. 42.6, p. 539-542.
- Moench, R.H., and Aleinikoff, J.N., 2003, Stratigraphy, geochronology, and accretionary terrane settings of two Bronson Hill arc sequences, northern New England: *Physics and Chemistry of the Earth*, v. 28, p. 113-160.
- Mount Washington Observatory (MWOB), Some Specific Hiking Routes: http://www.mountwashington.org/about/visitor/summer_visits/routes.php (accessed Oct 2014).
- Nesse, W.D., 2012, Introduction to Mineralogy: New York, Oxford University Press, 480 p.
- OlympusMicro.com, 2015, The Microscope Resource Center: olympusmicro.com (accessed January 2015)
- Oxman, G., 2015, Petrogenesis and paleostress analysis of the Mill Brook Dike Zone in the Mount Dartmouth 7.5' quadrangle, New Hampshire [Undergraduate thesis]: Bates College.
- Reusch, D.N., and van Staal, C.R., 2011, The Dog Bay-Liberty Line and its significance for Silurian tectonics of the northern Appalachian orogen: *Canadian Journal of Earth Sciences*, v. 49, p. 239-258.
- Robinson, P., Tucker, R.D., Bradley, D., Berry, H.N., and Osberg, P.H., 1998, Paleozoic orogens in New England, USA: *GFF*, v. 120, p. 119-148.

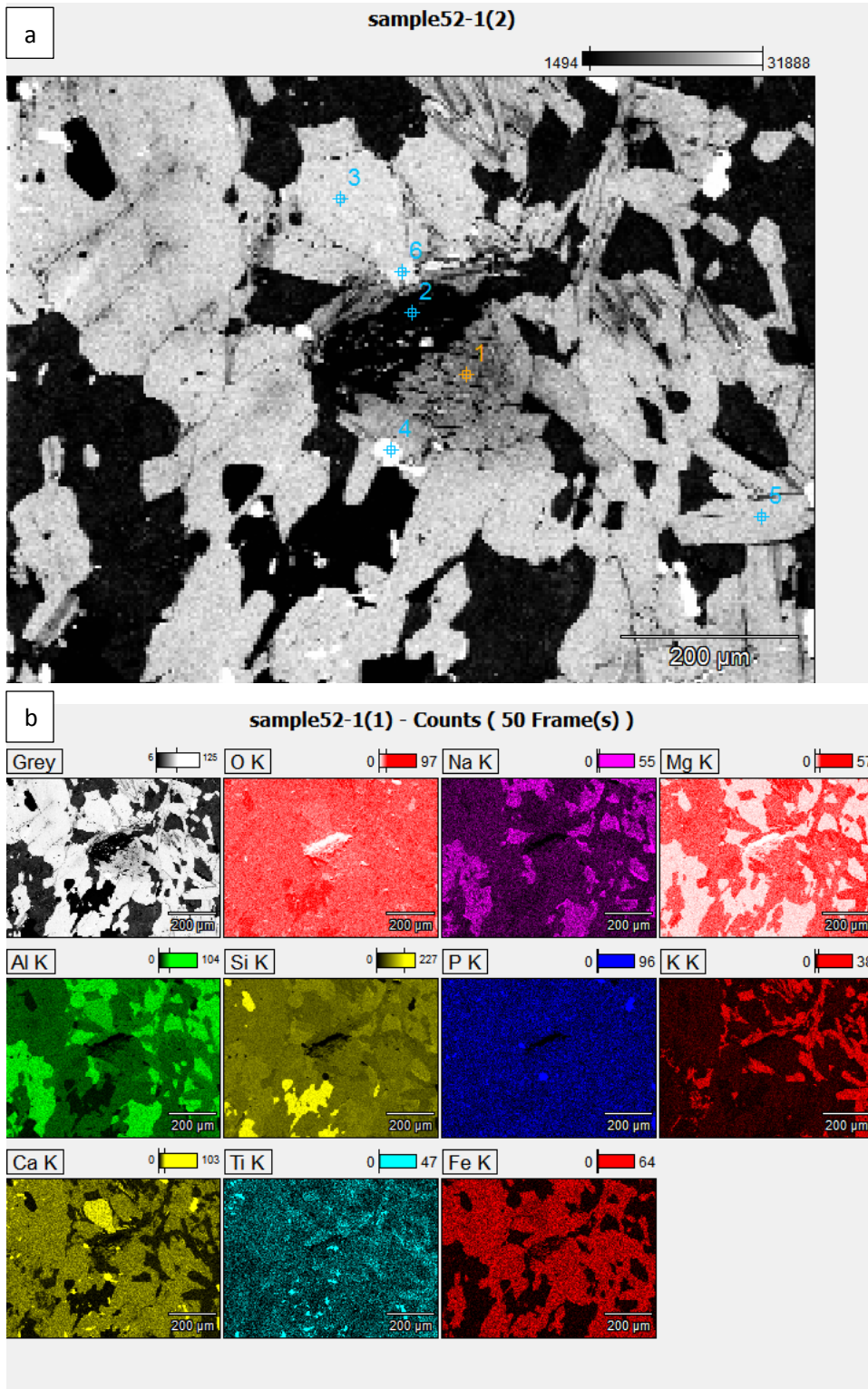
- Roden-Tice, M.K., and Tice, S.J., 2005, Regional-Scale Mid-Jurassic to Late Cretaceous Unroofing from the Adirondack Mountains through Central New England Based on Apatite Fission-Track and (U-Th)/He Thermochronology: *Journal of Geology*, v. 113, p. 535-552.
- Roden-Tice, M.K., West, Jr., D.P., Potter, J.K., Raymond, S.M., and Winch, J.L., 2009, Presence of Long-Term Lithospheric Thermal Anomaly: Evidence from Apatite Fission-Track Analysis in Northern New England: *Journal of Geology*, v. 117, p. 627-641.
- Schumacher, J.C. 1988, Stratigraphy and geochemistry of the Ammonoosuc Volcanics, Central Massachusetts and Southwestern New Hampshire. *American Journal of Science*, v. 288, p. 619-663.
- Solar, G.S., and Brown, M., 2001, Deformation partition during the transpression in response to Early Devonian oblique convergence, northern Appalachian orogeny, USA: *Journal of Structural Geology*, v. 23, p. 1043-1065.
- Swanson, M.T., 1999, Kinematic indicators for regional dextral shear along the Norumbega fault system in the Casco Bay area, coastal Maine: *GSA Special Papers*, v. 331, p.1-23.
- Thompson, J.B., Robinson, P., Clifford, T.N., and Newell, J.T., 1968, Nappes and Gneiss Domes in West-Central New England, *in* Zen, E-A., White, W.S., Hadley, J.B., and Thompson, J.B., eds., *Studies of Appalachian Geology: Northern and Maritime*: New York, NY, John Wiley and Sons, Inc., p. 203-218.
- van Staal, C.R., 2005, The Northern Appalachians: *Encyclopedia of geology* 4, p. 81-91.
- van Staal, C.R., Whalen, J.B., Valverde-Vaquero, P., Zagorevski, A., and Rogers, N., 2009, Pre-Carboniferous, episodic accretion-related, orogenesis along the Laurentian margin of the northern Appalachians: *Geological Society, London, Special Publications*, v. 327, p. 271-316.
- Waldron, W.F., and van Staal, C.R., 2001, Taconian orogeny and the accretion of the Dashwoods block: A peri-Laurentian microcontinent in the Iapetus Ocean: *Geology*, v. 29.9, p. 811-814.
- Xiao, S.M., 2015, *Bedrock Geology of the Mt. Dartmouth 7.5' Quadrangle, New Hampshire* [Undergraduate thesis]: Bates College.

APPENDIX

SEM-EDS imaging and data for following samples is presented as follows:

a) Backscatter image with Point and Shoot locations where elemental data was collected; b) X-ray map; and c) elemental quantification data corresponding to Point and Shoot locations.

A1. Sample 52 (Oal)



C: Elemental quantification results for Sample 52

Point 1:

Element	Net	Net	Int.	Int.	Element	Wt.%	Compnd	Num. of
Line	Counts	Error	Cps/nA	Error	Wt.%	Error	Formula	Cations
O K	188744 ±	858	4.63	4.63	43.52S	---	(null)	---
Na K	11709 ±	168	0.91	0.91	0.99 ±	0.01	Na2O	0.127
Mg K	147034 ±	653	3.52	3.52	6.65 ±	0.03	MgO	0.805
Al K	120734 ±	555	2.99	2.99	5.65 ±	0.03	Al2O3	0.616
Si L	0 ±	0	0.00	0.00	---	---	(null)	---
Si K	475975 ±	1709	9.21	9.21	21.95 ±	0.08	SiO2	2.299
K L	0 ±	0	0.00	0.00	---	---	(null)	---
K K	10398 ±	167	0.90	0.90	0.66 ±	0.01	K2O	0.050
Ca L	7 ±	5	0.03	0.03	---	---	(null)	---
Ca K	123961 ±	515	2.78	2.78	9.05 ±	0.04	CaO	0.664
Ti L	1750 ±	119	0.64	0.64	---	---	(null)	---
Ti K	2275 ±	119	0.64	0.64	0.25 ±	0.01	TiO2	0.015
Fe L	23617 ±	205	1.11	1.11	---	---	(null)	---
Fe K	55778 ±	294	1.58	1.58	11.26 ±	0.06	Fe2O3	0.593
					-----		-----	
Total					100.00			5.17

Point 2: Plucked mineral clast

Point 3:

Element	Net	Net	Int.	Int.	Element	Wt.%	Compnd	Num. of
Line	Counts	Error	Cps/nA	Error	Wt.%	Error	Formula	Cations
O K	187708 ±	853	4.60	4.60	43.08S	---	(null)	---
Al K	319402 ±	1232	6.64	6.64	13.28 ±	0.05	Al2O3	1.462
Si L	0 ±	0	0.00	0.00	---	---	(null)	---
Si K	407169 ±	1490	8.03	8.03	18.37 ±	0.07	SiO2	1.943

Ca L	6 ± 5	0.03	0.03	---	---	(null)	---
Ca K	248483 ± 862	4.65	4.65	17.51 ± 0.06	CaO	1.298	
Ti L	1991 ± 122	0.66	0.66	---	---	(null)	---
Ti K	544 ± 110	0.59	0.59	0.06 ± 0.01	TiO2	0.004	
Fe L	16635 ± 182	0.98	0.98	---	---	(null)	---
Fe K	39025 ± 244	1.32	1.32	7.70 ± 0.05	Fe2O3	0.410	
				-----		-----	
Total				100.00		5.12	

Point 4:

Element	Net	Net	Int.	Int.	Element	Wt.%	Compnd	Num. of
Line	Counts	Error	Cps/nA	Error	Wt.%	Error	Formula	Cations
O K	92163 ± 477		2.57	2.57	40.75S	---	(null)	---
Al K	2217 ± 155		0.84	0.84	0.09 ± 0.01		Al2O3	0.011
Si L	0 ± 0		0.00	0.00	---	---	(null)	---
Si K	6448 ± 170		0.92	0.92	0.25 ± 0.01		SiO2	0.028
P L	0 ± 0		0.00	0.00	---	---	(null)	---
P K	445066 ± 1568		8.45	8.45	18.90 ± 0.07		P2O5	1.916
Ca L	100 ± 13		0.07	0.07	---	---	(null)	---
Ca K	590876 ± 1801		9.71	9.71	39.81 ± 0.12		CaO	3.120
Fe L	13709 ± 160		0.86	0.86	---	---	(null)	---
Fe K	1091 ± 96		0.52	0.52	0.21 ± 0.02		Fe2O3	0.012
				-----		-----		
Total					100.00		5.09	

Point 5:

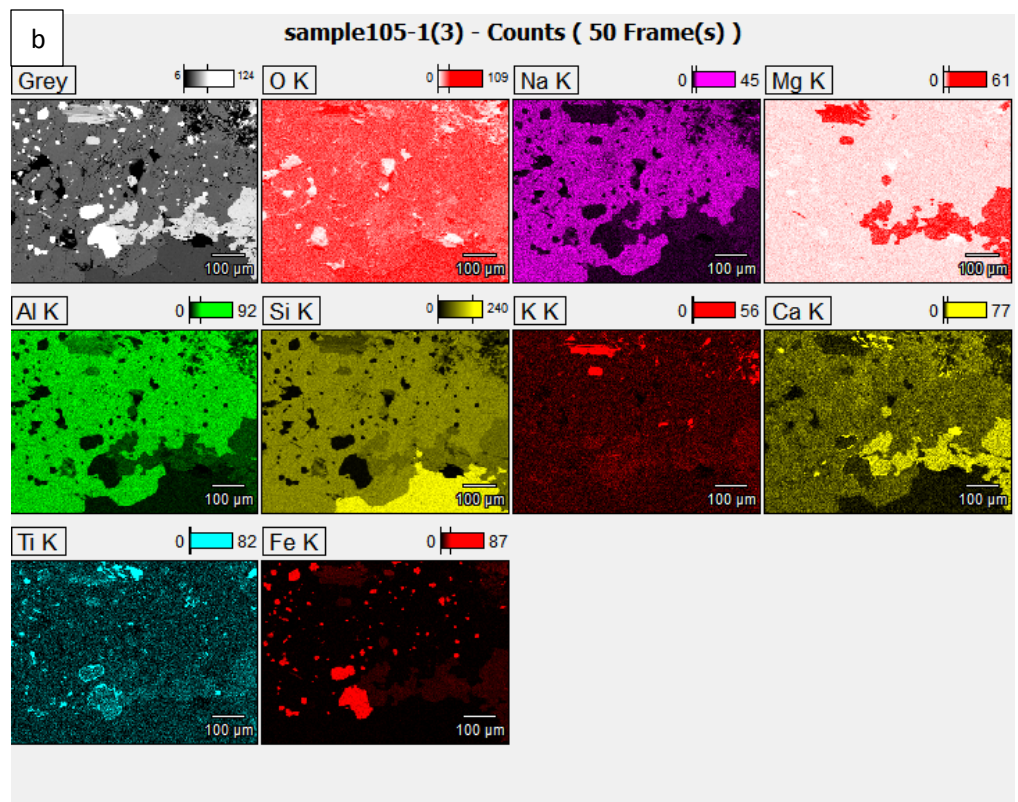
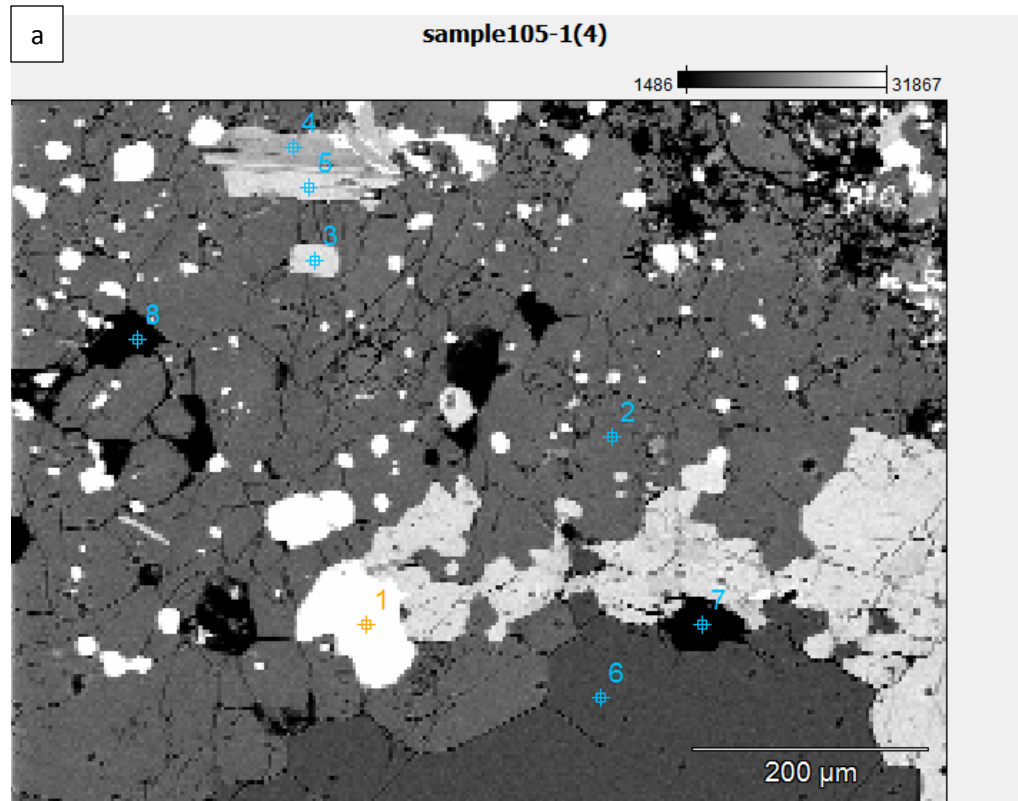
Element	Net	Net	Int.	Int.	k-ratio	Element	Wt.%	Norm.	Compnd	Num. of
Line	Counts	Error	Cps/nA	Error	(calc.)	Wt.%	Error	Wt.%	Formula	Cations
O K	230627 ± 1021		5.50	5.50	---	42.34S	---	42.34S	(null)	---
Na K	2127 ± 131		0.71	0.71	0.002	0.18 ± 0.01		0.18	Na2O	0.024
Mg K	173151 ± 746		4.02	4.02	0.108	7.90 ± 0.03		7.90	MgO	0.983

Al K	185309 ± 775	4.17	4.17	0.131	8.91 ± 0.04	8.91	Al2O3	0.998	
Si L	0 ± 0	0.00	0.00	---	---	---	(null)	---	
Si K	383020 ± 1408	7.58	7.58	0.304	18.68 ± 0.07	18.68	SiO2	2.010	
K L	0 ± 0	0.00	0.00	---	---	---	(null)	---	
K K	126025 ± 527	2.84	2.84	0.172	8.28 ± 0.03	8.28	K2O	0.640	
Ti L	1749 ± 129	0.69	0.69	---	---	---	(null)	---	
Ti K	10661 ± 159	0.86	0.86	0.024	1.20 ± 0.02	1.20	TiO2	0.075	
Fe L	28223 ± 226	1.22	1.22	---	---	---	(null)	---	
Fe K	60795 ± 309	1.66	1.66	0.258	12.52 ± 0.06	12.52	Fe2O3	0.678	
				-----		-----		-----	
Total					100.00	100.00		5.41	

Point 6:

Element	Net	Net	Int.	Int.	Element	Wt.%	Compnd	Num. of	
Line	Counts	Error	Cps/nA	Error	Wt.%	Error	Formula	Cations	
O K	167263 ± 776	4.18	4.18	42.19S	---	---	(null)	---	
Mg K	32839 ± 258	1.39	1.39	1.52 ± 0.01	MgO	0.190			
Al K	233836 ± 941	5.07	5.07	10.52 ± 0.04	Al2O3	1.183			
Si L	0 ± 0	0.00	0.00	---	---	---	(null)	---	
Si K	383169 ± 1410	7.59	7.59	17.99 ± 0.07	SiO2	1.943			
K L	0 ± 0	0.00	0.00	---	---	---	(null)	---	
K K	24397 ± 222	1.20	1.20	1.54 ± 0.01	K2O	0.120			
Ca L	7 ± 5	0.03	0.03	---	---	---	(null)	---	
Ca K	194445 ± 713	3.84	3.84	14.27 ± 0.05	CaO	1.080			
Ti L	1632 ± 118	0.64	0.64	---	---	---	(null)	---	
Ti K	6787 ± 142	0.76	0.76	0.77 ± 0.02	TiO2	0.049			
Fe L	21943 ± 201	1.08	1.08	---	---	---	(null)	---	
Fe K	54870 ± 292	1.57	1.57	11.21 ± 0.06	Fe2O3	0.609			
				-----		-----		-----	
Total					100.00			5.17	

A2. Sample 105 (Oo1bc)



C: Elemental quantification results for Sample 105

Point 1:

Element	Net	Net	Int.	Int.	Element	Wt.%	Compnd	Num. of
Line	Counts	Error	Cps/nA	Error	Wt.%	Error	Formula	Cations
O K	238868	± 1049	5.55	5.55	30.23S	---		---
Al K	4961	± 159	0.84	0.84	0.26	± 0.01	Al ₂ O ₃	0.020
Si L	0	± 0	0.00	0.00	---	---		---
Si K	3859	± 161	0.85	0.85	0.18	± 0.01	SiO ₂	0.013
Ti L	0	± 0	0.00	0.00	---	---		---
Ti K	474	± 140	0.74	0.74	0.04	± 0.01	TiO ₂	0.002
Fe L	138021	± 591	3.13	3.13	---	---		---
Fe K	426041	± 1272	6.73	6.73	69.29	± 0.21	Fe ₂ O ₃	2.627
					-----		-----	
Total					100.00			2.66

Point 2:

Element	Net	Net	Int.	Int.	Element	Wt.%	Compnd	Num. of
Line	Counts	Error	Cps/nA	Error	Wt.%	Error	Formula	Cations
O K	308348	± 1311	6.94	6.94	47.90S	---		---
Na K	121922	± 574	3.04	3.04	7.47	± 0.04	Na ₂ O	0.868
Al K	339711	± 1297	6.86	6.86	12.36	± 0.05	Al ₂ O ₃	1.224
Si L	0	± 0	0.00	0.00	---	---		---
Si K	725143	± 2530	13.39	13.39	28.94	± 0.10	SiO ₂	2.754
Ca L	12	± 5	0.03	0.03	---	---		---
Ca K	50749	± 298	1.58	1.58	3.34	± 0.02	CaO	0.222
					-----		-----	
Total					100.00			5.07

Point 3:

Element	Net	Net	Int.	Int.	Element	Wt.%	Compnd	Num. of
Line	Counts	Error	Cps/nA	Error	Wt.%	Error	Formula	Cations
O K	249051 ± 1093		5.78	5.78	42.06S	---		---
Mg K	194122 ± 820		4.34	4.34	8.19 ± 0.03		MgO	1.539
Al K	164665 ± 707		3.74	3.74	7.33 ± 0.03		Al ₂ O ₃	1.240
Si L	0 ± 0		0.00	0.00	---	---		---
Si K	425368 ± 1550		8.20	8.20	18.88 ± 0.07		SiO ₂	3.069
Cl L	0 ± 0		0.00	0.00	---	---		---
Cl K	2702 ± 147		0.78	0.78	0.15 ± 0.01		Cl	0.019
K L	0 ± 0		0.00	0.00	---	---		---
K K	142036 ± 576		3.05	3.05	8.56 ± 0.03		K ₂ O	0.999
Ti L	3476 ± 143		0.76	0.76	---	---		---
Ti K	20587 ± 200		1.06	1.06	2.12 ± 0.02		TiO ₂	0.202
Fe L	36074 ± 254		1.34	1.34	---	---		---
Fe K	67122 ± 329		1.74	1.74	12.71 ± 0.06		Fe ₂ O ₃	1.039
					-----		-----	
Total					100.00			8.11

Point 4:

Element	Net	Net	Int.	Int.	Element	Wt.%	Compnd	Num. of
Line	Counts	Error	Cps/nA	Error	Wt.%	Error	Formula	Cations
O K	401610 ± 1677		8.87	8.87	42.23S	---		---
F K	8252 ± 255		1.35	1.35	2.20 ± 0.07		F	0.526
Na K	3830 ± 134		0.71	0.71	0.34 ± 0.01		Na ₂ O	0.068
Mg K	223610 ± 918		4.86	4.86	10.52 ± 0.04		MgO	1.967
Al K	208266 ± 851		4.50	4.50	10.50 ± 0.04		Al ₂ O ₃	1.770
Si L	0 ± 0		0.00	0.00	---	---		---
Si K	307982 ± 1159		6.13	6.13	15.70 ± 0.06		SiO ₂	2.542
Ca L	2 ± 4		0.02	0.02	---	---		---
Ca K	2296 ± 133		0.70	0.70	0.17 ± 0.01		CaO	0.019

Ti L	5012 ± 155	0.82	0.82	---	---	---	---
Ti K	283 ± 112	0.59	0.59	0.03 ± 0.01	TiO2	0.003	
Fe L	29856 ± 334	1.77	1.77	---	---	---	
Fe K	90924 ± 393	2.08	2.08	18.31 ± 0.08	Fe2O3	1.490	
				-----		-----	
Total				100.00		8.39	

Point 5:

Element	Net	Net	Int.	Int.	Element	Wt.%	Compnd	Num. of
Line	Counts	Error	Cps/nA	Error	Wt.%	Error	Formula	Cations
O K	261574 ± 1135		6.01	6.01	40.56S	---		---
F K	14083 ± 267		1.41	1.41	3.71 ± 0.07	F		0.925
Mg K	182793 ± 779		4.12	4.12	7.55 ± 0.03	MgO		1.470
Al K	180959 ± 761		4.03	4.03	7.80 ± 0.03	Al2O3		1.368
Si L	0 ± 0		0.00	0.00	---	---		---
Si K	417689 ± 1522		8.05	8.05	18.01 ± 0.07	SiO2		3.035
Cl L	0 ± 0		0.00	0.00	---	---		---
Cl K	2737 ± 145		0.77	0.77	0.15 ± 0.01	Cl		0.019
K L	0 ± 0		0.00	0.00	---	---		---
K K	135801 ± 557		2.95	2.95	7.90 ± 0.03	K2O		0.956
Ti L	3897 ± 141		0.75	0.75	---	---		---
Ti K	15279 ± 180		0.95	0.95	1.52 ± 0.02	TiO2		0.150
Fe L	22395 ± 316		1.67	1.67	---	---		---
Fe K	70190 ± 337		1.78	1.78	12.82 ± 0.06	Fe2O3		1.087
				-----		-----		
Total					100.00			9.01

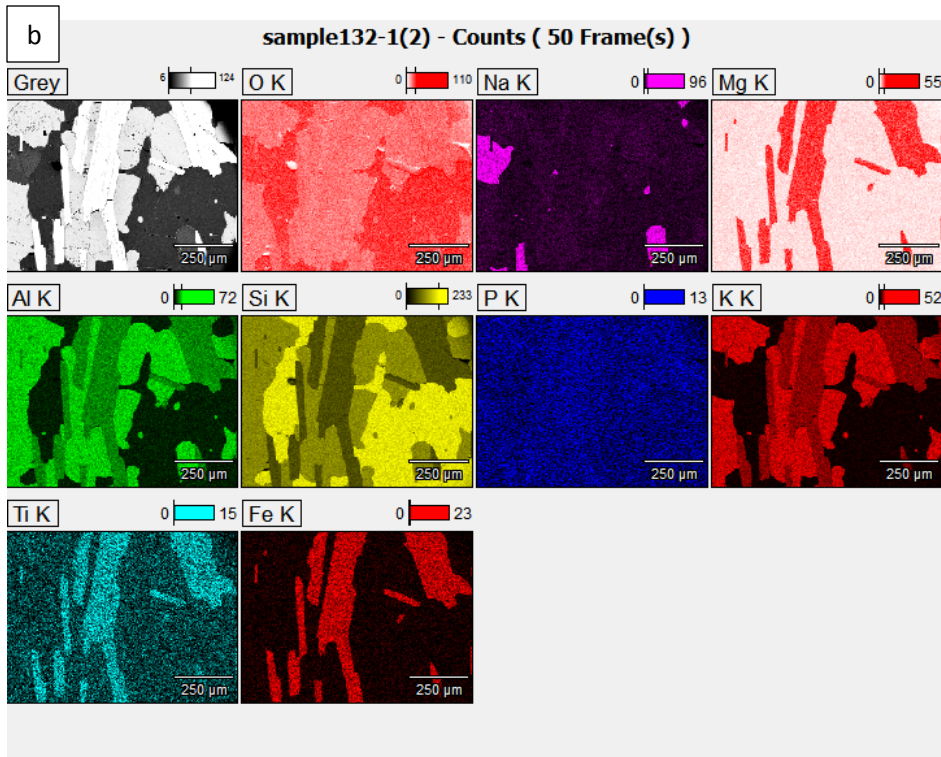
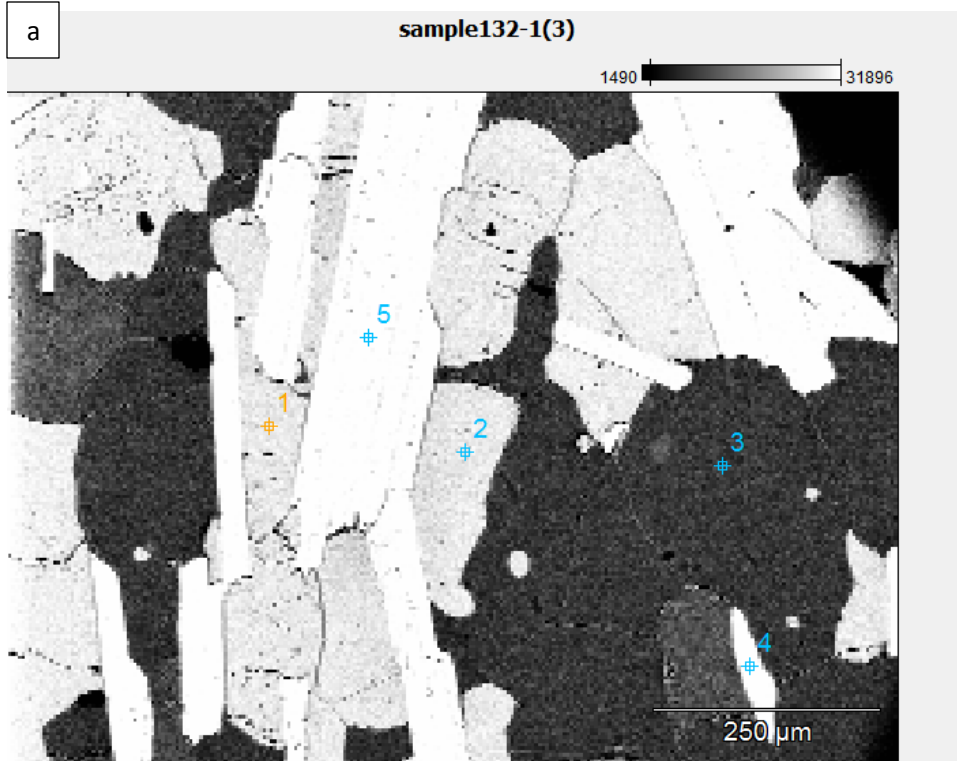
Point 6:

Element	Net	Net	Int.	Int.	Element	Wt.%	Compnd	Num. of
Line	Counts	Error	Cps/nA	Error	Wt.%	Error	Formula	Cations

O K	381096 ± 1591	8.42	8.42	53.22S	---	---
Al K	9752 ± 174	0.92	0.92	0.34 ± 0.01	Al ₂ O ₃	0.030
Si L	0 ± 0	0.00	0.00	---	---	---
Si K	1350384 ± 4627	24.48	24.48	46.45 ± 0.16	SiO ₂	3.977
				-----		-----
Total				100.00		4.01

Point 7 and 8: Plucked mineral clast.

A3. Sample 132 (Oo1hx)



C: Elemental quantification results for Sample 132

Point 1:

Element	Net	Net	Int.	Int.	Element	Wt.%	Compnd	Num. of
Line	Counts	Error	Cps/nA	Error	Wt.%	Error	Formula	Cations
O K	0	± 0	0.00	0.00	46.14S	---	---	---
Na K	8906	± 161	0.92	0.92	0.64	± 0.01	Na2O	0.077
Al K	255538	± 1009	5.75	5.75	9.93	± 0.04	Al2O3	1.021
Si L	0	± 0	0.00	0.00	---	---	---	---
Si K	716382	± 2488	14.18	14.18	30.20	± 0.10	SiO2	2.983
K L	279	± 21	0.12	0.12	---	---	---	---
K K	202905	± 743	4.24	4.24	13.09	± 0.05	K2O	0.928
					-----		-----	
Total					100.00			5.01

Point 2:

Element	Net	Net	Int.	Int.	Element	Wt.%	Compnd	Num. of
Line	Counts	Error	Cps/nA	Error	Wt.%	Error	Formula	Cations
O K	192288	± 902	5.14	5.14	46.02S	---	---	---
Na K	8550	± 161	0.92	0.92	0.61	± 0.01	Na2O	0.074
Al K	257133	± 1017	5.80	5.80	9.90	± 0.04	Al2O3	1.021
Si L	0	± 0	0.00	0.00	---	---	---	---
Si K	719411	± 2504	14.28	14.28	30.07	± 0.10	SiO2	2.977
K L	0	± 0	0.00	0.00	---	---	---	---
K K	209666	± 763	4.35	4.35	13.40	± 0.05	K2O	0.953
					-----		-----	
Total					100.00			5.03

Point 3:

Element	Net	Net	Int.	Int.	Element	Wt.%	Compnd	Num. of
Line	Counts	Error	Cps/nA	Error	Wt.%	Error	Formula	Cations
O K	333125	± 1399	7.98	7.98	53.21S	---	---	---

Al K	10424 ± 168	0.96	0.96	0.39 ± 0.01	Al ₂ O ₃	0.035
Si L	0 ± 0	0.00	0.00	---	---	---
Si K	1249372 ± 4264	24.32	24.32	46.40 ± 0.16	SiO ₂	3.974
				-----	-----	
Total				100.00		4.01

Point 4:

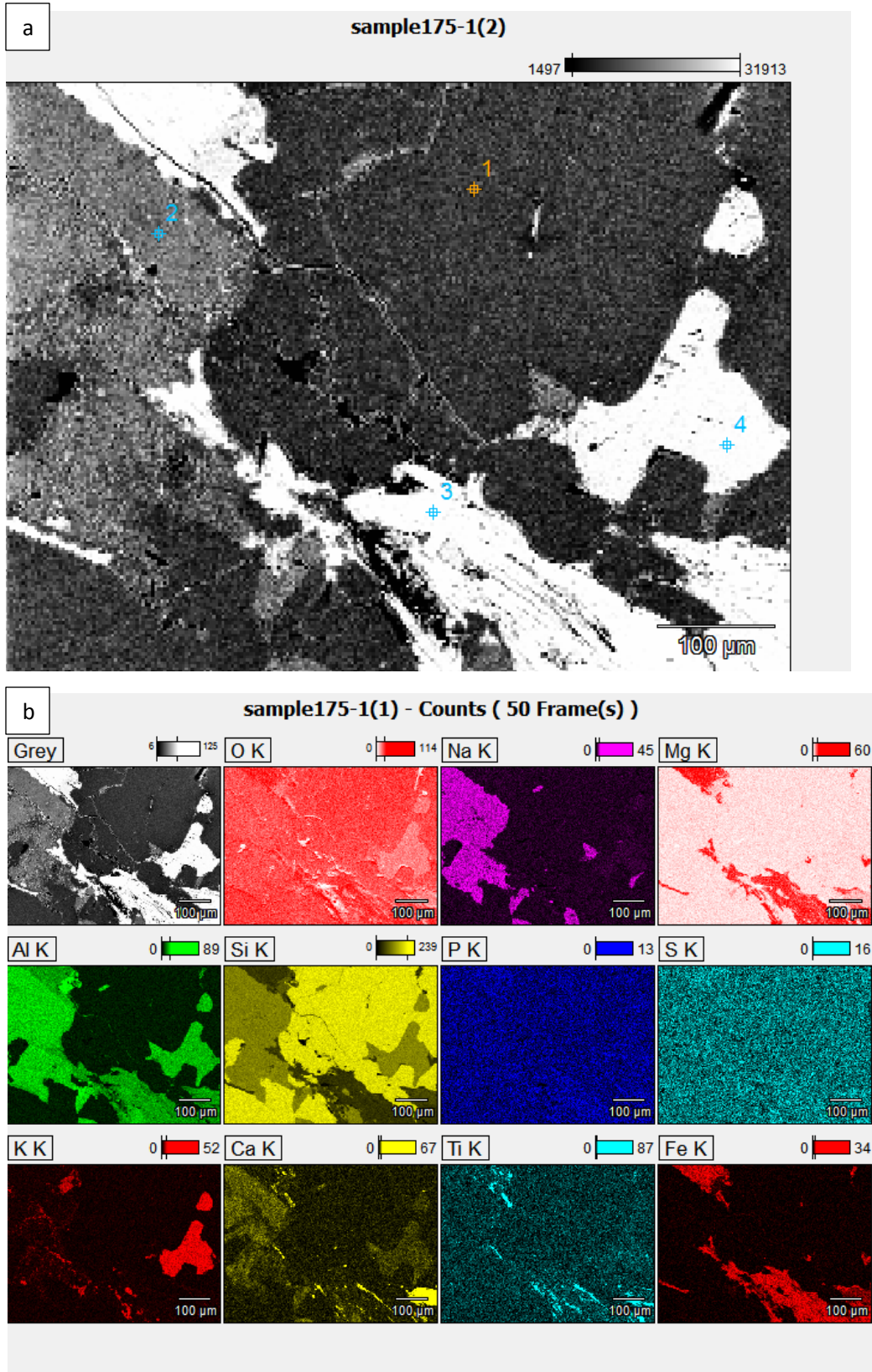
Element	Net	Net	Int.	Int.	Element	Wt.%	Compnd	Num. of
Line	Counts	Error	Cps/nA	Error	Wt.%	Error	Formula	Cations
O K	212228 ± 951	5.42	5.42	42.22S	---	---	---	---
Na K	2312 ± 127	0.72	0.72	0.20 ± 0.01	Na ₂ O	0.040		
Mg K	184345 ± 783	4.47	4.47	8.60 ± 0.04	MgO	1.609		
Al K	159519 ± 687	3.92	3.92	7.91 ± 0.03	Al ₂ O ₃	1.333		
Si L	0 ± 0	0.00	0.00	---	---	---		
Si K	382266 ± 1405	8.01	8.01	19.01 ± 0.07	SiO ₂	3.078		
K L	0 ± 0	0.00	0.00	---	---	---		
K K	128823 ± 534	3.05	3.05	8.67 ± 0.04	K ₂ O	1.009		
Ti L	2162 ± 125	0.71	0.71	---	---	---		
Ti K	9880 ± 155	0.88	0.88	1.14 ± 0.02	TiO ₂	0.108		
Fe L	27385 ± 219	1.25	1.25	---	---	---		
Fe K	58015 ± 301	1.72	1.72	12.25 ± 0.06	Fe ₂ O ₃	0.997		
				-----	-----			
Total				100.00		8.17		

Point 5:

Element	Net	Net	Int.	Int.	Element	Wt.%	Compnd	Num. of
Line	Counts	Error	Cps/nA	Error	Wt.%	Error	Formula	Cations
O K	189659 ± 861	4.91	4.91	42.01S	---	---	---	---
Mg K	180818 ± 769	4.39	4.39	8.18 ± 0.03	MgO	1.539		
Al K	161113 ± 690	3.93	3.93	7.69 ± 0.03	Al ₂ O ₃	1.303		
Si L	0 ± 0	0.00	0.00	---	---	---		

Si K	389895 ± 1426	8.13	8.13	18.63 ± 0.07	SiO2	3.031
K L	0 ± 0	0.00	0.00	---	---	---
K K	136721 ± 556	3.17	3.17	8.84 ± 0.04	K2O	1.033
Ti L	1641 ± 119	0.68	0.68	---	---	---
Ti K	17131 ± 182	1.04	1.04	1.90 ± 0.02	TiO2	0.181
Fe L	26876 ± 216	1.23	1.23	---	---	---
Fe K	62774 ± 314	1.79	1.79	12.75 ± 0.06	Fe2O3	1.044
				-----		-----
Total				100.00		8.13

A4. Sample 175 (Oo1b)



C: Elemental quantification results for Sample 175

Point 1:

Element	Net	Net	Int.	Int.	k-ratio	Element	Wt.%	Norm.	Compnd	Num. of
Line	Counts	Error	Cps/nA	Error	(calc.)	Wt.%	Error	Wt.%	Formula	Cations
O K	331884 ± 1401		7.66	7.66	---	53.22S	---	53.22S	(null)	---
Al K	9648 ± 169		0.92	0.92	0.007	0.35 ± 0.01		0.35	Al2O3	0.031
Si L	0 ± 0		0.00	0.00	---	---	---	---	(null)	---
Si K	1298211 ± 4483		24.50	24.50	0.992	46.32 ± 0.16		46.32	SiO2	3.966
P L	0 ± 0		0.00	0.00	---	---	---	---	(null)	---
P K	1898 ± 115		0.63	0.63	0.002	0.11 ± 0.01		0.11	P2O5	0.009
						-----		-----		-----
Total						100.00		100.00		4.01

Point 2:

Element	Net	Net	Int.	Int.	k-ratio	Element	Wt.%	Norm.	Compnd	Num. of
Line	Counts	Error	Cps/nA	Error	(calc.)	Wt.%	Error	Wt.%	Formula	Cations
O K	264911 ± 1143		6.25	6.25	---	48.04S	---	48.04S	(null)	---
Na K	123351 ± 578		3.16	3.16	0.111	7.84 ± 0.04		7.84	Na2O	0.909
Al K	314720 ± 1212		6.62	6.62	0.233	11.95 ± 0.05		11.95	Al2O3	1.180
Si L	0 ± 0		0.00	0.00	---	---	---	---	(null)	---
Si K	708492 ± 2475		13.52	13.52	0.588	29.40 ± 0.10		29.40	SiO2	2.789
P L	0 ± 0		0.00	0.00	---	---	---	---	(null)	---
P K	1636 ± 119		0.65	0.65	0.002	0.09 ± 0.01		0.09	P2O5	0.008
Ca L	10 ± 5		0.03	0.03	---	---	---	---	(null)	---
Ca K	38993 ± 260		1.42	1.42	0.066	2.68 ± 0.02		2.68	CaO	0.178
						-----		-----		-----
Total						100.00		100.00		5.06

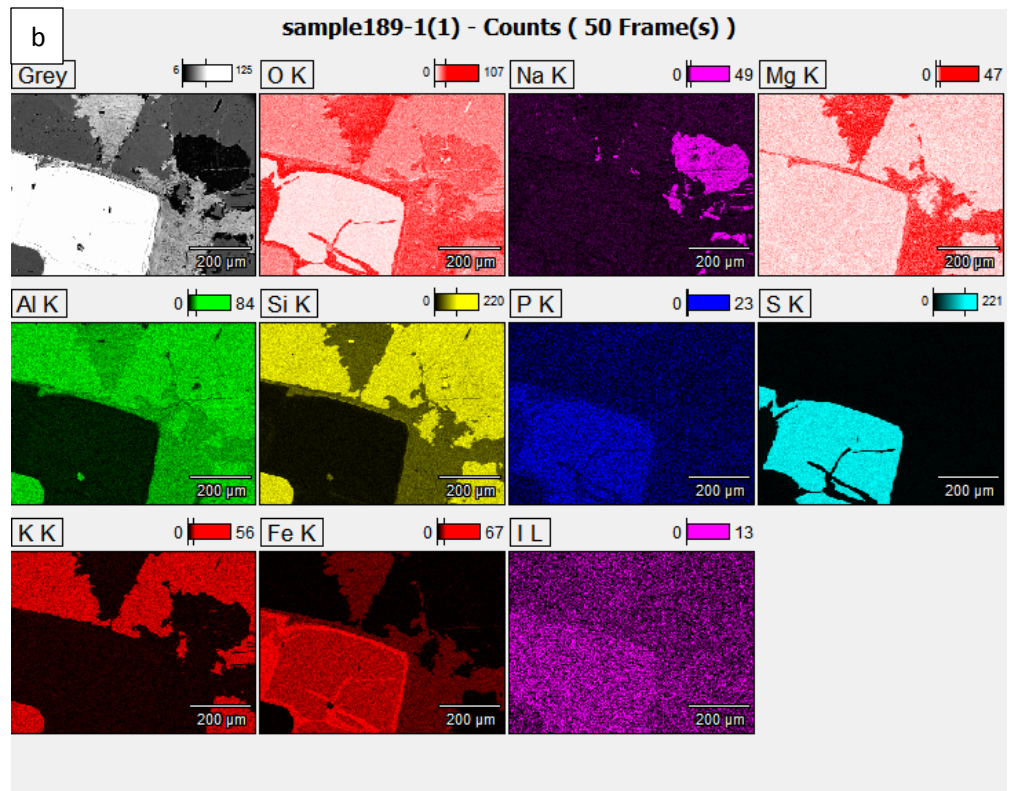
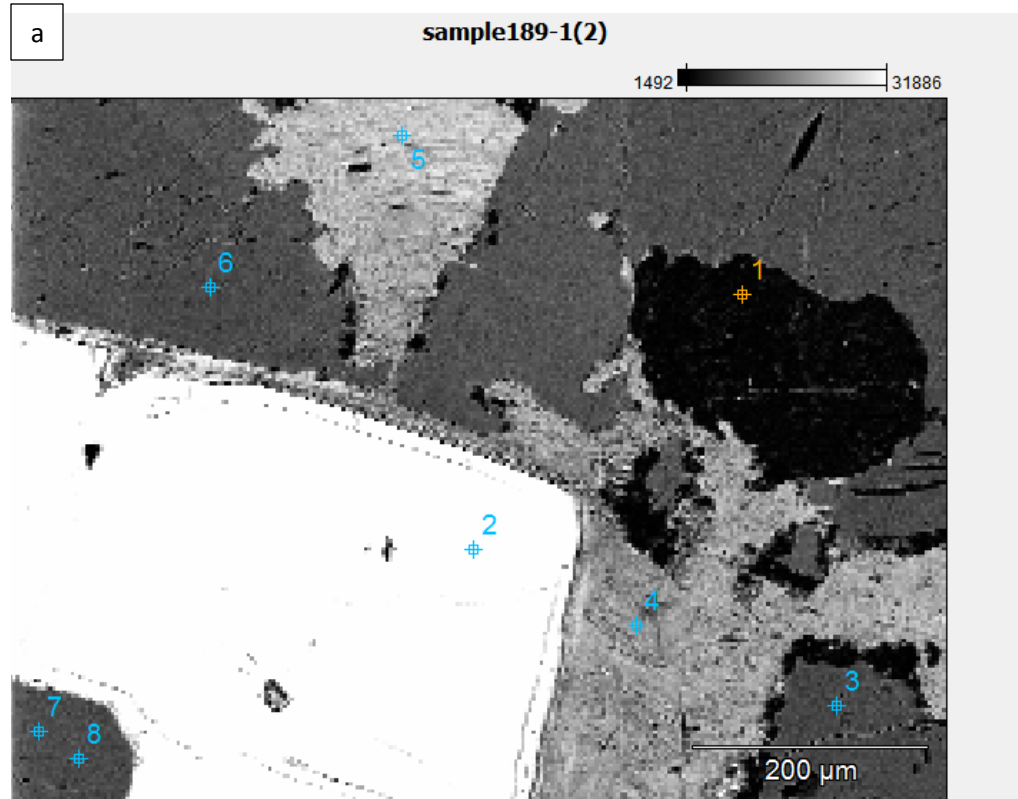
Point 3:

Element	Net	Net	Int.	Int.	Element	Wt.%	Compnd	Num. of
Line	Counts	Error	Cps/nA	Error	Wt.%	Error	Formula	Cations
O K	299244 ±	1290	7.05	7.05	42.30S	---	(null)	---
Mg K	160692 ±	703	3.84	3.84	8.53 ±	0.04	MgO	1.062
Al K	232145 ±	934	5.10	5.10	12.82 ±	0.05	Al ₂ O ₃	1.438
Si L	0 ±	0	0.00	0.00	---	---	(null)	---
Si K	239339 ±	937	5.12	5.12	13.62 ±	0.05	SiO ₂	1.468
Fe L	35137 ±	252	1.38	1.38	---	---	(null)	---
Fe K	103445 ±	425	2.32	2.32	22.72 ±	0.09	Fe ₂ O ₃	1.231
					-----		-----	
Total					100.00			5.20

Point 4:

Element	Net	Net	Int.	Int.	k-ratio	Element	Wt.%	Norm.	Compnd	Num. of
Line	Counts	Error	Cps/nA	Error	(calc.)	Wt.%	Error	Wt.%	Formula	Cations
O K	220690 ±	969	5.30	5.30	---	46.17S	---	46.17S	(null)	---
Na K	9999 ±	168	0.92	0.92	0.009	0.76 ±	0.01	0.76	Na ₂ O	0.092
Al K	243332 ±	971	5.31	5.31	0.178	10.09 ±	0.04	10.09	Al ₂ O ₃	1.037
Si L	0 ±	0	0.00	0.00	---	---	---	---	(null)	---
Si K	664916 ±	2326	12.71	12.71	0.547	29.91 ±	0.10	29.91	SiO ₂	2.953
P L	0 ±	0	0.00	0.00	---	---	---	---	(null)	---
P K	3357 ±	133	0.73	0.73	0.003	0.21 ±	0.01	0.21	P ₂ O ₅	0.019
K L	0 ±	0	0.00	0.00	---	---	---	---	(null)	---
K K	178029 ±	674	3.68	3.68	0.251	12.18 ±	0.05	12.18	K ₂ O	0.863
Ba M	4363 ±	202	1.10	1.10	---	---	---	---	(null)	---
Ba L	3836 ±	167	0.91	0.91	0.012	0.67 ±	0.03	0.67	BaO	0.014
						-----		-----		-----
Total						100.00		100.00		4.98

A5. Sample 189 (Oo1hx), capture 1



C: Elemental quantification of Sample 189, capture 1

Point 1:

Element	Net	Net	Int.	Int.	Element	Wt.%	Compnd	Num. of
Line	Counts	Error	Cps/nA	Error	Wt.%	Error	Formula	Cations
O K	267488 ± 1150		6.42	6.42	48.41S	---	(null)	---
Na K	129579 ± 604		3.37	3.37	9.09 ± 0.04		Na2O	1.045
Al K	249811 ± 996		5.56	5.56	10.67 ± 0.04		Al2O3	1.046
Si L	0 ± 0		0.00	0.00	---	---	(null)	---
Si K	679156 ± 2381		13.29	13.29	31.28 ± 0.11		SiO2	2.945
K L	0 ± 0		0.00	0.00	---	---	(null)	---
K K	7993 ± 148		0.83	0.83	0.55 ± 0.01		K2O	0.037
					-----		-----	
Total					100.00			5.07

Point 2:

Element	Net	Net	Int.	Int.	Element	Wt.%	Compnd	Num. of
Line	Counts	Error	Cps/nA	Error	Wt.%	Error	Formula	Cations
O K	0 ± 0		0.00	0.00	50.16S	---	(null)	---
Al K	5408 ± 170		0.95	0.95	0.11 ± 0.00		Al2O3	0.011
Si L	0 ± 0		0.00	0.00	---	---	(null)	---
Si K	8969 ± 186		1.04	1.04	0.17 ± 0.00		SiO2	0.016
S L	0 ± 0		0.00	0.00	---	---	(null)	---
S K	1312189 ± 4161		23.17	23.17	26.77 ± 0.09		SO3	2.130
Fe L	169522 ± 653		3.64	3.64	---	---	(null)	---
Fe K	260800 ± 827		4.60	4.60	22.78 ± 0.07		Fe2O3	1.041
					-----		-----	
Total					100.00			3.20

Point 3:

Element	Net	Net	Int.	Int.	Element	Wt.%	Compnd	Num. of
Line	Counts	Error	Cps/nA	Error	Wt.%	Error	Formula	Cations
O K	0	± 0	0.00	0.00	46.10S	---	---	---
Na K	7168	± 336	1.87	1.87	0.49	± 0.02	Na2O	0.059
Al K	260952	± 1082	6.03	6.03	9.65	± 0.04	Al2O3	0.993
Si L	0	± 0	0.00	0.00	---	---	---	---
Si K	759853	± 1925	10.73	10.73	30.38	± 0.08	SiO2	3.003
K L	0	± 0	0.00	0.00	---	---	---	---
K K	211471	± 959	5.35	5.35	12.94	± 0.06	K2O	0.919
Fe L	0	± 0	0.00	0.00	---	---	---	---
Fe K	571	± 158	0.88	0.88	0.11	± 0.03	Fe2O3	0.005
Ba M	0	± 202	1.13	1.13	---	---	---	---
Ba L	2168	± 250	1.39	1.39	0.34	± 0.04	BaO	0.007
					-----		-----	
Total					100.00			4.99

Point 4:

Element	Net	Net	Int.	Int.	Element	Wt.%	Compnd	Num. of
Line	Counts	Error	Cps/nA	Error	Wt.%	Error	Formula	Cations
O K	0	± 0	0.00	0.00	42.09S	---	---	---
F K	0	± 0	0.00	0.00	0.00	± 0.00	F	0.000
Mg K	121244	± 845	4.69	4.69	6.47	± 0.05	MgO	1.823
Al K	197532	± 1192	6.62	6.62	10.65	± 0.06	Al2O3	2.699
Si L	0	± 0	0.00	0.00	---	---	---	---
Si K	279992	± 1072	5.96	5.96	15.25	± 0.06	SiO2	3.714
Ca L	0	± 0	0.00	0.00	---	---	---	---
Ca K	1137	± 183	1.02	1.02	0.09	± 0.01	CaO	0.015
Ti L	152215	± 1405	7.81	7.81	---	---	---	---
Ti K	626	± 168	0.93	0.93	0.07	± 0.02	TiO2	0.010
Fe L	0	± 918	5.10	5.10	---	---	---	---

Fe K	118652 ± 687	3.82	3.82	25.38 ± 0.15	Fe2O3	3.110
				-----	-----	
Total				100.00		11.37

Point 5:

Element	Net	Net	Int.	Int.	Element	Wt.%	Compnd	Num. of
Line	Counts	Error	Cps/nA	Error	Wt.%	Error	Formula	Cations
O K	0	± 0	0.00	0.00	40.94S	---	---	---
F K	0	± 140	0.78	0.78	0.00	± 0.00	F	0.000
Mg K	104291	± 792	4.40	4.40	5.63	± 0.04	MgO	1.630
Al K	194188	± 1167	6.48	6.48	10.38	± 0.06	Al2O3	2.707
Si L	0	± 0	0.00	0.00	---	---	---	---
Si K	250160	± 1021	5.67	5.67	13.39	± 0.05	SiO2	3.355
Fe L	0	± 144	0.80	0.80	---	---	---	---
Fe K	142952	± 745	4.14	4.14	29.65	± 0.15	Fe2O3	3.734
					-----	-----		
Total					100.00			11.43

Point 6:

Element	Net	Net	Int.	Int.	Element	Wt.%	Compnd	Num. of
Line	Counts	Error	Cps/nA	Error	Wt.%	Error	Formula	Cations
O K	0	± 0	0.00	0.00	46.27S	---	---	---
Na K	7746	± 335	1.86	1.86	0.53	± 0.02	Na2O	0.064
Al K	259919	± 1080	6.00	6.00	9.64	± 0.04	Al2O3	0.988
Si L	0	± 0	0.00	0.00	---	---	---	---
Si K	762377	± 1928	10.71	10.71	30.60	± 0.08	SiO2	3.014
K L	0	± 21	0.12	0.12	---	---	---	---
K K	210318	± 958	5.32	5.32	12.96	± 0.06	K2O	0.917
					-----	-----		
Total					100.00			4.98

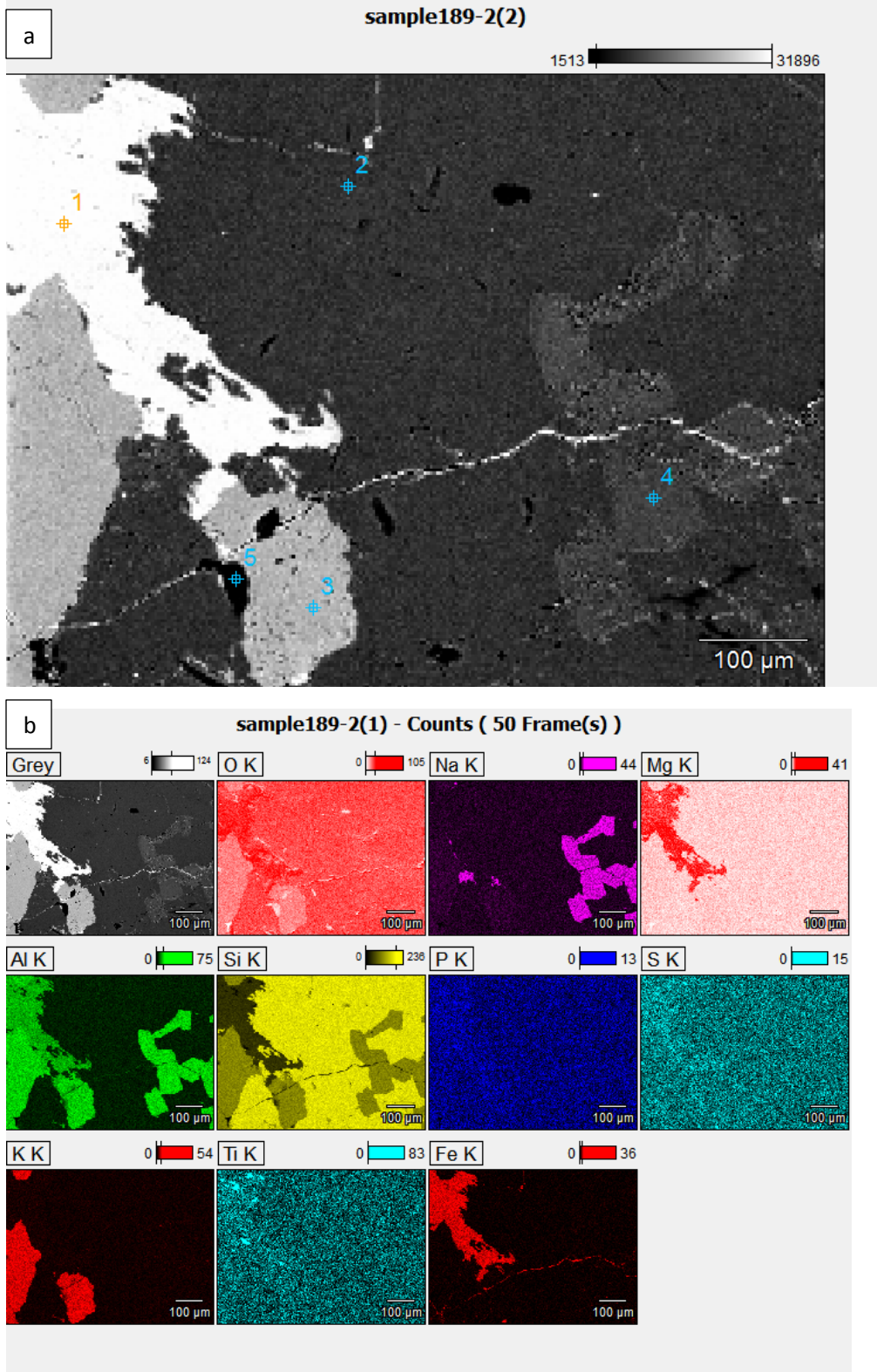
Point 7:

Element	Net	Net	Int.	Int.	Element	Wt.%	Compnd	Num. of
Line	Counts	Error	Cps/nA	Error	Wt.%	Error	Formula	Cations
O K	0	± 0	0.00	0.00	46.22S	---	---	---
Na K	7604	± 332	1.85	1.85	0.53	± 0.02	Na2O	0.064
Al K	255554	± 1068	5.94	5.94	9.58	± 0.04	Al2O3	0.983
Si L	0	± 0	0.00	0.00	---	---	---	---
Si K	753027	± 1910	10.63	10.63	30.53	± 0.08	SiO2	3.010
K L	0	± 0	0.00	0.00	---	---	---	---
K K	207779	± 950	5.29	5.29	12.93	± 0.06	K2O	0.915
Fe L	0	± 121	0.67	0.67	---	---	---	---
Fe K	1089	± 160	0.89	0.89	0.21	± 0.03	Fe2O3	0.010
					-----		-----	
Total					100.00			4.98

Point 8:

Element	Net	Net	Int.	Int.	Element	Wt.%	Compnd	Num. of
Line	Counts	Error	Cps/nA	Error	Wt.%	Error	Formula	Cations
O K	0	± 0	0.00	0.00	46.27S	---	---	---
Na K	7623	± 334	1.86	1.86	0.53	± 0.02	Na2O	0.064
Al K	255552	± 1068	5.94	5.94	9.60	± 0.04	Al2O3	0.985
Si L	0	± 0	0.00	0.00	---	---	---	---
Si K	753024	± 1910	10.63	10.63	30.62	± 0.08	SiO2	3.016
K L	0	± 69	0.38	0.38	---	---	---	---
K K	207779	± 950	5.29	5.29	12.98	± 0.06	K2O	0.918
					-----		-----	
Total					100.00			4.98

A5. Sample 189 (Oo1hx), capture 2



C: Elemental quantification of Sample 189, capture 2

Point 1:

Element	Net	Net	Int.	Int.	Element	Wt.%	Compnd	Num. of
Line	Counts	Error	Cps/nA	Error	Wt.%	Error	Formula	Cations
O K	0	± 0	---	---	41.07S	---	(null)	---
Mg K	95066	± 765	---	---	5.24	± 0.04	MgO	1.512
Al K	205613	± 1175	---	---	11.19	± 0.06	Al2O3	2.908
Si L	0	± 0	---	---	---	---	(null)	---
Si K	241106	± 1005	---	---	13.25	± 0.06	SiO2	3.309
Fe L	0	± 285	---	---	---	---	(null)	---
Fe K	137631	± 732	---	---	29.25	± 0.16	Fe2O3	3.672
					-----		-----	
Total					100.00			11.40

Point 2:

Element	Net	Net	Int.	Int.	Element	Wt.%	Compnd	Num. of
Line	Counts	Error	Cps/nA	Error	Wt.%	Error	Formula	Cations
O K	0	± 0	0.00	0.00	53.25S	---		---
Al K	905	± 274	1.53	1.53	0.03	± 0.01	Al2O3	0.001
Si L	0	± 0	0.00	0.00	---	---		---
Si K	1322454	± 2825	15.78	15.78	46.72	± 0.10	SiO2	0.999
Fe L	0	± 115	0.64	0.64	---	---		---
Fe K	0	± 67	0.37	0.37	0.00	± 0.00	Fe2O3	0.000
					-----		-----	
Total					100.00			1.00

Point 3:

Element	Net	Net	Int.	Int.	Element	Wt.%	Compnd	Num. of
Line	Counts	Error	Cps/nA	Error	Wt.%	Error	Formula	Cations
O K	194897	± 896	10.01	10.01	46.12S	---	(null)	---

Na K	6012 ± 155	1.73	1.73	0.43 ± 0.01	Na2O	0.052
Al K	257741 ± 1023	11.43	11.43	9.91 ± 0.04	Al2O3	1.019
Si L	0 ± 0	0.00	0.00	---	(null)	---
Si K	723939 ± 2529	28.25	28.25	30.22 ± 0.11	SiO2	2.986
K L	0 ± 0	0.00	0.00	---	(null)	---
K K	208186 ± 761	8.50	8.50	13.31 ± 0.05	K2O	0.945

Total				100.00		5.00

Point 4:

Element	Net	Net	Int.	Int.	Element	Wt.%	Compnd Num. of
Line	Counts	Error	Cps/nA	Error	Wt.%	Error	Formula Cations
O K	274947 ± 1225	13.68	13.68	48.31S	---	(null)	---
Na K	130165 ± 604	6.74	6.74	8.52 ± 0.04	Na2O	0.982	
Al K	283007 ± 1107	12.36	12.36	11.18 ± 0.04	Al2O3	1.098	
Si L	0 ± 0	0.00	0.00	---	(null)	---	
Si K	714207 ± 2496	27.87	27.87	30.57 ± 0.11	SiO2	2.884	
Ca L	13 ± 5	0.06	0.06	---	(null)	---	
Ca K	20041 ± 195	2.18	2.18	1.43 ± 0.01	CaO	0.094	

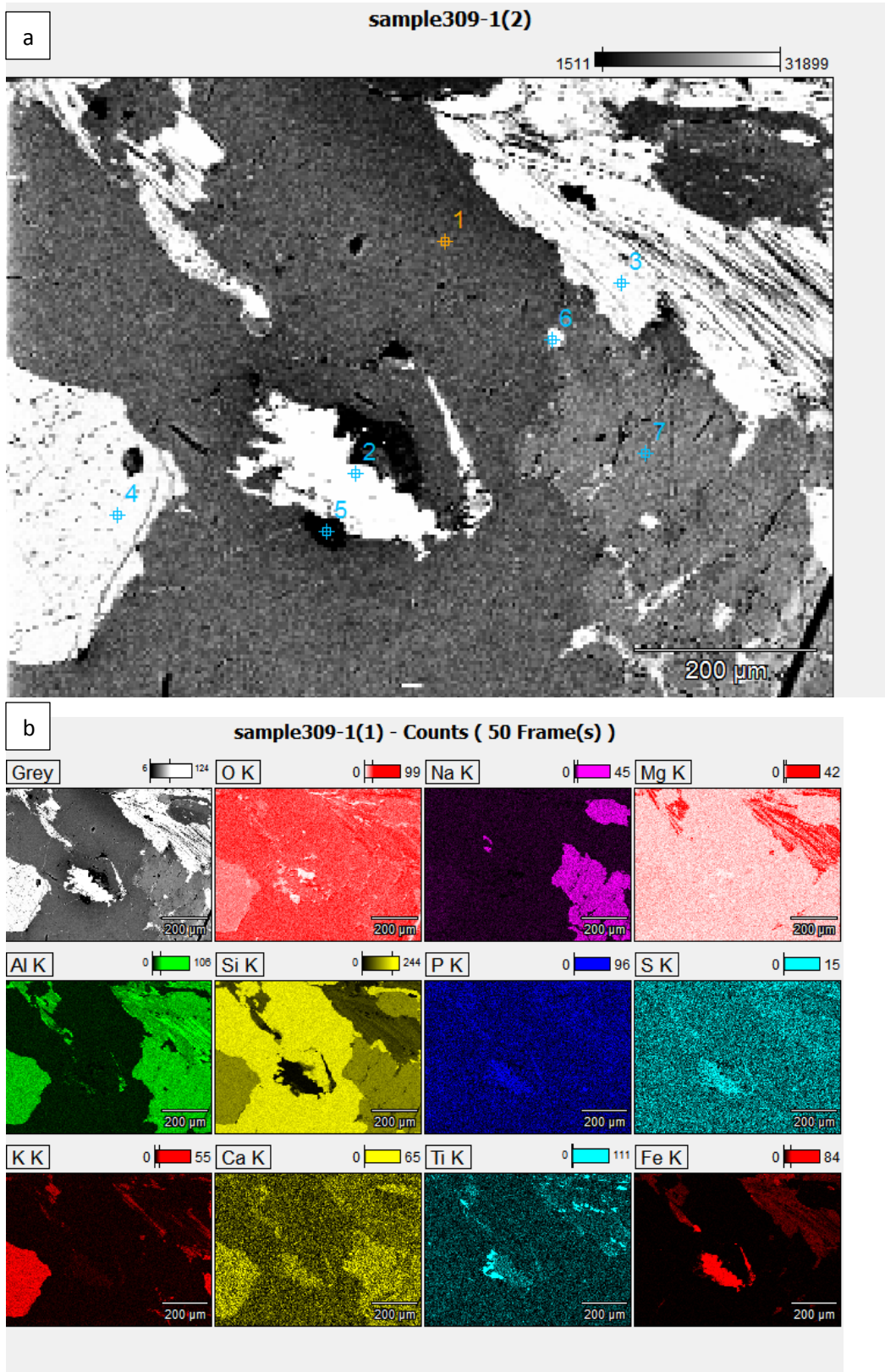
Total				100.00		5.06	

Point 5:

Element	Net	Net	Int.	Int.	Element	Wt.%	Compnd Num. of
Line	Counts	Error	Cps/nA	Error	Wt.%	Error	Formula Cations
O K	0 ± 0	0.00	0.00	43.12S	---	(null)	---
Na K	30706 ± 385	4.30	4.30	4.40 ± 0.06	Na2O	0.569	
Al K	95261 ± 643	7.18	7.18	7.73 ± 0.05	Al2O3	0.851	
Si L	0 ± 0	0.00	0.00	---	(null)	---	
Si K	301020 ± 973	10.87	10.87	25.64 ± 0.08	SiO2	2.709	
S L	0 ± 0	0.00	0.00	---	(null)	---	

S K	18277 ± 252	2.82	2.82	1.96 ± 0.03	SO3	0.182
Cl L	0 ± 0	0.00	0.00	---	---	---
Cl K	40495 ± 507	5.66	5.66	4.78 ± 0.06	Cl	0.400
K L	0 ± 0	0.00	0.00	---	---	---
K K	92466 ± 625	6.98	6.98	12.22 ± 0.08	K2O	0.928
Fe L	0 ± 77	0.86	0.86	---	---	---
Fe K	347 ± 132	1.47	1.47	0.14 ± 0.05	Fe2O3	0.008
				-----		-----
Total				100.00		5.65

A6. Sample 309 (Oo1b)



C: Elemental quantification of Sample 309

Point 1:

Element	Net	Net	Int.	Int.	Element	Wt.%	Compnd	Num. of
Line	Counts	Error	Cps/nA	Error	Wt.%	Error	Formula	Cations
O K	0	± 0	0.00	0.00	53.26S	---	---	---
Si L	0	± 0	0.00	0.00	---	---	---	---
Si K	1361743±	2898	15.56	15.56	46.74 ±	0.10	SiO2	1.000
					-----		-----	
Total					100.00			1.00

Point 2:

Element	Net	Net	Int.	Int.	Element	Wt.%	Compnd	Num. of
Line	Counts	Error	Cps/nA	Error	Wt.%	Error	Formula	Cations
O K	213362 ±	955	5.13	5.13	30.21S	---	(null)	---
Al K	3061 ±	169	0.91	0.91	0.17 ±	0.01	Al2O3	0.026
Si L	0	± 0	0.00	0.00	---	---	(null)	---
Si K	4251 ±	178	0.96	0.96	0.20 ±	0.01	SiO2	0.031
Fe L	130691 ±	570	3.06	3.06	---	---	(null)	---
Fe K	405280 ±	1184	6.37	6.37	69.42 ±	0.20	Fe2O3	5.266
					-----		-----	
Total					100.00			5.32

Point 3:

Element	Net	Net	Int.	Int.	Element	Wt.%	Compnd	Num. of
Line	Counts	Error	Cps/nA	Error	Wt.%	Error	Formula	Cations
O K	287458 ±	1247	6.70	6.70	43.10S	---	(null)	---
Na K	2720 ±	131	0.70	0.70	0.28 ±	0.01	Na2O	0.036
Mg K	33443 ±	258	1.39	1.39	1.77 ±	0.01	MgO	0.217
Al K	237750 ±	957	5.15	5.15	12.10 ±	0.05	Al2O3	1.331
Si L	0	± 0	0.00	0.00	---	---	(null)	---

Si K	339962 ± 1271	6.83	6.83	17.97 ± 0.07	SiO2	1.900
K L	0 ± 0	0.00	0.00	---	(null)	---
K K	2793 ± 140	0.75	0.75	0.19 ± 0.01	K2O	0.015
Ca L	8 ± 5	0.03	0.03	---	(null)	---
Ca K	2192 ± 134	0.72	0.72	0.17 ± 0.01	CaO	0.013
Fe L	37843 ± 264	1.42	1.42	---	(null)	---
Fe K	114754 ± 455	2.45	2.45	24.42 ± 0.10	Fe2O3	1.298

Total				100.00		4.81

Point 4:

Element	Net	Net	Int.	Int.	Element	Wt.%	Compnd Num. of
Line	Counts	Error	Cps/nA	Error	Wt.%	Error	Formula Cations
O K	207834 ± 923	4.96	4.96	46.03S	---	(null)	---
Na K	5850 ± 151	0.81	0.81	0.40 ± 0.01	Na2O	0.048	
Al K	269804 ± 1061	5.70	5.70	9.89 ± 0.04	Al2O3	1.019	
Si L	0 ± 0	0.00	0.00	---	(null)	---	
Si K	757691 ± 2634	14.16	14.16	30.13 ± 0.10	SiO2	2.983	
K L	0 ± 0	0.00	0.00	---	(null)	---	
K K	222660 ± 802	4.31	4.31	13.56 ± 0.05	K2O	0.964	

Total				100.00		5.01	

Point 5 and 6: Plucked mineral clast

Point 7:

Element	Net	Net	Int.	Int.	Element	Wt.%	Compnd Num. of
Line	Counts	Error	Cps/nA	Error	Wt.%	Error	Formula Cations
O K	280791 ± 1404	7.55	7.55	48.08S	---	(null)	---
Na K	151250 ± 674	3.62	3.62	9.03 ± 0.04	Na2O	1.046	
Al K	311729 ± 1198	6.44	6.44	11.31 ± 0.04	Al2O3	1.116	

Si L	0 ± 0	0.00	0.00	---	---	(null)	---
Si K	765613 ± 2657	14.28	14.28	30.10 ± 0.10		SiO2	2.853
Ca L	9 ± 5	0.03	0.03	---	---	(null)	---
Ca K	22687 ± 204	1.10	1.10	1.48 ± 0.01		CaO	0.098
				-----			-----
Total				100.00			5.11